EVALUATION OF REMOTE SENSING DATA SOURCES FOR RAINFALL- RUNOFF MODELING: A CASE STUDY OF NYABARONGO CATCHMENT AREA, RWANDA
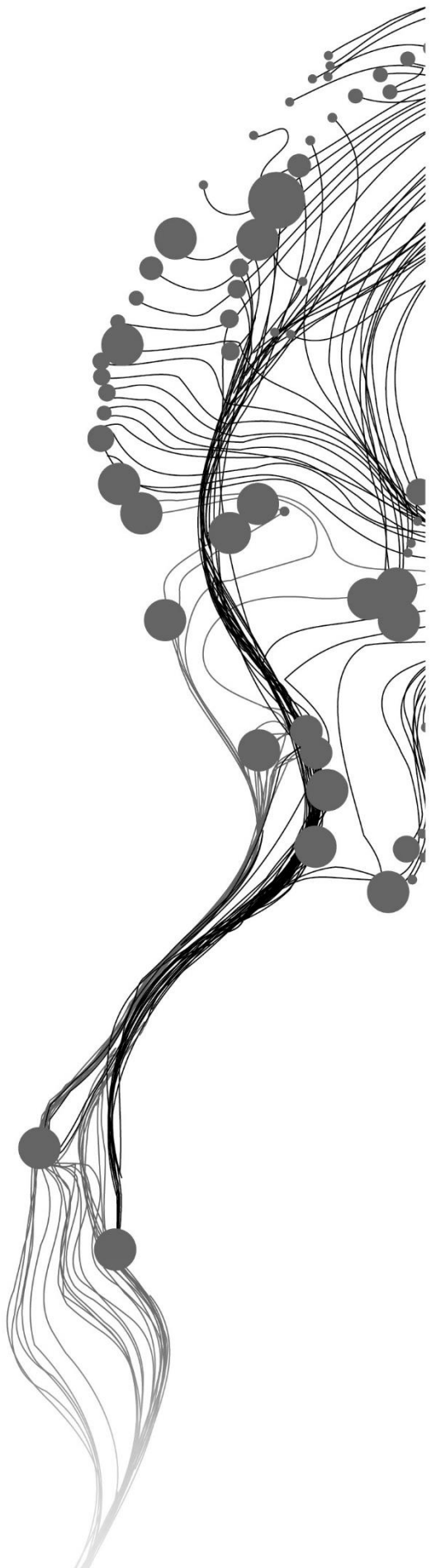
EMMANUEL NTEZIYAREMYE
August, 2024

SUPERVISORS:
DR ING. T..M. RIENTJES
IR G.N PARODI

EVALUATION OF REMOTE SENSING DATA SOURCES FOR RAINFALL-RUNOFF MODELING: A CASE STUDY OF NYABARONGO CATCHMENT AREA, RWANDA

EMMANUEL NTEZIYAREMYE
Enschede, The Netherlands, August 2024

SUPERVISORS:
DR. ING. T.H.M. RIENTJES
IR. G.N. PARODI

THESIS ASSESSMENT BOARD:
Dr. Ir. Christiaan Van Der Tol (Chair)
Dr. Demelash Wondimagegnehu Goshime (PhD) (External Examiner, Arba Minch University)
Dr. Ing. T.H.M. Rientjes (First supervisor)
Ir. G.N. Parodi (Second supervisor)
Dr. B.H.P. Maathuis (Procedural Advisor)

ABSTRACT

Rainfall-runoff modelling is required for effective water resource management, flood risk assessment, and environmental planning, particularly in locations such as the Nyabarongo catchment area in Rwanda, where in-situ data are insufficient and of poor quality. Remote sensing data such as Digital Elevation Models (DEMs), Land Use Land Cover (LULC) maps, soil data, and Satellite Rainfall Estimates (SREs) such as CHIRPS, CMORPH, and GPM-IMERG, can be alternative sources of data for hydrologic modelling in such a context of limited data. The main objective of this study is to assess how remote sensing data sources affect the performance of rainfall-runoff modelling in the Nyabarongo catchment area. This study developed a semi-distributed HEC-HMS model using four model combinations of data sources: Local DEM (10m × 10m) with in-situ or SREs rainfall and Sentinel-2, Local DEM (10m × 10m) with in-situ or SREs rainfall and LandSat-8, SRTM (30m × 30m) with in-situ or SREs rainfall and Sentinel-2, and SRTM (30m × 30m) with in-situ or SREs rainfall and LandSat-8. The Local DEM (10m × 10m) with in-situ rainfall and Sentinel-2 served as a reference case because it showed high performance for the first run compared to the other models developed. The preliminary effect assessment of different data sources showed that the LULC map from Sentinel-2 provided a more detailed land cover type than LandSat-8. For DEMs, the Local DEM 10m × 10m provided more detailed topographic information and stream network delineation, and low volume-water storage compared to the SRTM DEM 30m×30m, which contributed to better runoff simulation and model performance within the Nyabarongo catchment area. The analysis of both in-situ and SRE products showed that CHIRPS and GPM-IMERG overestimated the in-situ rainfall, and CMORPH underestimated it. The effects of data sources on model performance, the HEC-HMS model that used high-resolution data of the Local DEM 10m × 10m, Sentinel-2 LULC map, and in-situ rainfall outperformed other model developed, achieving a Nash-Sutcliffe Efficient (NSE) of 0.89, and Relative Volume Error (RVE) of 2.9%. The study also evaluated and corrected errors in SREs, finding that the Power Transform (PT) bias correction technique was the most effective in reducing errors compared to other techniques (Time Space variant and Distribution Transformation). Additionally, the study assessed different time window sizes for bias correction using a Sequential Window approach and showed that a 7-day window is most effective. Furthermore, the effects of error propagation from these data sources on streamflow simulations were analysed. The uncorrected SREs showed an increase in error. However, applying bias correction effectively reduced these errors. Finally, a runoff coefficient evaluation showed that the highest coefficients occurred with the model using the Local DEM, Sentinel-2 LULC, and in-situ rainfall data, as well as the corrected SREs with the Power Transform.

Keywords: Remote sensing data, Rainfall-runoff modelling, Nyabarongo catchment, HEC-HMS, SREs, LULC, Digital Elevation Model, In-situ data, bias correction techniques.

ACKNOWLEDGEMENTS

TABLE OF CONTENTS

LIST OF FIGURES

LIST OF TABLES

1. INTRODUCTION

1.1.   Background

Hydrologic modelling provides essential information for environmental planning, water resource management and flood risk assessment (Chalkias et al., 2016). The quality and sources of the remote sensing input data, such as Land Use Land Cover, Digital Elevation Model, Soil types, and rainfall products, have a significant impact on the performance of the model, particularly the HEC-HMS model (Santos et al., 2022). In areas with inadequate and poor in-situ data, remote sensing data can serve as the origin of data for rainfall-runoff modelling (Mushore et al., 2019). This study focused on evaluating the effect of various input data sources on the performance of the HEC-HMS model in the Nyabarongo catchment area.

Remote sensing data provide spatially distributed observations, allowing the building of both simple and more complicated models, which are important for rainfall-runoff modelling (Khan et al., 2011). Predicting rainfall-runoff processes in the Nyabarongo catchment area is difficult because of the spatial distribution and variations in rainfall and discharge records (Manyifika, 2015). Due to its broad spatial coverage and temporal frequency, remote sensing data are often assumed to overcome the limitations of in situ data; however, remote sensing data may be inaccurate and even be of poor quality. As such, the use of remote sensing data may result in very different model performance depending on the quality of the data.

For modelling hydrological processes, the applying of remote sensing data, such as Digital Elevation Models and LULC data, provides essential information on the topography and land cover needed by the model. Sentinel-2 and LandSat-8 LULC images provide high-resolution maps that help in differentiating between various land use types, which have an immediate impact on evapotranspiration and runoff processes (Ahn et al., 2014). These high-resolution maps enable detailed mapping and capture of the landscape, which is essential for understanding the spatial distribution of different land use types and how they affect rainfall runoff responses (Koneti et al., 2018). Therefore, the simulation of surface runoff for rainfall-runoff models may be greatly impacted by LULC data. For instance, compared with urban or built-up areas, which are defined by impermeable surfaces that cause increased runoff and less infiltration, forested areas often have higher infiltration rates and lower surface runoff (Manyifika, 2015). Precise land use cover data (LULC) ensures improved model performance as land cover affects hydrological processes. In contrast, DEM is essential for catchment delineation and stream network analysis (Rocha et al., 2020). It provides the topographic information necessary to define and identify the boundaries and flow paths of runoff within a watershed (Moges et al., 2023a). The resolution of a DEM directly affects the capacity of model

performance to simulate runoff processes, such as overland flow, flow within channel, and the movement of water through the surface (Roostaee & Deng, 2020).

Soil properties, particularly texture and hydraulic conductivity, significantly affect infiltration and surface runoff (Trinh et al., 2018). Using precise soil data can improve the performance of hydrological models (Trinh et al.2018). The soil properties, such as structure, texture, and hydraulic conductivity, may be provided by the FAO Digital Soil Map of the World, which are necessary to accurately simulate soil-water interactions in rainfall-runoff models. Therefore, the soil data helps to capture the spatial variation in soil characteristics across the catchment, which affects the performance of the hydrologic model. However, the impact of soil data on the model performance can vary. Loague (1992) found that using soil texture data to estimate hydraulic conductivity can reduce model performance, whereas Lannoy (2014) reported significant improvements in a land surface model's simulation of soil moisture and hydrological flows when using new soil texture data. Van Tol (2020) and Trinh (2018) demonstrated the role of detailed soil data in rainfall runoff modelling, showing that more detailed soil data can improve simulation efficiency.

The temporal and spatial coverage offered by Satellite Rainfall Estimates (SREs) is particularly helpful in areas where ground-based rainfall observations are insufficient (Belayneh et al., 2020). These estimations provide a high-resolution alternative to traditional in situ measurements because they are obtained from remote sensing data. The SRE products are not free from errors that can be random or systematic by nature; thus, before applying them to rainfall-runoff modelling, rigorous evaluation and error correction are required (Belayneh et al., 2020). It is essential to evaluate these satellite data for hydrological modelling, specifically in the Nyabarongo catchment area, which varies with different land cover, topography, and climate, and with frequent and extreme floods where hydrological stations and rain gauges are scarce (REMA, 2019).

Hydrologic models, especially the HEC-HMS model, may be applied as lumped or semi-distributed models to simulate hydrological processes and rely mainly on rainfall, the Digital Elevation Model, curve number grid, and runoff time series as input data. The HEC-HMS model has been applied in numerous researches to simulate hydrological processes within a watershed. For instance, Asadi (2013) showed that the semi-distributed model was more effective than the lumped model in simulating the peak runoff discharge and total runoff volume. Similarly, Tibangayuka (2022) and Mind'je (2021) confirmed the high performance of the HEC-HMS model in simulating streamflow, peak flow, and volume. The HEC-HMS model requires in situ data such as discharge and rainfall measurements for calibration and validation purposes. These data provide a ground-truth reference that helps adjust model parameters to improve the performance of the objective function selected by research (Asadi & Boustani, 2013).

1.2.   Problem statement

Rainfall-runoff modelling frequently suffers from inaccuracies due to errors in the input data, which include both in-situ and remote sensing sources. This issue is particularly evident in the Nyabarongo catchment area in Rwanda. Previous studies, such as Manyifika (2015) and Huang (2018), have used satellite and in-situ data to model urban floods and inflow discharges within the Nyabarongo catchment area, highlighting the significant impact of data quality on the model performance for streamflow simulations. Sendama (2015) further assessed satellite data products, such as TRMM, RFE, and CMORPH, for streamflow modelling using the HBV-light model in the Nyabarongo catchment area. The findings indicated that rainfall was typically less estimated by satellite rainfall products before error correction, and showed good performance of the model when these errors were fixed.

These studies have identified the critical issues of data availability and quality. Manyifica (2015) noted the scarcity and poor quality of rainfall and hydrological data, suggesting the integration of remote sensing products to address this issue for rainfall-runoff modelling. Huang (2018) identified gaps in in-situ data coverage and the low density of rain gauges, which limit the reliability and performance of rainfall-runoff models. This study proposed the adoption of advanced data techniques, including satellite-based data, to solve the identified issue. Sendama pointed out the challenges of limited and unreliable hydrological data, suggesting that future studies should apply and evaluate remote sensing data to improve the model performance in other parts of the Nyabarongo catchment.

Recent studies in Rwanda by Ntawukuriryayo (2022) showed that the error and uncertainty in model input data should be addressed by using and evaluating SRE rainfall products. By integrating various remote sensing products, such as SREs, Land Use Land Cover (LULC) data, Digital Elevation Models (DEMs), and soil data, it is possible to address the limitations of ground-based measurements. These data sources can enhance and affect the performance of hydrologic models differently, particularly in areas with sparse in-situ data, such as the Nyabarongo catchment area. Assessment of the effectiveness of these remote sensing data sources, particularly through error correction, propagation, and comparison with in-situ data as a reference, is essential for improving model performance and reliability However, the selection of data sources and model combinations must be carefully considered, as different datasets can significantly affect model outcomes (Elaji & Ji, 2020).

1.3. Research objectives

1.3.1. Global objective

The main objective of this study is to assess how remote sensing data affect the performance of rainfall-runoff modelling in the Nyabarongo catchment area.

1.3.2. Specific objectives

The specific objectives of this study are as follows:

1. To develop a semi-distributed HEC-HMS rainfall-runoff model for the Nyabarongo catchment area.
2. To assess and compare the performance of the semi-distributed HEC-HMS rainfall-runoff model by applying SRE products and in situ rainfall data, as well as analyzing the effects of various data sources such as Land Use Land Cover and Digital Elevation Model on the performance of the model.
3. To evaluate the accuracy and perform bias correction for the CHIRPS, CMORPH, and GPM-IMERG satellite rainfall products in the Nyabarongo catchment area.
4. To assess how errors in different data source sets affect the error in streamflow simulation with a semi-distributed HEC HMS model.
5. To assess the changes in runoff coefficient resulting from the application of remote sensing data (SREs, DEMs, LULC) and in situ rainfall data in the Nyabrongo catchment area.

1.4. Research questions

This study addressed the following questions that align with the previously stated objectives:

1. What is the ability of a semi-distributed HEC-HMS model to simulate rainfall-runoff processes in the Nyabarongo catchment area?
2. To what performance level does the semi-distributed HEC-HMS rainfall-runoff model use various remote sensing data and in-situ rainfall data as a benchmark?
3. How accurate are bias-corrected and uncorrected CHIRPS, CMORPH, and GPM-IMERG satellite rainfall products for estimating rainfall in the Nyabarongo catchment area?
4. What are the most effective bias correction techniques for satellite rainfall products, and the extent to which bias correction improves accuracy?
5. How does error propagation in various data sources affect the accuracy of streamflow simulations using a semi-distributed HEC-HMS model?
6. How does the use of satellite data (SREs, DEMs, and LULC) affect the catchment runoff coefficient compared with in-situ rainfall data as a reference in the Nyabarongo catchment?

1.5.   Research structure

The conceptual framework of this study includes the following essential components. The first chapter discusses the study background, problem statements, objectives, and questions. The next chapter details the relevant literature. The third chapter describes the study area, including the datasets, and how they were preprocessed. The fourth chapter focuses on the research methodology. The fifth chapter covers the research findings and provides a thorough discussion. Finally, the sixth chapter concludes and summarizes the findings, suggests recommendations, and acknowledges the limitations of this study.

2.   LITERATURE REVIEW

2.1.   Hydrologic modeling

Rainfall-runoff models are designed to simulate the movement, distribution, and quality of water in the real world (Islam, 2011). Rientjes (2016) describes different model approaches. The descriptions are adopted below and are sometimes paraphrased. Models are simplified representations of real-world phenomena using mathematical formulations, and consider catchment, meteorological, and boundary conditions. Hydrologic models are grouped into three types, including empirical, conceptual, and physically based models, with each varying in complexity and level of detail in representing hydrological processes (Devia et al., 2015). Hydrologic models are categorized depending on their input, structure, and parameters as well as the application of physical concepts, and they can be lumped, semi-distributed, or fully distributed (all adopted from Rientjes, 2016).

The lumped models consider the catchment as a single entity, where the input data and outputs are averaged over the entire area, and this simplification makes lumped models computationally efficient. The semi-distributed models divide the catchment into different sub-catchments based on terrain, which are considered as single units during computation. The semi-distributed approach is more detailed than lumped models but requires more data and computational resources (Knudsen et al., 1986). The fully distributed models discretize the catchment into fine grids, where each cell is individually modeled. These are most detailed and allow a full representation of spatial variations in rainfall, topography, soil moisture, and other factors within the catchment, but they significantly cost data requirements and computational time (Godara, 2019).

Rainfall-runoff models include WeSpa, HBV, HEC-HMS, SWAT, and MIKE SHE exists, and the application of these models is highly dependent on their purpose, with some used for research and others for decision-making (Moradkhani & Sorooshian, 2009). These models require calibration to improve their performance in simulating real-world processes (Rientjes 2016). Model performance evaluation is an important aspect of hydrologic modeling, as it contributes to the accuracy and reliability of the model simulation. The validation, on the other hand, tests the model's prediction or simulation capability using a different dataset than that used for the calibration (Morrison et al.2013).

Hydrologic models require input data, including in-situ data, such as rainfall and discharge data; remote sensing data, such as Digital Elevation Models (DEMs), which provide detailed topographic information; and Land Use and Land Cover (LULC) data, SRE products, and soil data. These data sources are essential for understanding and modeling water movement and distribution because they provide the necessary information on the terrain and land surface characteristics that influence rainfall-runoff processes. The

HEC- HMS semi-distributed model was selected and applied in this research because of its ability to manage complex hydrological conditions efficiently, despite that the model concept is relatively simple. It has been shown in research carried out in the Upper Blue Nile River Basin to provide reliable and accurate predictions under various conditions, which is crucial for the Nyabarongo area with complex water systems (Gebre, 2015). Furthermore, the model has demonstrated good performance in analyzing its applicability and hydrological simulation in the Abbay River, making it a suitable choice for the Nyabarongo watershed (Zelelew & Melesse, 2018).

2.2.   Satellite rainfall

2.2.1.   Infrared-based approaches

Infrared-based techniques use IR band sensors on board of geostationary satellites. These sensors are crucial for determining the rainfall intensity by observing various stages of cloud formation (Amorati et al., 2000). Approaches based on infrared imaging, as well as algorithms that consider seasonal changes, regional variations, and cloud-top temperatures, help in precipitation estimation (Dold, 2016). These techniques are based on the idea that colder, higher-altitude clouds are more likely to precipitate, though it should be emphasized that not all cold clouds, such as high cirrus clouds, produce rainfall (Amorati et al., 2000). Although infrared technologies can detect rainfall, they are less precise in determining its depth (D'souza et al., 1990).

2.2.2. Microwave-based approaches

Microwave (MW)-based approaches for estimating rainfall use the properties of MW radiation to directly observe precipitation, unlike visible or infrared techniques, which can be masked by clouds (Aonashi & Ferraro, 2020). This approach, based on Planck's radiation law, detects precipitation particles by analysing the microwave energy that is emitted or scattered (Kidd et al., 2003). To provide detailed precipitation data, the position of MW sensors on low-Earth orbit satellites results in less frequent and limited coverage compared to geostationary satellites (Levizzani et al., 2007).

2.2.3. Integrating Microwave and Infrared Techniques

Integrated Microwave and Infrared techniques offer unique ways to estimate rainfall, each with its own strengths and weaknesses. Thermal Infrared (IR) approaches are appreciated for their simplicity and the ability to provide data around the clock. However, they are not perfect (Marzano et al., 2004) and one of the main issues at the time with IR techniques was that they tend to estimate rainfall amounts that are extremely high. Additionally, there is usually a delay when they try to measure rainfall, meaning that what they report has already happened a bit ago, making them less reliable for real-time observations. On the other hand, microwave (MV) approaches offer a different approach to estimating rainfall. These methods

are known to provide estimates with less frequent updates, which means that they might not capture every change in rainfall intensity as quickly as desired. Despite this, MW techniques have a crucial advantage in that they offer direct insights into cloud and rainfall characteristics, which can lead to more accurate rainfall estimates (Feudale & Manzato, 2014).

To overcome the inherent limitations of using either IR or MW techniques alone, a blending approach has been developed. This innovative method combines data from both IR and MW satellite sensors. By doing this, it benefits from the frequent updates available from IR images and more accurate and direct measurements of rainfall from MW images. This blend leads to a more reliable and timely estimation of the rainfall. Notable SREs such as TRMM 3B42, CMORPH, and RFE apply this blended approach. They used the precision of MW sensors to refine and improve the estimates derived from the IR temperatures of geostationary satellites, ensuring accurate rainfall measurements (Feudale & Manzato, 2014).

2.2.4. SRE products

Inaccurate precipitation data may result in poor simulation outcomes, leading to incorrect conclusions regarding hydrological processes in the catchment (Vrugt et al., 2005). For instance, precise estimations of rainfall can be obtained from in-situ measurements that rely on the use of rain gauges (Brocca et al., 2019). Haile et al. (2009) indicate that local topography, hill slope and convergence, terrain elevation, and slope gradient are some examples of aspects that could affect the variations in rainfall. To improve rainfall representation in space and time, in situ rainfall observations can be integrated with rainfall measured by satellites (Lanza & Vuerich, 2009). Therefore, accurate in situ and SRE data are also pertinent.

Satellite rainfall products, including TRMM-3B427, CHIRPS, CMORPH, and GPM-IMERG, have been used in various hydrometeorological applications (Stisen & Sandholt, 2010). For instance, the CMORPH was most effective in streamflow simulation among four SRE products evaluated using a fully distributed rainfall runoff model (Bitew & Gebremichael, 2011), and the daily CHIRPS SRE was more effective and reliable as input data for rainfall-runoff modelling (Guermazi et al., 2019). The GPM SRE product offered high-resolution and showed good performance for daily rainfall estimation and detecting precipitation events in mountain high-slope areas characterized by significant variations in rainfall patterns and often inadequate coverage of rain gauges, which are usually scattered and irregularly spaced (C. Zhang et al., 2018). Hussein (2023) compared in situ rainfall data to GPM-IMERG and CHIRPS and confirmed that the HEC-HMS model performed well with both products (Hussein & Baylar, 2023). Brocca et al. (2013) reported that daily SRE products showed good results for the performance of rainfall-runoff modelling in areas with poor or no in situ rainfall data, but most studies indicate large estimations of errors. Belayneh et al. (2020) indicates that both TMPA-3B42v7 and CHIRPS satellite data performed well and can be useful for providing good rainfall data for hydrologic modelling. Moreover, because of their high accuracy and temporal and spatial

resolutions, SREs such as CMORPH, GPM-IMERG, TRMM, and PERSIANN, have become more applicable for large-scale rainfall-runoff models (Stisen & Sandholt, 2010).

The accuracy of satellite rainfall estimates varies based on satellite type, data processing algorithms, and geographical location (Bitew & Gebremichael, 2011). According to previous studies, estimates are more reliable on land than on water and can be influenced by the presence of mountains and variable topography (Zambrano-Bigiarini et al., 2016). To overcome these problems, techniques such as the Global Precipitation Measurement (GPM) mission's Integrated Multi-satellite Retrievals for GPM (IMERG), have been developed, resulting in increased precipitation detection and measurement accuracy under different conditions (Meng et al., 2021).

2.2.5. SREs bias correction

Satellite Rainfall Estimates (SREs) can have inaccuracies due to random and systematic errors, which may result in incorrect simulation outcomes when applied (Gumindoga et al., 2017). To correct for these errors, a technique called bias correction must be used prior to their application to reduce errors in SREs. The goal of applying bias-correction techniques is to improve the precision of SREs for the desired application.
Various methods have been investigated. For instance, Gumindoga et al. (2019) assessed five bias correction techniques. These techniques are Spatio-Temporal (STB), Elevation Zone (EZ), Power Transform (PT), Distribution Transformation (DT), and Quantile Mapping using empirical distribution (QME) algorithms on the CMORPH SRE product. The findings showed that the STB and EZ approaches were significantly more effective than the other approaches. Similarly, Habib et al. (2014) evaluated three versions of the STB techniques such as time-space variable (TSV), time variable (TV), and time-space fixed (TSF), and confirmed that the TSV technique reduced bias in the CMORPH SRE product.

Satellite rainfall estimations are essential for flood forecasting, agricultural planning, and drought monitoring. Despite their advantages, satellite rainfall estimates have limitations, particularly in terms of ground validation and under or overestimation of the rainfall intensity (Amekudzi et al., 2016). The challenge of validating satellite data with ground observations remains critical, as differences can arise owing to differences in spatial and temporal resolution between satellite measurements and ground-based sensors (Amekudzi et al., 2016).

2.3.   Land Use Land Cover, and soil data for rainfall-runoff modeling

Soil properties and LULC are crucial for hydrological analysis and have a significant impact on the interaction between rainfall and runoff in a watershed (Chow et al., 1988). Land cover features have a direct effect on water infiltration, storage, and runoff (Babaremu, 2024), and the relationship between LULC and hydrological processes is a well-established concept in environmental studiesClick or tap here to enter text.. Several types of land cover, such as urban areas, forests, and farmlands, respond to rainfall in different ways to determine the amount of water flowing into rivers and seeps into the ground (Afonso de Oliveira Serrão et al., 2022); (Zhou, 2020). This relationship is essential for understanding and predicting the movement of water within a catchment, where varied land use impacts water resources (Babaremu, 2024).

Soil characteristics influence water infiltration, retention, and discharge within a watershed and are important when studying hydrological processes (Chow et al., 1988). The capacity of different soil types to retain and absorb water varied. Soil properties such as texture, porosity, and organic matter content significantly affect hydrological processes. These characteristics determine the ability of the soil to absorb water, thereby influencing groundwater recharge and surface runoff patterns (McCauley et al., 2005). For example, sandy soils with high porosity allow for more water infiltration and minimize surface runoff, whereas clay-based soils with low porosity cause more runoff because of the reduced infiltration rate (J.Herben Huddleston, 1996). Soil and LULC maps were used to create a curve number grid that served as the input for the HEC-HMS semi-distributed model.

Remote sensing technology, using satellites such as Landsat-8 and Sentinel-2, is a helpful tool for monitoring and mapping LULC and soil properties across large areas and over time (Nasiri et al., 2022). These satellites capture high-resolution images that can be used to accurately and consistently identify changes in land cover. This aspect is particularly useful in areas where ground-based inspection of LULC change detection is difficult or impractical. The apply of remote sensing data for LULC analysis enables an understanding of how land changes affect hydrological processes and, as a result, rainfall-runoff modelling (Govender et al., 2022).

Furthermore, digital soil maps, such as the Digital Soil Map of the World sourced from the FAO, provide detailed information about the soil characteristics in various landscapes (Sanchez et al., 2009). When combined with remote sensing data, these maps provide a thorough overview of the physical and chemical properties of the soil at different depths (Richer-de-Forges et al., 2023). This integrated approach improves the accuracy of hydrological models by combining spatially detailed data from both the land surface and soil profiles. As a result of this research, a model that incorporates detailed LULC and soil data from remote sensing and digital soil maps is better able to predict the dynamics of rainfall-runoff processes in the Nyabarongo catchment area, which is critical for successful water resource management and planning.

2.4.   Topographic data for rainfall-runoff modeling

Topographic data sources are important in hydrologic modeling because they offer complete details of the physical characteristics of the terrain (Vaze & Teng, 2007). They provide full elevation and terrain features for the study area, which are required to simulate runoff processes. This information is critical for understanding how water moves across landscapes, which influences rainfall-runoff processes and model performance (Lee et al., 2009). According to previous studies, high-resolution topographic data can considerably improve the performance of hydrological models (Ma et al., 2016). This is because a finer spatial resolution provides more detailed representations of topographical features, which are essential for calculating water flow patterns and accumulation areas. Topographic data can often be generated from remote sensing sources, such as Digital Elevation Models (DEM) and the Shuttle Radar Topography Mission (SRTM), which provide crucial information about the physical characteristics of the land surface (Smith & Sandwell, 2003). The elevation and slope obtained from DEM and SRTM are essential for determining the direction and speed of surface water flow, both of which are important components in modeling rainfall-runoff dynamics.

3. STUDY AREA, DATA ACQUISITION AND PROCESSING

3.1. Study area description

The focus of this research was the Nyabarongo catchment, as shown in Figure 1, which is located between -1.962584° 'S and 30. 003816° 'E and occupies a total area of 8,876.42 Km². The catchment serves various activities, such as agricultural irrigation, settlement, hydropower production, water treatment plants and supply, groundwater recharge, and as a habitat for biodiversity. The mean yearly precipitation of the catchment varies from 992 to 1,128 mm and it is defined as a moderate tropical climate. In this catchment, the annual evapotranspiration varies from 503 to 1,050 mm, and the catchment average temperature changes between 17°C and 20°C. The catchment has two major rainy seasons: one from March to early May and the other from late September to late December. The mean elevation is 1,342 m above sea level in the catchment, and it can reach approximately 4,480 m above sea level in the northern area (RoR, 2018).
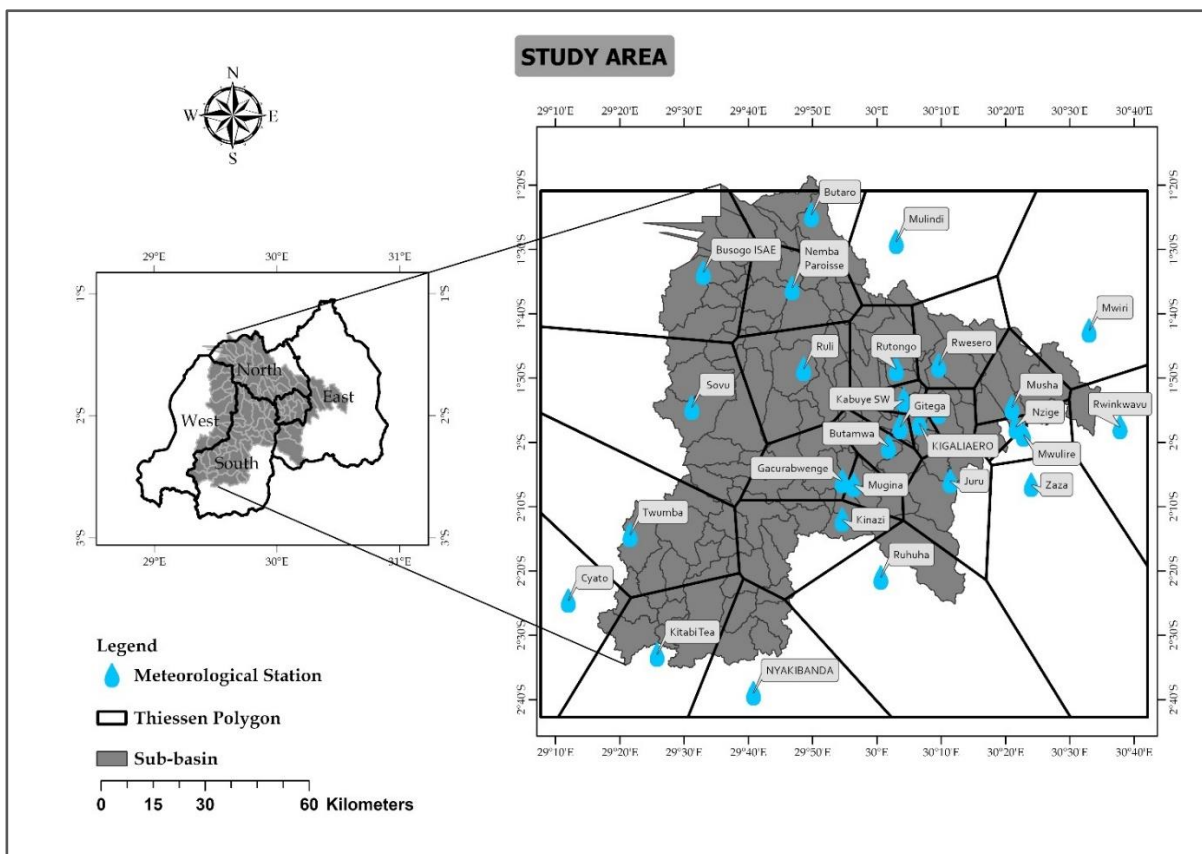
Figure 1: Location map of the study area

3.2.   Data acquisition

The Nyabarongo catchment has suffered flooding in recent years; however, local in-situ data recording are limited, mostly for measuring water streamflow. This study intends to assess how remote sensing data can affect the performance of hydrologic modeling in the catchment. Therefore, various data, including in-situ rainfall data, satellite-based precipitation products, river discharge data, LULC and soil characteristics data, and topographic data, were used to accomplish this research, as summarized in Table 1.

Table 1: Datasets used in the research

Data category	Dataset	Spatial resolution	Temporal resolution	Source of data	Role of dataset
Meteorological data	Rainfall	gauge	Daily	Rwanda Meteorology Agency	Model input
Hydrological data	Stage and discharge	gauge	Daily	Rwanda Water Board	Model calibration and validation
Topographic data	DEM	10m×10m	-	Rwanda National Land Authority	Terrain model processing
	SRTM	30m×30m	-	Earth data(nasa.gov), USGS Earth Explorer	Terrain model processing
LULC	Sentinel-2	10m×10m	-	USGS Earth Explorer	To create a curve number grid for model input
	Landsat-8	30m×30m	-	USGS Earth Explorer	
Soil type		-	-	FAO/USDA	Soil classification
Satellites rainfall Data	CHIRPS	5Km×5Km	Daily	http://chg.geog.ucsb.edu/data/ chirps/ or CHG, USGs	Model input
	GPM-IMERG	10Km×10Km	Daily	NASA GPM Data Access	Model input
	CMORPH	8Km×8Km	Daily	https://CMORPH CDR/National Centers for Environmental (NCEI) (noaa.gov) or ftp://ftp.cpc.ncep.n oaa.gov/precip/	Model input

3.2.1.   Rainfall data

This study used in-situ and SRE products. The in-situ rainfall data were provided by the Rwanda Meteorological Agency, which covered precipitation values from 2016 to 2020. This dataset served as the basis for the analysis, allowing us to assess the detailed patterns of rainfall throughout the study area after processing. Three satellite rainfall products were evaluated: CMORPH, GPM-IMERG, and CHIRPS.

Furthermore, the intended time window for these SRE products was from 2016 to 2020. Daily time series were used for all in situ rainfall data and SRE products.

3.2.2.   In situ streamflow data

In Rwanda, pressure sensors, radar, float-operated shaft encoders, staff gauges, and other devices are used to measure and record the water level. On the other hand, dilution gauging, radar point velocity meters, acoustic Doppler current profilers, and mechanical current meters are used to measure river flow, which is also referred to as streamflow discharge (RoR, 2018). Acquiring reliable streamflow time-series data is important for calibrating and validating hydrologic models. Data on the water level of the Nyabarongo River were obtained from the Rwanda Water Board for use in this study, with a special focus on Rwinzoka station as the catchment outlet.

3.2.3.   Topographic data

The Digital Elevation Model (DEM) is crucial for hydrologic modelling. It provides full elevation and topographical data for the study area, which are required for guiding the runoff process simulation. The study area is divided into smaller cells using a mesh or grid created from this DEM, and each cell has its elevation value, which originates from the Digital Elevation Model (Adugna, 2021). Different techniques can be applied to generate Digital Elevation models (DEMs), such as Mesa-Mingorance and Aiza-Lopez (2020) explained. LIDAR, photogrammetry, interferometry, and topographic surveys are examples of these techniques. In this study, two Digital Elevation Models (DEMs), including a local DEM with a spatial resolution of 10m × 10m from the Rwanda National Land Authority and SRTM data with a spatial resolution of 30m × 30m, were applied and evaluated.

3.2.4.   Soil type, Land Use, and Land Cover data

Soil type has effect on the interaction between rainfall and runoff in a catchment (Chow et al., 1988). They are required to define curve number values at pixel level that is an input to the HEC-HMS model (see Section 4.4). The surface characteristics of the area can change because of LULC changes such as urbanization or deforestation, and both the quantity of rainfall that becomes surface runoff and the amount that penetrates the ground are affected by these changes (Afonso de Oliveira Serrão et al., 2022). For example, the natural capacity of vegetation to intercept and absorb rainfall decreases when forests are converted to urban areas or agricultural land. The increased surface runoff frequently causes erosion and flooding. To effectively predict the effects on runoff amounts and patterns, rainfall-runoff models consider these LULC changes (Guide & Manual, 2008). Two sets of Land Use and Land Cover (LULC) data, one from the Sentinel-2 satellite and one from the Landsat-8 satellite were processed and used in this study.

In addition, soil characteristics influence water infiltration, retention, and discharge within a catchment, and are important when studying hydrological processes (Chow et al., 1988). For example, the ability of different soil types to hold and absorb water varies. Chow et al. (1988) reported that clay soils have different rainfall patterns because of their fine particle structure and high water-retention capacity, in contrast to sandy soils, which have larger particles and lower water retention capacities. Accurately simulating the change in precipitation into runoff and ground penetration in various parts of the catchment depends on this variation (Guide and Manual, 2008). In this study, soil data were sourced from the Food and Agriculture Organization (FAO) Digital Soil Map of the World (DSMW).

3.3. Data processing

3.3.1. In-situ rainfall data

The Thiessen Polygon approach was used to represent the amount of rainfall for each sub-catchment station entering the entire catchment. Twenty-eight rain gauge stations, both inside and outside the study area, were selected for this study, as shown in Figure 2.

S/N	Station name	Longitude	Latitude
1	Kinazi	29.91	-2.2
2	Mugina	29.94	-2.11
3	Mwulire	30.38	-1.98
4	Gacurabwenge	29.91	-2.1
5	Juru	30.19	-2.1
6	Zaza	30.4	-2.11
7	Gitega	30.06	-1.96
8	Kabuye SW	30.07	-1.89
9	Rutongo	30.05	-1.81
10	KIGALI AERO	30.11	-1.95
11	Rubungo RAB	30.16	-1.92
12	Musha	30.35	-1.91
13	Rwesero	30.16	-1.8
14	Butamwa	30.03	-2.01
15	Nzige	30.36	-1.96
16	Cyato	29.2	-2.41
17	Kitabi Tea	29.43	-2.55
18	Nyakibanda	29.68	-2.65
19	Twumba	29.36	-2.24
20	Ruhuha	30.01	-2.35
21	Sovu	29.52	-1.91
22	Ruli	29.81	-1.81
23	Busogo ISAE	29.55	-1.56
24	Nemba Paroisse	29.78	-1.6
25	Butaro	29.83	-1.41
26	Mulindi	30.05	-1.48
27	Mwiri	30.55	-1.71
28	Rwinkwavu	30.63	-1.96

Figure 2: Location of selected meteorological stations

Manyifika (2015) described that the rainfall station's weight in a selected catchment was determined by dividing the effect of the Thiessen polygon by the desired catchment area. Equation 1 was used to determine the weighting:

$$\bar{P} = \frac{1}{A}\sum_{s=1}^{s=n}(A_s P_s)$$

<div style="text-align:right">Equation 1</div>

Where $\bar{P}$ represents the average rainfall and Ps represents the precipitation of the station. The intended catchment area is indicated by A, the impact area of the station within the intended catchment by As, and the number of precipitation stations affecting the target catchment by n.

Juru station incorrectly recorded two days of rainfall on May 6th and 7, 2018, with a rainfall of -9,999 mm. Similarly, Kigali Aero, Cyato, Kitabi Tea, Gacurabwenge, and Rwinkwavu stations also reported incorrect rainfall of -9,999mm for five days from May 6th to May 10th, 2018. The arithmetic mean approach was used to fill gaps in the precipitation data, as shown in Equation 2.

$$PX = \frac{1}{m}\sum_{i=1}^{m} Pi \qquad\qquad\qquad \text{Equation 2}$$

Where Px is the missing rainfall data, m represents the number of neighboring stations, and Pi is the rainfall recorded at the ith station.

After the precipitation data were gap-filled, the consistency of the data from each station was assessed. To verify this, a double mass curve analysis was conducted, and this method was calculated by comparing the cumulative daily precipitation at one station to the total accumulated daily precipitation at nearby stations, as shown in Figure 3 (Manyifika, 2015).
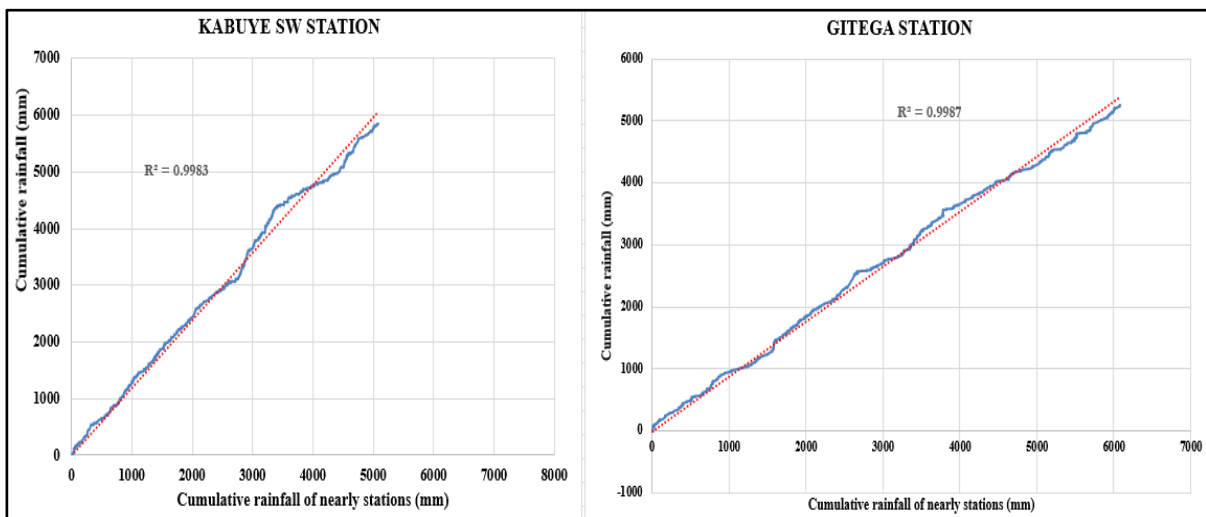
Figure 3: Example of double mass curve analysis of in-situ rain gauge stations

Figure 3 shows the cumulative rainfall data for the Kabuye SW station compared to nearby stations, while the right graph shows the same data for the Gitega station. Both graphs show good linearity, with R-squared values of 0.9983 for Kabuye SW and 0.9987 for Gitega. This high linear correlation indicates that the rainfall data from these stations are consistent with those of nearby stations, indicating that the recordings are reliable. All stations explained the consistent rainfall. The Rwinkwavu station consistently underestimated the daily rainfall compared to the other stations, whereas the Sovu station recorded significantly higher annual rainfall.

3.3.2. In-situ streamflow data

The rainfall-runoff model requires stream flow time series data for model calibration and validation. A stage-discharge relationship was developed using accessible field visit recordings of the water stage for the Rwinzoka station obtained from the Rwanda Water Board. Rwinzoka station is considered the river outlet location for the entire catchment. After the stage-discharge relationship, the obtained water level data were transformed into discharge flow using Equation 3, as explained by Manyifika (2015).
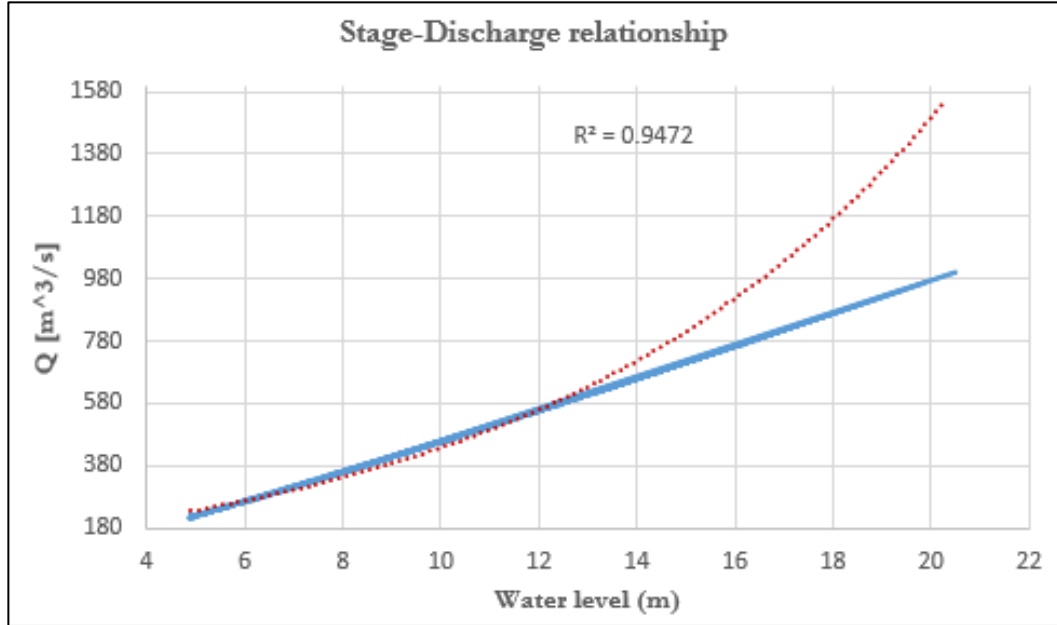
Figure 4: Stage-discharge relationship at outlet sink

$$Q = C * (h - a)^b \hspace{3cm} \text{Equation 3}$$

Where h represents the water level in meters, and Q represents the flow rate expressed in m³/s. The meaning of a is the water stage when there is no flow, C and b are calibrating constants, b is the logarithmic gradient of the rating curve, and C represents the flow rate at which the effective water flow depth (the sum of h and a) equals one. In Equation 3, Manyifika (2015) fully explained the processes used to determine the coefficients a, C, and b. Once the coefficients have been calculated, the relationship between the stage and discharge is estimated, as shown in Equation 4.

$$Q = 32.39817 * (h - 0.45)^{1.127994} \hspace{2cm} \text{Equation 4}$$

After deducing the stage-discharge relationship, it was essential to analyse the streamflow data from the outlet sink of the catchment to verify how the catchment responds to rainfall, as shown in Figure 5. Equations 5 and 6 were used to adjust the ratio values in the streamflow data to guarantee a steady or consistent streamflow for the outlet station, as well as to correct the recorded streamflow data (Goez, 2011).

$$\Delta P = P_t - P_{t-1} \text{ \& } \Delta Q = Q_t - Q_{t-1} \hspace{2cm} \text{Equation 5}$$

$$Ratio = \frac{|\Delta P|}{\Delta Q} \qquad \qquad \text{Equation 6}$$

Where ΔP represents the variations in precipitation and ΔQ represents the observed discharge. P_{t-1} and Q_{t-1}, respectively indicate the previous precipitation and streamflow of day. P_t and Q_t indicate the current rainfall and streamflow of the day, respectively.
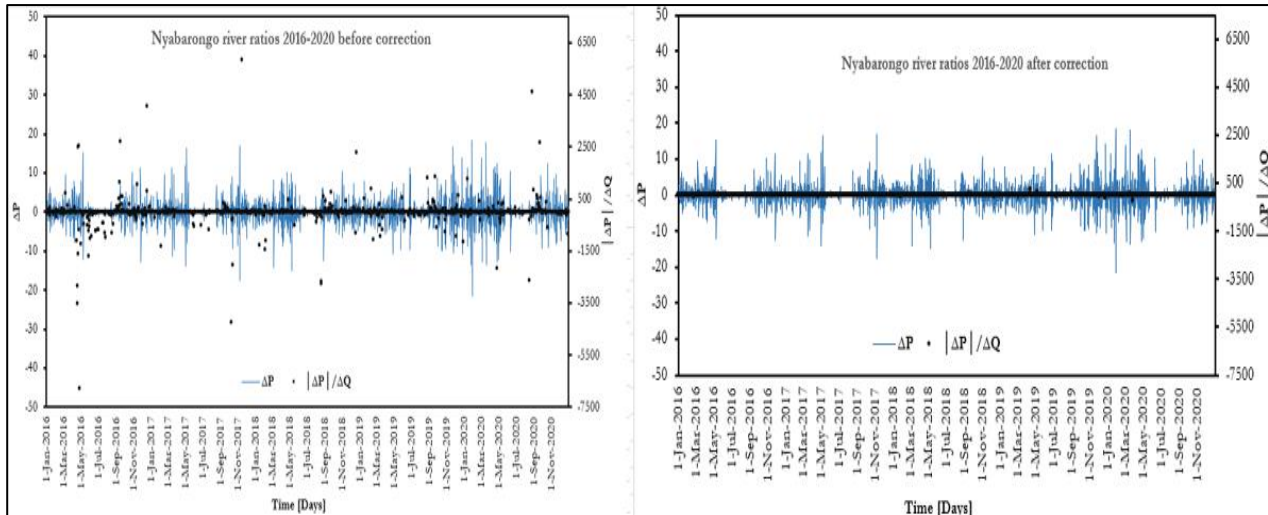
Figure 5: Nyabarongo River variation ratios 2016-2020 before and after discharge correction

Figure 5 shows the Nyabarongo streamflow variation ratios from 2016 to 2020 before and after discharge correction. The analysis focused on two main variables: ΔP (blue line) and the ratio $|\Delta P|/\Delta Q$ (black dots). ΔP represents precipitation changes, ΔQ represents the change in streamflow and $|\Delta P|/\Delta Q$ represents the ratio of absolute precipitation to streamflow. The plot shows a consistent relationship between precipitation variations and streamflow responses, with most of the $|\Delta P|/\Delta Q$ values falling between -450 and 450. Outliers (-7500-6500) indicate significant anomalies and indicate an error in observed P or Q. All ratios within the outlier values (-450 to 450 and -7500 to 6500) were adjusted and corrected within a range values of -10 and 10 to obtain the final discharge data used in this study, as shown in Figure 6.
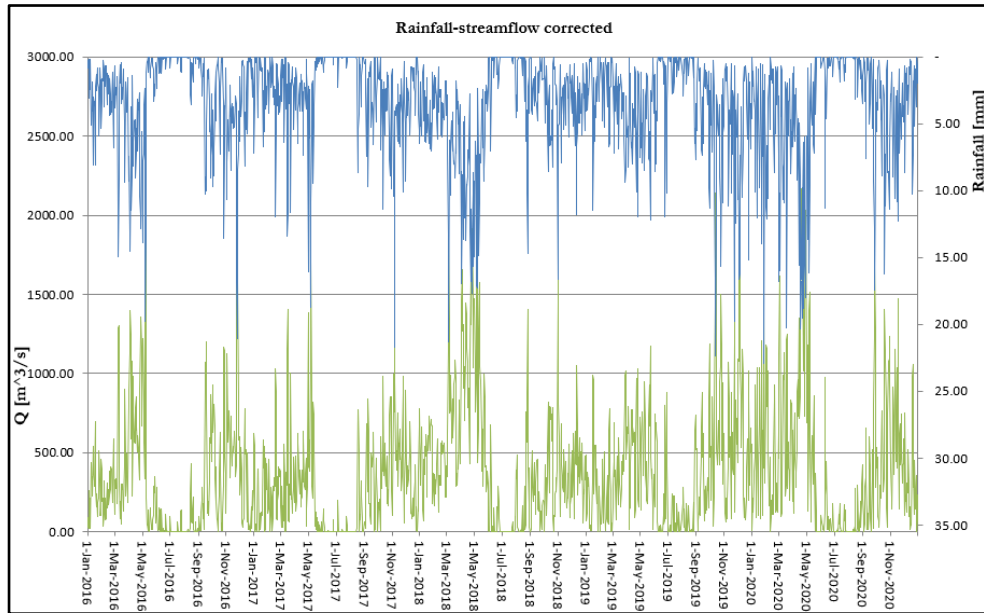
Figure 6: Nyabarongo River corrected streamflow

3.3.3.   Topographic data

Two different topographic datasets were used in this research, including a local DEM and SRTM of 10m ×
10m and 30m × 30m spatial resolutions, respectively. These datasets were harmonized to a spatial resolution
of 30m × 30m, ensuring that they aligned the analysis and consistency for semi-distributed HEC-HMS
rainfall-runoff. Furthermore, the bilinear interpolation method has been demonstrated to be more effective
than other methods, including nearest neighbour and bicubic resampling techniques, when applications
require a smoothing representation from fine to coarse resolution (Omondi, 2017). Bilinear interpolation
was adopted to harmonize the local DEM and SRTM data with a commonly selected spatial resolution of
30m × 30m.
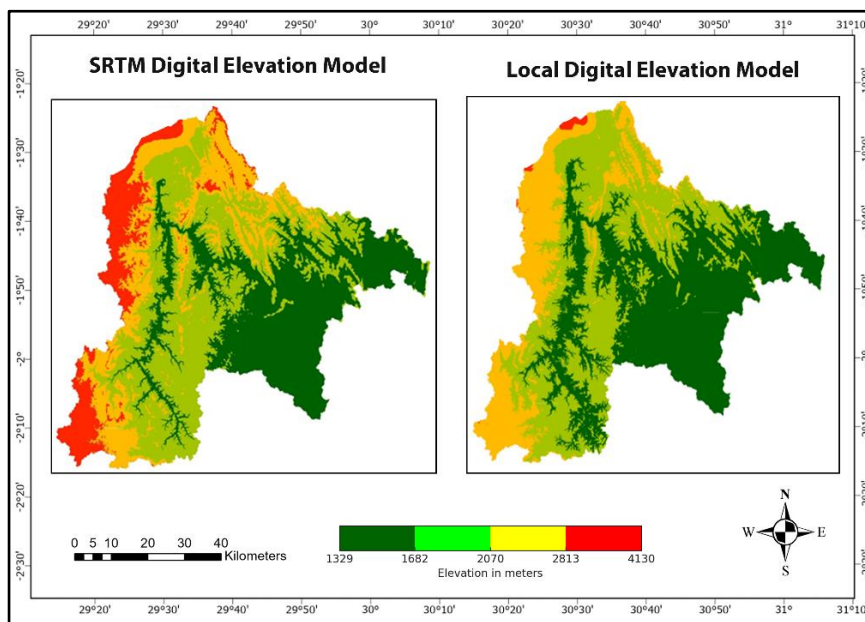
Figure 7: Topographic maps of Nyabarongo catchment (Local DEM-10m and SRTM-30m)

3.3.4.   Soil type, Land Use, and Land Cover data

3.3.4.1.   Soil type

In the Nyabarongo catchment area, accurate soil data are essential for the effective simulation of the rainfall-runoff model. The soil data used in this study were obtained from the FAO Digital Soil Map of the World (DSMW,2007). This map contains complete worldwide soil information, which is necessary to understand the soil characteristics of the research area. The soil map was carefully downloaded and processed to extract the area of interest of the Nyabarongo catchment area. The soil map was classified after extracting the study area. The method involves dividing the soil into different types based on its properties. The reclassification identified seven soil types in the Nyabarongo catchment including clay, loam, silty clay, clay loam, sandy clay, and sandy loam as shown in Figure 8. Each of these soil types has different characteristics that influence water infiltration and runoff, making them crucial for effective hydrological modelling.
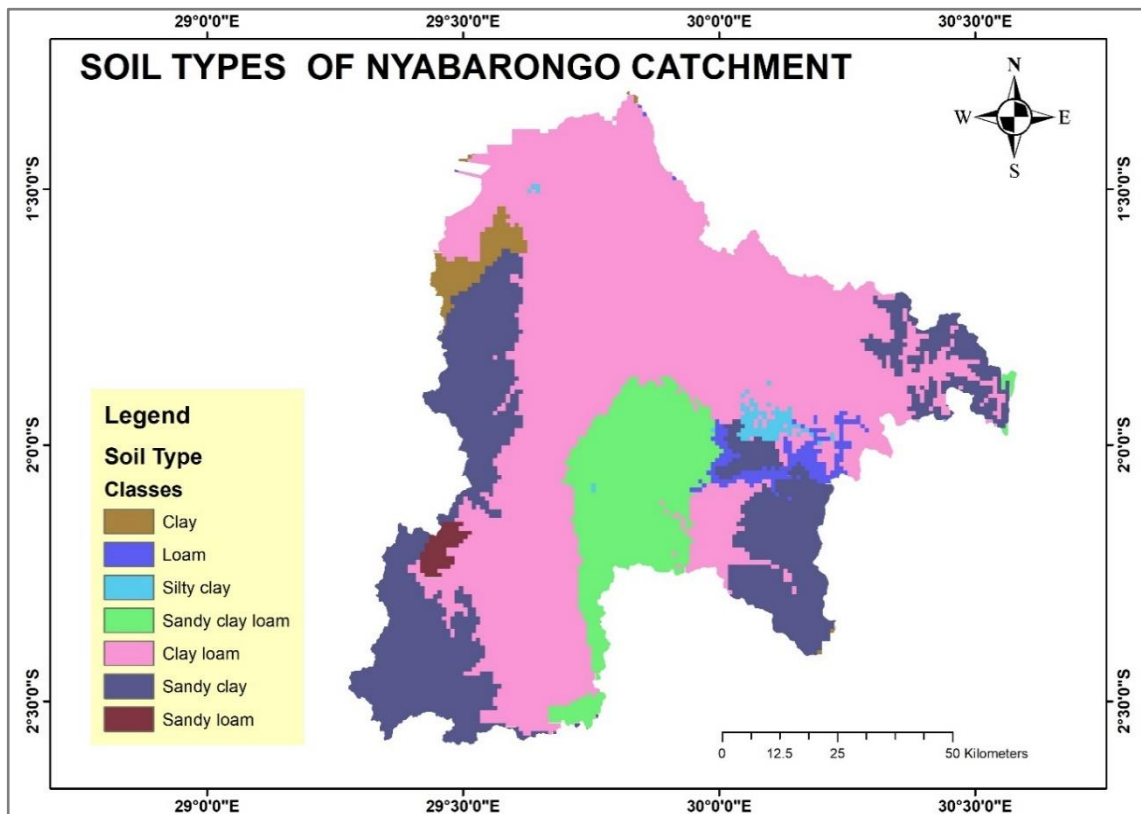
Figure 8: Soil map of the Nyabarongo catchment area

The reclassified soil map was then used to generate Curve Number (CN) grids, which were required for the HEC-HMS semi-distributed model in this study. CN values are essential for estimating runoff potential from various land use and soil combinations (Ara & Zakwan, 2018). These values were assigned to different land use and hydrologic soil group (HSG) classifications based on remote sensing data from Sentinel-2 and Landsat-8.

3.3.4.2. Land Use Land Cover from Sentinel-2 and LandSat-8

Land Use and Land Cover (LULC) maps are important for evaluating remote sensing data for hydrologic modeling. These LULC maps were created using maps from Sentinel-2 and Landsat 8 satellites. A Sentinel-2 map with a spatial resolution of 10m × 10m and a Landsat-8 map with a spatial resolution of 30m × 30m were extracted to generate useful data for the research area. LULC maps were downloaded using Google Earth Engine. After extraction of the Nyabarongo catchment area, the LULC maps were reclassified applying a supervised classification technique. The dataset was split among 70% training samples and 30% testing samples, with more than 50 samples to conduct classification.

The classification process found six main LULC classes, such as built-up areas, croplands, water bodies forests, grasslands, and bare land, as indicated in Figure 10. The final LULC map created using Sentinel-2 data had an overall accuracy of 78.8%, whereas the Landsat-8-derived map had an accuracy of 73.1%. These LULC maps, when combined with soil maps, were useful for generating the Curve Numbers (CN) grid, which was an essential input for the semi-distributed HEC-HMS model.
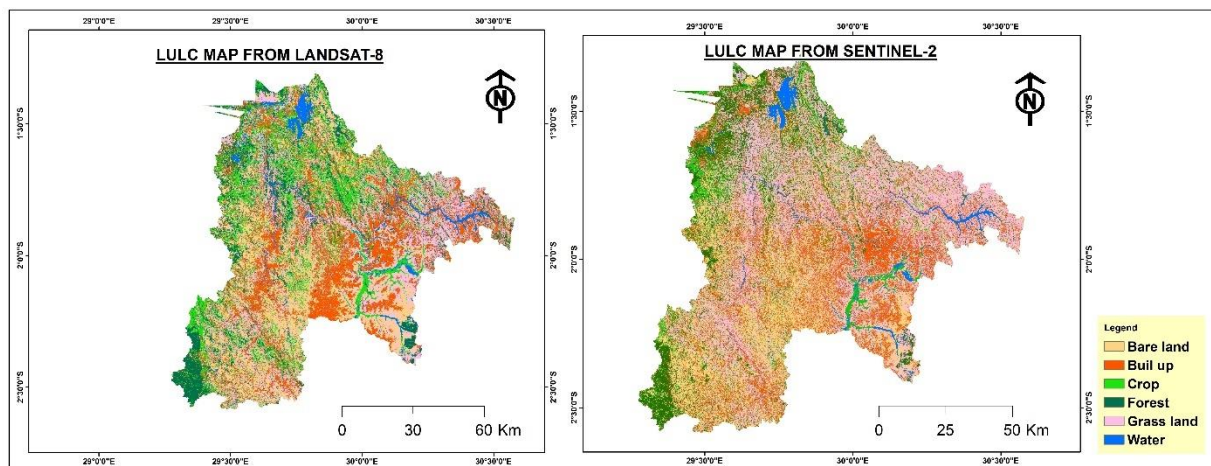
Figure 9: LULC maps of Nyabarongo catchment area (Sentinel-2 and LandSat-8)

3.3.5. SREs products

3.3.5.1. CMORPH

The CMORPH rainfall product was assessed from 2016 to 2020, using 28 meteorological stations located throughout the catchment area. CPC Morphing methodology (CMORPH) is an advanced precipitation estimation technique that generates high-resolution global precipitation datasets from passive microwave (PMW) and infrared (IR) data. The CMORPH covers latitudes ranging from 60°N to 60°S and provides data with a spatial precision of approximately 0.08° and a temporal resolution of 30min, allowing for a detailed investigation of rainfall patterns (Joyce et al., 2004).

The download and processing sequence for CMORPH data on a half-hour basis began with the CMORPH-8 km data from an FTP location (a specific server location where the CMORPH datasets are stored). The data were loaded into the ILWIS raster format and underwent initial processing, which included producing a 30-minute data maplist and mirror rotation. The next step was to subset the 30-minute images to the area of interest (AOI) and reproject them accordingly (WGS 84 datum applying UTM Zone 36S). These images were then mosaicked to provide hourly equivalents and aggregated into daily totals to match the temporal resolution required for comparison with ground-based gauge data. The result is the daily precipitation in millimeters per day, which was saved in a Microsoft Excel sheet for further analysis.

3.3.5.2. CHIRPS

For this product, time series data from the Climate Hazards Group InfraRed Precipitation with Stations (CHIRPS) were downloaded and processed for 28 meteorological stations within the catchment area from 2016 to 2020. The data, which are quasi-global and extend from 50°S to 50°N, were available using the FTP location of the Climate Hazards Group. The downloading process included obtaining daily rainfall data with a spatial precision of 0.05°, which were then organized and saved for further analysis. These high-resolution data were beneficial for capturing the variability and distribution of rainfall throughout the entire basin. CHIRPS data combine infrared Cold Cloud Duration (CCD) observations and in situ measurements to produce full precipitation estimates (Funk et al., 2015).

3.3.5.3. GPM-IMEWRG

NASA and JAXA developed the GPM-IMERG product, which offers daily worldwide precipitation estimates at a spatial resolution of 0.10°×0.10°. It uses data from numerous satellite sources including microwave and infrared sensors (Huffman et al., 2019). Downloading and processing GPM-IMERG data require numerous important stages to obtain accurate and relevant precipitation data. GPM-IMERG data from 28 meteorological stations in the catchment area between 2016 and 2020 were downloaded. These data were obtained from the NASA Earth data website, which provides access to GPM-IMERG datasets (Huffman et al., 2019). After downloading, the data files, which were often in the HDF5 format, were pre-processed to convert them to a usable format, such as NetCDF and CSV, for further analysis. Finally, data were extracted to match the specific coordinates and time ranges of the 28 meteorological stations.

The obtained data for the SREs were verified for consistency before their application, as shown in Figure 12.
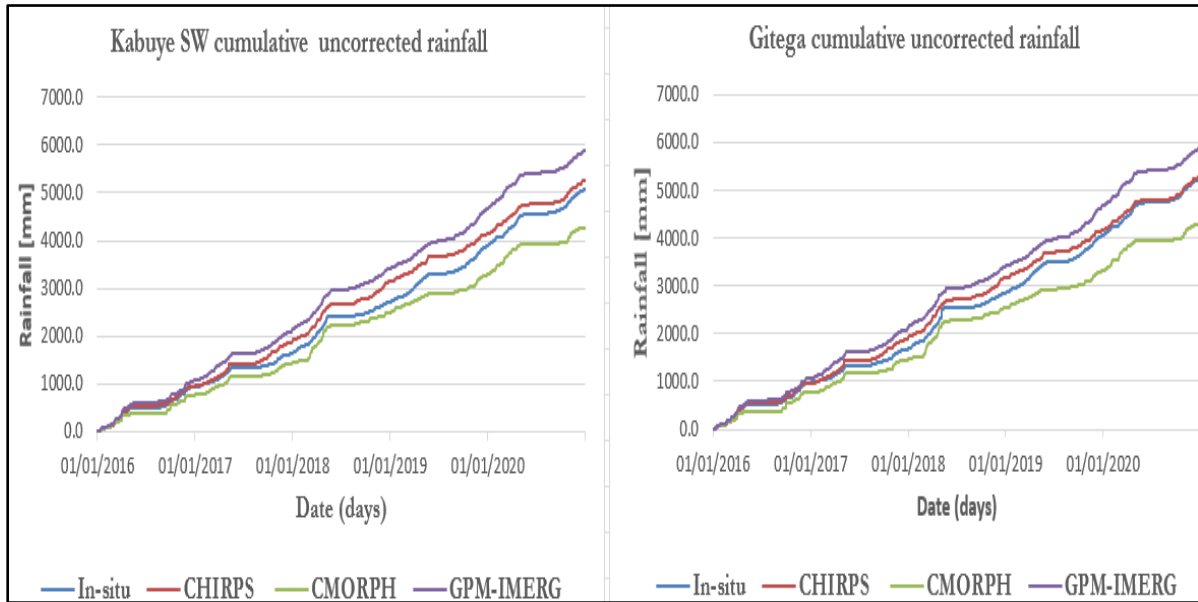
Figure 10: Example of uncorrected SRE cumulative rainfall for some rain gauge stations

Figure 10 shows the cumulative uncorrected rainfall data for the Kabuye SW and Gitega stations, comparing the in-situ data to three satellite-based rainfall estimating (SRE) products: CHIRPS, CMORPH, and GPM-IMERG. Examination of 28 stations showed a consistent relationship between the SRE data and in-situ measurements. Specifically, CHIRPS and GPM-IMERG overestimated rainfall compared with in situ data, but CMORPH underestimated rainfall.

4. RESEARCH METHODOLOGY

4.1. Schematic framework

In-situ and satellite data were used in this research. The HEC-HMS semi-distributed model was applied for rainfall-runoff modelling, and the NSE and RVE performance metrics were employed as indicators for model performance. Therefore, in situ rainfall data, satellite-based precipitation products, river discharge data, LULC, soil characteristic data, and topographic data were examined. The main steps adopted in this study are illustrated in Figure 11.
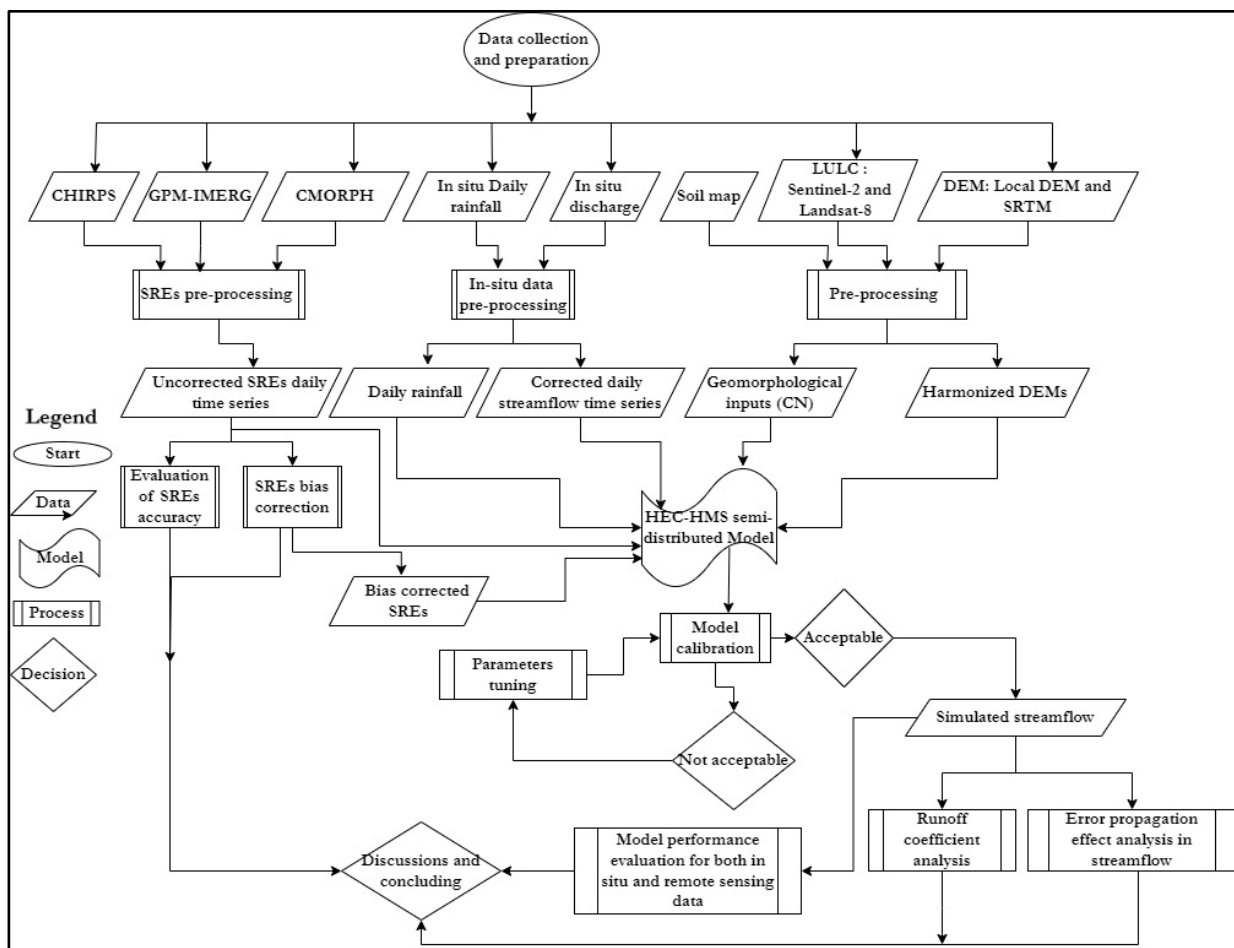
Figure 11: Conceptual flowchart

4.2. Evaluation of Satellite rainfall products

The assessment of satellite rainfall products (SREs) has focused on assessing the differences between ground-based and satellite rainfall data. A reference dataset was created using observations from 28 meteorological monitoring stations located both within and outside the catchment, and the observations ranged from 2016 to 2020. The Thiessen Polygon method was used for a reliable spatial representation of

rainfall over the catchment. This method maps each station's recorded rainfall to specified locations, resulting in a thorough spatial rainfall distribution (Ball & Luk, 1998). A set of statistical function indicators was used, including the Mean Error (ME), correlation coefficient (R^2), relative bias (rBias), and Root Mean Square Error (RMSE), to evaluate these SREs products, as shown in Table 2 (Solakian et al., 2020). Negative values signify underestimation, and positive values show overestimation by the satellite.

Table 2: Statistical performance metrics used to evaluate SREs and error propagation

Statistical metric	Values	Units	Accurate value
$RMSE = \sqrt[2]{\dfrac{\sum_{1=1}^{n}(S-G)^2}{N}}$	[0 to ∞]	mm	0
$ME = \dfrac{\sum_{i=1}^{n}(S-G)}{N}$	[-∞ to +∞]	mm	0
$rBias = \dfrac{\sum_{i=1}^{n}(S-G)}{\sum_{i=1}^{n}G} * 100$	[-∞ to +∞]	%	0
$R^2 = \dfrac{\sum_{i=1}^{n}(S_i - \bar{S}_i)(G_i - \bar{G}_i)}{\sqrt{\sum_{i=1}^{n}(S_i - \bar{S}_i)^2}\sqrt{\sum_{i=1}^{n}(G_i - \bar{G}_i)^2}}$	[-1 to 1]	[-]	1

Where S is the rainfall data gathered using satellites or the simulated streamflow derived from satellite data. G is the recording from gauge stations (in situ rain gauge observation) or simulated observed streamflow (from in situ reference rain gauge), and N symbolizes the total count of the recorded observations.

The correlation coefficient (R^2) assesses the linear correlation between satellite and in-situ rainfall estimates, whereas RMSE measures the standard deviation of differences (precipitation errors from SREs products). Relative Bias (rBias) indicates overestimation or underestimation of real rainfall (between satellite and in-situ). The Mean Error (ME) determines the errors or accuracy direction related to the underestimation or overestimation of the SRE products.

After rigorous statistical analysis was carried out to determine the errors and evaluate the correlation between satellite and ground-based rainfall estimations, graphical summaries, such as scatter plots and error distribution charts, were created to visually show the relative performance of each satellite product, as demonstrated in the Results and Discussion section.

4.3. Satellites rainfall bias correction

SRE products are not free from errors, and these errors can generally occur either randomly or systematically from different sources (Aghakouchak et al., 2012). Before applying SRE products for rainfall-runoff modelling, it is necessary to identify, evaluate, and fix these biases. Therefore, bias or error correction techniques have been established to enhance the accuracy of rainfall in terms of spatial and temporal representations just before being applied in rainfall-runoff modelling (Najmaddin et al., 2017). In this study, bias correction was performed on the SRE products, including CMORPH, CHIRPS, and GPM-IMERG.

According to their effectiveness proven by various studies, the following three bias correlation techniques, including Time and Space Variant (TSV), Distribution Transformation, and Power Transform bias correction methods, were assessed and tested in this research to prove the most effective bias correction technique, which indicates improvement in the accuracy of SRE products and to be applied in this research.

- **Time and Space Variant (TSV) bias correction technique**

The results of Omondi (2017), Habib et al., (2014), and Gumindoga et al., (2019) in their studies indicated that Time and Space Variant was the most effective bias correction approach. As they explained, the TVSV relies on the following equation and was applied in this study:

$$BF_{TSV} = \frac{\sum_{t=d}^{t=d-l} G(i,t)}{\sum_{t=d}^{t=d-l} S(i,t)} \qquad \text{Equation 7}$$

Where BF represents the daily bias factor, G and S indicate the daily recorded precipitation data in mm/day (daily gauge and satellite), d is the day number, i is the number of rain gauge locations, t is the Julian day number, and l indicates the defined period over which the bias was assessed and calculated (time window).

- **Distribution Transformation (DT) bias correction method**

Based on research by Omondi (2017), the Distribution Transformation (DT) and Time and Space Variant (TSV) methods showed good performance among other bias correction techniques in terms of correcting mean rainfall and eliminating daily bias. Regarding the matching concept, the differences in the variance and mean value are fixed according to the chosen time, as explained in the following equations (Gumindoga et al., 2016). Equation (8) determines the bias correction factor for mean values.

$$DT_\mu = \frac{G_\mu}{S_\mu} \qquad \text{Equation 8}$$

S_μ represents the mean value of the selected time window size of satellite rainfall estimate products, and G_μ shows the mean value of the selected time window size of gauged rainfall observation. Equation 9 shows the variance bias correction factor (standard deviation) for the gauge (G_τ) and SREs (S_τ).

$$DT_\tau = \frac{G_\tau}{S_\tau} \qquad \text{Equation 9}$$

Finally, Equation 10 was applied to determine the corrected SREs for daily estimates (S_{DT}) after determining the bias correction factors within a chosen time window. Therefore, correction factors were used for the daily satellite rainfall estimates ($S_{i,t}$).

$$S_{DT} = DT_\tau(S_{i,t} - S_\mu) + DT_\mu S_\tau \qquad \text{Equation 10}$$

- **Non-linear Power Transform (PT) bias correction technique**

A nonlinear power transform bias correction approach can be used to remove satellite data errors for hydrological modelling (Vernimmen et al., 2012). This bias correction technique was more effective and effective in providing precipitation, as confirmed by Gumindoga et al. (2019) in their study. This approach focused on adjusting the standard deviation of the rainfall series through an exponential form, and Equation 11 was applied.

$$PT = \alpha G(i,t)^\beta \qquad \text{Equation 11}$$

G represents the gauged daily precipitation in mm/day, signifies the pre-factor set to equalize the mean values for the transformed SREs and observed gauged rainfall, β is a coefficient calculated to match the coefficient of variation (CV) of the SREs to that of the gauged data, t represents the day number, and i signifies the gauge number. The final values for α and β were derived from the optimization approach, allowing for a more precise correction of satellite-derived rainfall data (Gumindoga et al., 2019). The optimizing process of the α and β coefficients aimed to minimize the difference between the measured (in situ) and corrected satellite rainfall values. This could be achieved through an algorithm that minimizes the root mean square error (RMSE) between the corrected satellite rainfall values and in situ values (Fylstra et al., 1998).

4.3.1. Testing and determining the most effective bias correction approach

This study aimed to obtain an appropriate bias correction approach for satellite rainfall estimates (SREs), including the CMORPH, CHIRPS, and GPM-IMERG datasets, in the context of evaluating remote sensing data for rainfall-runoff modelling in the Nyabarongo catchment area. The assessment was conducted using data from 28 meteorological stations inside and beyond the catchment area interpolated through the Thiessen Polygon method, which ranges from 2016 to 2020.

To assess the effectiveness of the bias correction methods mentioned above, this study tested them on a hundred sample time series recorded during the 2020 rainy season, from February 12th to May 21st. Testing was carried out at four meteorological stations: Gitega, Kabuye SW, Kigali Aero, and Gacurabwenge. The BF for each approach was determined over a seven-day period window and applied to daily satellite rainfall data. For the Power Transform method, further tests were performed without a preset time window. These approaches were evaluated by comparing corrected SREs with gauge-based rainfall data using performance indicators, such as Mean Error (ME), correlation coefficient (R²), relative bias (rBias), and Root Mean Square

Error (RMSE), as noted in the preceding section. The results of this evaluation test are detailed in Table 3 of the results section, providing a full overview of the performance indicators for each tested method.

The most effective bias correction technique was then applied to all 28 rain-gauge locations in the study area. Other less effective methods were also used in part throughout the same time window for comparison purposes. The purpose of implementing these methods was to produce an improved rainfall dataset for each method. The uncorrected and corrected data were then used to analyze the performance of the HEC-HMS semi-distributed rainfall-runoff model, and the impact of bias correction on the model was established by comparing its performance to rainfall corrected data using the most and least effective methods throughout the time series of the same year.

Due to the computational time for optimizing the coefficients (α and β) for the Power Transform method across several time series, this optimization was fully completed and limited to data from 2016, 2017 and 2018 due to the limited time to perform all bias correction. The others remaining 2019 and 2020 years timeseries, on the α and β values the average from 2016 to 2018 was used per station and the obtained values for α and β were applied to the others remaining years (2019 and 2020).

4.3.2. Time Window defining

Sequential Window (SW), the most applicable approach, was used to estimate the size of the time window, as recommended by Habib et al. (2014). The daily SREs in this study were corrected using a multiplicative bias factor, which is often known as the multiplicative shift approach. To obtain a biased adjusted rainfall estimate, the ratio of gauge-to-satellite estimates was calculated and multiplied by satellite estimates. Therefore, to remove bias in SREs, the Sequential (SW) approach was used. The windows of 3,5,7, 9, and 17 days were analysed and tested on four rain gauge stations, and the errors spread among in situ observations and SREs were assessed by determining the root mean square error (RMSE). The objective was to find an optimum window length to be applied to all 28 rain gauge stations, which accurately captures the SRE bias and effectively corrects it for rainfall-runoff model simulations.

4.4. HEC-HMS rainfall-runoff modeling

4.4.1. Model description

A HEC-HMS semi-distributed model was used to meet the objectives of this study. HEC-HMS is an acronym for Hydrologic Engineering's Center Hydrologic Modelling System, which was developed by the U.S. Army Corps of Engineers (USACE, 2022). The HEC-HMS model is a commonly used software for simulating rainfall-runoff processes, and it was specifically designed to manage the complexity of hydrological processes in various catchments (Feldman, 2000). This model simulates the effects of precipitation, evaporation, and transpiration on runoff, making it appropriate for evaluating the hydrological

responses in catchment areas (Singh & Woolhiser, 2003).The semi-distributed approach for HEC-HMS provides a more detailed representation of spatial variability within the catchment than lumped models, which treat the entire watershed as a single unit (Beven, 2012). The semi-distributed model divides the catchment into sub-basins, each with distinct characteristics, improving the precision of the runoff predictions.

4.4.2. Model setup

The selected approach for processing the rainfall transforms into runoff at the sub-basins and reaches the element level within the entire Nyabarongo catchment area in this study, as shown in Figure 12.
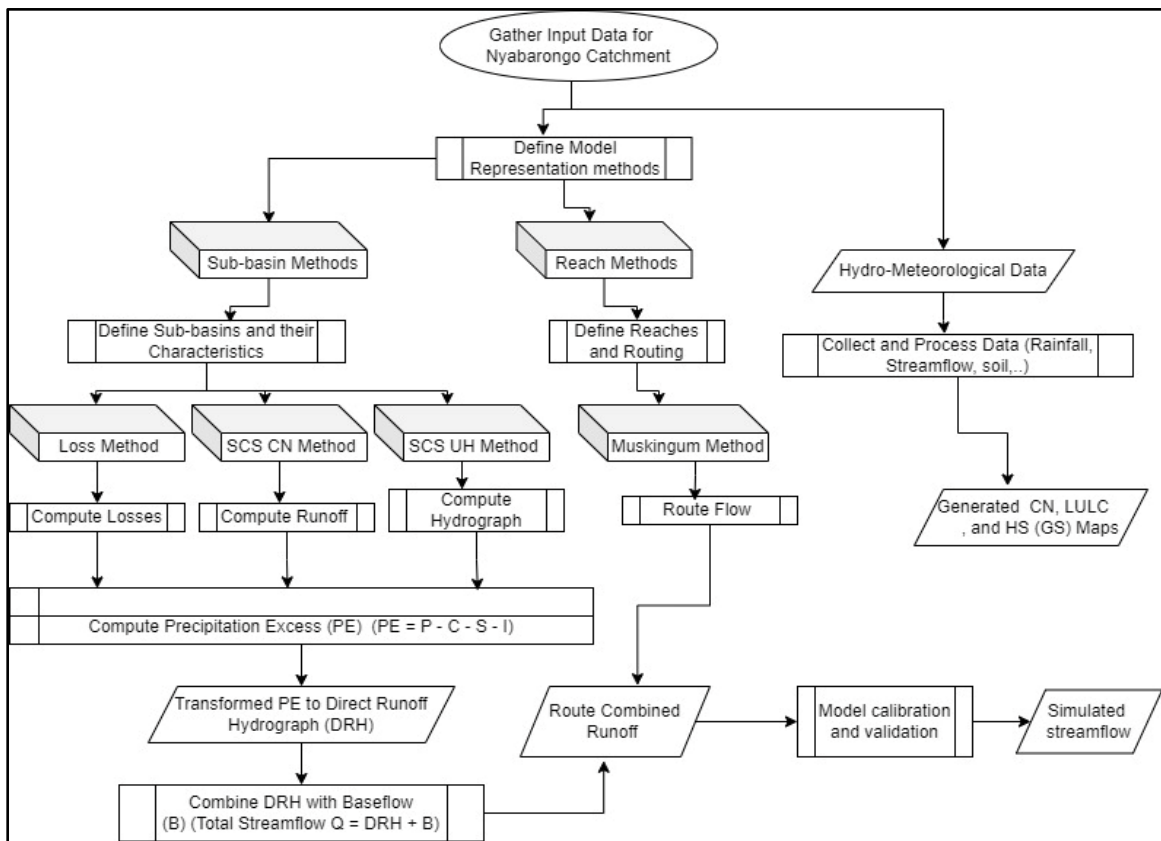
Figure 12: Semi-distributed HEC-HMS model used methods

In the flow chart, C represents the canopy interception of rainfall, S represents the rainfall stored in the surface depressions, I is the rainfall lost due to infiltration, and P is the precipitation.

The four models were set including Local DEM (10m × 10m) with in-situ or SREs rainfall and Sentinel-2, Local DEM (10m × 10m) with in-situ or SREs rainfall and LandSat-8, SRTM (30m × 30m) with in-situ or SREs rainfall and Sentinel-2, and SRTM (30m × 30m) with in-situ or SREs rainfall and LandSat-8.

The process of developing the HEC-HMS semi-distributed rainfall-runoff model for the Nyabarongo catchment area was conducted and separated into the following main steps.

- **Initial setup and basin model**

The HEC-HMS model was established by first developing the basin model, which involved specifying the physical representation of the Nyabarongo catchment area. This is often done using Geographic Information System (GIS) data, including the Terrain Model. The basin model comprises sub-basins, reaches, junctions, and reservoirs in the Nyabarongo catchment, all of which are necessary for defining the catchment and understanding the movement of water within it.

- **GIS pre-processing**

For this study, GIS pre-processing included the use of GIS tools to process spatial data, such as terrain or digital elevation models (DEMs), land use data, and soil data. These processed data were applied to precisely delineate the sub-basins and extract relevant hydrological characteristics for the model.

- **Assigning Curve Numbers to sub-basins**

Assigning Curve Numbers (CN) to each sub-basin was an important step in developing the HEC-HMS model for the Nyabarongo catchment area. CN values, which are based on land use and soil data, are crucial for predicting direct runoff from rainfall. These numbers were derived from standardized tables created by the USDA's Natural Resources Conservation Service (NRCS) and incorporated into the model for each sub-basin (Manyifika, 2015).

Initially, the obtained a soil map as explained in the section of data processing which included various soil types such as clay, loam, silty clay, clay loam, sandy clay, and sandy loam. Each of these soils was classified based on their Hydraulic Conductivity (in/h) using SCS HGS results. Using ArcGIS, these classified soil groups were crossed with SCS Curve Numbers, which are defined for different Land Use Land Cover (LULC) types present in the study area. This combination process produces a curve-number grid map. Subsequently, using ArcGIS Pro, the Zonal Statistics as Table tool was used to intersect or join the Curve Number grid with the subbasins delineated in the model. This final step allowed us to determine the specific Curve Numbers for each sub-basin, which were the input data for the HEC-HMS model.

- **Assigning Lag Time and Muskingum Parameters**

The Lag time, described as the interval time between peak rainfall and peak runoff, was assigned to each sub-basin in the model for the Nyabarongo catchment area (Feldman 2000). Furthermore, Muskingum parameters (K, X) were defined to simulate the movement of water across the river network. These factors are crucial for effectively estimating the time and degree of runoff within the Nyabarongo catchment area. The proper assignment of lag times and Muskingum parameters ensured that the model could accurately simulate hydrological processes within the catchment. The Lag Time within the Nyabarongo catchment area was calculated from the following equations (12,13 and 14), as detailed by the HEC-HMS User's Manual, Version 2022, upgraded by the US Army Corps of Engineers.

$$TC = \frac{l^{0.8}(S+1)^{0.7}}{1,140Y^{0.5}}$$ Equation 12

$$Y = \frac{1000}{CN} - 10$$ Equation 13

Lag=$0.6T_C$ Equation 14

Where T_C indicates the Time of Concentration (in hours), which is the period needed for rainfall drop to travel from the farthest point in the catchment to the outlet. The l is the flow length (ft), Y is the mean catchment land slope (%), S is the maximum potential retention, and CN represents the Curve Number. Lag is the Lag Time expressed in hours.

- **Creating a meteorologic model**

Creating a meteorological model for the Nyabarongo catchment in the HEC-HMS setting up required describing the catchment's rainfall input (time series), which included entering rainfall data from various sources such as in situ stations and remote sensing data (SREs).

- **Creating control specifications and simulation run**

The final stage in the Nyabarongo HEC-HMS model setup was to create control specifications that defined the time and intervals of the simulation. This involved determining the start and end dates (time) for the simulation period in the Nyabarongo catchment area. A simulation was conducted by connecting the basin model, meteorological model, and control specifications, allowing the modeler to run the model and view the results.

4.4.3. Calibration and performance evaluation of the model

Rainfall–runoff modelling must be calibrated to generate a match or fit of the time series for the simulated and observed stream flow. The calibration process refers to the fine-tuning of the model parameters (model parameter optimization), boundary conditions, and meteorological factors to obtain the best possible model input and create precise and reliable model simulations (Rientjes, 2016). To analyse the performance of the model, the validation process requires a different meteorological dataset that is not used for calibration (Legates & McCabe, 1999). Visual assessment and comparison of the observed and simulated hydrographs and objective functions were employed to assess the model performance. The performance metrics, including the Nash-Sutcliffe coefficient of efficiency (NSE) and Relative Volume Error (RVE), were used to assess the matching between the observed and simulated hydrographs, as described by Rientjes (2016). The NSE evaluates the resemblance between simulated and observed hydrograph shapes, while the RVE shows the difference in volume between the observed and simulated hydrographs. A description of the equations for the statistical criteria used in this study is provided in Table 3, as indicated by Rientjes (2016).

Table 3: Performance metrics

Performance metrics	Equations	Values	Performance indicator
Nash-Sutcliffe coefficient of efficiency (NS)	$NS = 1 - \dfrac{\sum_{n-1}^{N}(Q_{obs(i)} - Q_{sim(i)})^2}{\sum_{n-1}^{N}(Q_{obs(i)} - \overline{Qobs(\iota)})^2}$	$-\infty$ to 1	Range
		1	Perfect
		0.9-1	Extremely good
		0.8-0.9	Very good
		0.6-0.8	Reasonably good
		<0.6	Poor
Relative Volume Error (RVE)	$RVE = [\dfrac{\sum_{i=1}^{n}(Q_{sim(i)} - Q_{obs(i)}}{\sum_{n=1}^{n} Q_{obs(i)}}] \times 100$	$-\infty$ to $+\infty$	Range
		0	Best
		-5% to +5%	Good
		$\pm5\%$ to ±10	Reasonable

4.5.   Evaluation of data sources on the performance of hydrologic model

Before incorporating the datasets into the model (DEMs, LULC maps, and rainfall data), individual comparisons were performed to understand their preliminary impact on the model and reliability. First, a local DEM with a 10m ×10m resolution and SRTM with a 30m × 30m resolution were assessed. These DEMs were compared by determining the differences in surface storage (sinks) and their ability to delineate stream networks within the catchment. Local DEM and DEM generated from SRTM were filled using a fill sink tool to eliminate some depressions, which led to the continuous flow of water on the terrain. Moreover, the filled DEM helps determine the direction of water flow for each cell in the DEM. Therefore, the flow accumulation is derived from the flow direction, where it calculates the accumulated flow of water into each cell by showing potential stream locations. The flow accumulation data produced were used to assign an order to each segment of the stream network.

This comparison allowed us to understand how their accuracy differs and may affect hydrological modelling before and after being received by the model. Next, the two LULC maps were crossed and compared, including Sentinel-2 with a 10m × 10m resolution and LandSat-8 with a 30m × 30m resolution. Both LULC maps were combined with the digital soil map of the world from FAO to produce Curve Number (CN) grids, which were necessary input data for the model. These LULC maps were compared by analysing the surface areas across different land cover classes. For the rainfall data, the daily mean rainfall selected in the rainy season of two months ranged from 01/03 to 30/04 for 5 years' time series for both in situ measurements, and uncorrected SREs were compared by generating rainfall maps and delta maps. To differentiate between these rainfall data, the IN-SITU map was subtracted from each SRE map, resulting in different maps showing variation in precipitation values. Finally, maps are prepared that show the difference between IN-SITU data and GPM-IMERG, IN-SITU and CMORPH, and IN-SITU and CHIRPS rainfall data, in the following these maps will be referred to as DELTA maps. After the preliminary assessment and

comparison, the impacts of these different data sources on model performance were evaluated using four models with different input data developed. These models were evaluated using performance metrics, such as the Nash-Sutcliffe efficiency (NSE) and Relative Volume Error (RVE). The in-situ rainfall, local DEM, and Sentinel-2 LULC map served as reference data for comparison with other datasets and model evaluation.

4.6. Evaluation the effects of error propagation in streamflow simulations

The error propagation of data sources, primarily in SREs within the model, was evaluated by checking the variations in streamflow employing statistical indices such as the Mean Absolute Error (MAE), Root Mean Square Error (RMSE), and Correlation Coefficient (CC). The ratios of these metrics ($RMSE_{Qs}/RMSE_R$, MAE_{Qs}/MAE_R, and CC_{Qs}/CC_R) for discharge and precipitation were determined to assess the influence of error propagation within the model across data sources. Therefore, when the ratios for $RMSE_{Qs}/RMSE_R$ and MAE_{Qs}/MAE_R were below 1 and the ratio for CCQ/CCR was greater than 1, the errors decreased or attenuated (Gumindoga et al., 2021). The statistical metrics (RMSE, MAE, and CC) for both rainfall and streamflow were calculated using the equations listed in Table 2.

4.7. Runoff coefficient assessment resulting from the incorporation of different data sources

In this study, various data sources were evaluated for their effectiveness in assessing the runoff coefficient using the HEC-HMS semi-distributed model. These data sources, as mentioned in the section above, were used to analyse the runoff coefficient across the total outlet volume water generated by the four models developed as discussed above. The model outputs (outlet discharge) were divided by the input rainfall data sources to calculate the runoff coefficient. To compare the performance of different data sources, the model using in-situ rainfall data, local DEM, and Sentinel-2 LULC map was considered as benchmark.

5. RESULTS AND DISCUSSION

This chapter contains research findings based on the objectives stated in the introduction part. The findings are compared to previous scientific studies and related studies.

5.1. HEC-HMS rainfall runoff modelling

5.1.1. Model runs and calibration

5.1.1.1. Hydrological Soil Groups and Curve Number

Table 4 shows the grouping of the different soil types obtained based on their hydraulic conductivity, measured in inches per hour (in/h). This grouping is based on four SCS Hydrologic Soil Groups (A, B, C, and D) based on factors such as hydraulic conductivity, texture, and drainage properties, which help in understanding the infiltration rates and water movement through the soil in the study area (Abraham et al., 2019). For example, clay soil and Sandy Clay with a hydraulic conductivity of 0.03 in/h were grouped as HSG D, indicating low permeability and high runoff (Sartika et al., 2020). Therefore, they have low infiltration rate within the study area. Conversely, Sandy Loam with a much higher conductivity of 1.98 in/h also falls into HSG A, Loam and Sandy Clay Loam with hydraulic conductivity respectively of 0.73 and 0.31 in/h both also fall into HSG A groups, demonstrating significant infiltration rate within the study area according within their soil groups (Abraham et al., 2019; Sartika et al., 2020). They have low runoff and a high infiltration rate.

The grouping also showed that soils with intermediate conductivity values, such as silty clay (0.15 in/h) and Clay Loam (0.18 in/h), were classified into group B. This corresponds to the established knowledge that these soils have moderate infiltration rates (Sartika et al., 2020). The ranges of hydraulic conductivity for each HSG were provided, e.g., HSG A soils generally have conductivities greater than 0.30 in/h, confirming that soils with higher permeability are grouped together for hydrological modelling purposes.

Table 4: SCS Hydrologic Soil Groups identified in the study area

S/N	Soil type	Hydraulic conductivity (in/h) results for Soil Type	SCS HSG	Range of Hydraulic Conductivity (in/h) for SCS HSG	SCS HGS results for Soil Type
1	Clay	0.03	A	>0.30	D
2	Loam	0.73	B	0.15-0.3	A
3	Silty Clay	0.15	C	0.05-0.15	B
4	Sandy Clay Loam	0.31	D	0.00-0.05	A
5	Clay Loam	0.18			B
6	Sandy Clay	0.03			D
7	Sandy Loam	1.98			A

Table 5 presents SCS Curve Numbers (CN) assigned to different land use and land cover (LULC) types, differentiated by HSG. Curve numbers are used to predict the direct runoff or infiltration from rainfall (Hong & Adler, 2008). For instance, built-up areas have higher CN values (77-92) across all HSGs, indicating a higher runoff potential due to impervious surfaces, as indicated in their study; urban areas typically have higher CN values, indicating a greater runoff potential (Rawls et al., 1981). Water bodies have a CN of 100, indicating no infiltration, which aligns with the expectations for open water surfaces, as explained by the USDA NRCS, 1986. Agricultural lands (crops) have varying CN values (67-89), reflecting differences in soil management and vegetative cover. Forested areas have the lowest CN values (30-77), indicating high infiltration rates and low runoff, consistent with findings of their study conducted on the impact of LULC on runoff (Rietz & Hawkins, 2004).

Table 5: SCS Curve Numbers defined per Land Use Land Cover (Ottawa, 2017)

		Hydrologic Soil Groups			
S/N	LULC	A	B	C	D
1	Built up	77	85	90	92
2	Water	100	100	100	100
3	Crop	67	78	85	89
4	Forest	30	55	70	77
5	Grass Land	49	69	79	84
6	Bare Land	76	85	90	93

As illustrated in Figure 13, the CN maps from Landsat-8 and Sentinel-2 indicate visual representations of CN values in the study area. The CN values vary differently within subbasins across land cover and soil conditions after joining curve numbers obtained per LULC classes with SCS HGS identified in the study area. Higher CN values suggest areas with a higher runoff potential, often due to impervious surfaces or compacted soils. Conversely, lower CN values indicated areas with high infiltration and low runoff. The comparison of the CN between the two satellite-LULC maps can highlight temporal changes in land cover and soil types affecting runoff potential. Sentinel-2, with its higher spatial resolution, may provide more detailed and accurate representations of the hydrological characteristics of the study area. For instance, studies have shown that Sentinel-2 data can enhance the precision of hydrological models because of their finer resolution and higher revisit frequency (Forkuor et al., 2018a).
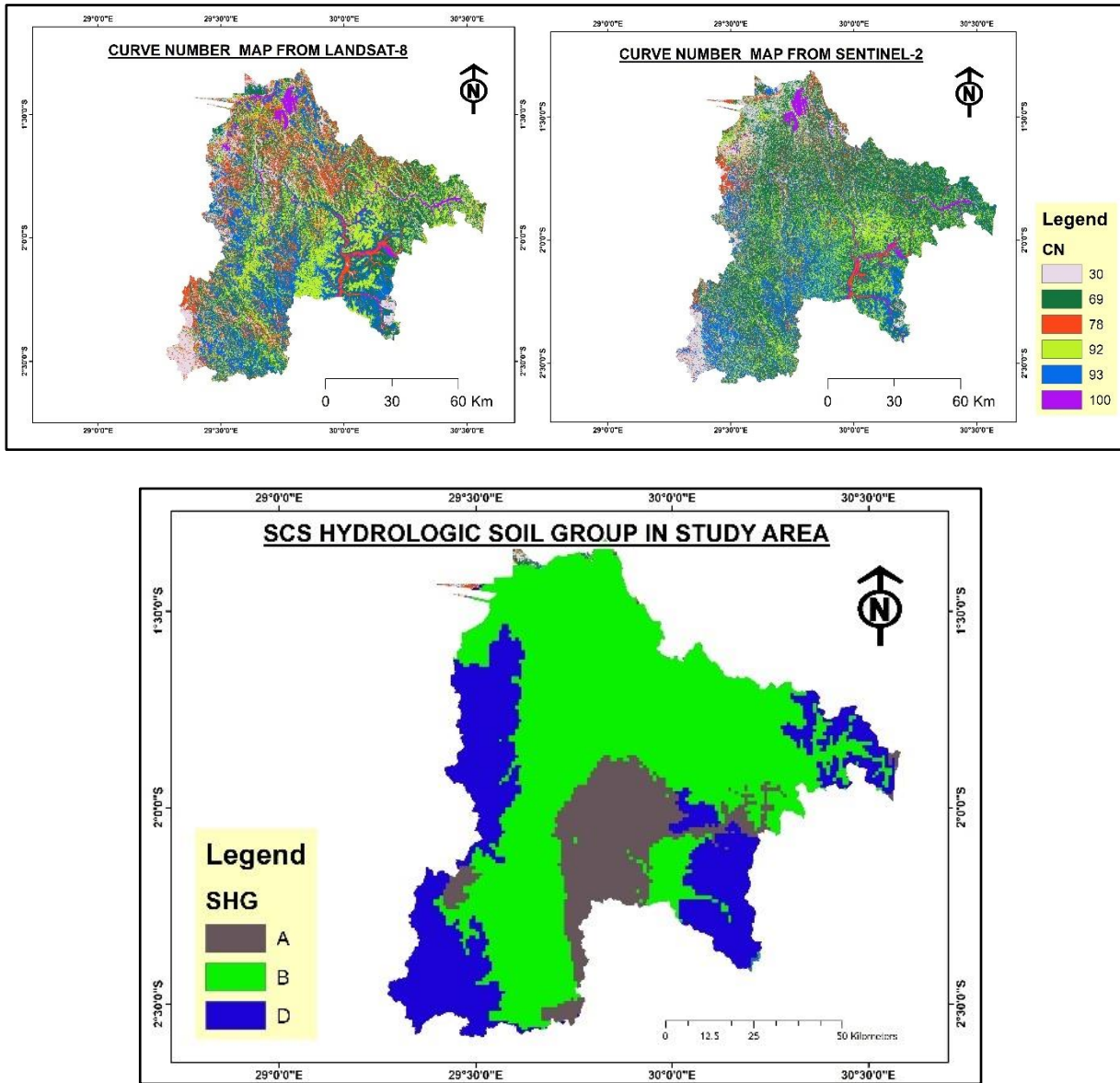
Figure 13: Hydrological Soil Groups and Curve Number

5.1.1.2. Model runs

Figure 14 shows the simulated and observed discharge hydrographs as outcomes of the first run of streamflow simulations using the HEC-HMS semi-distributed model. It includes four scenarios combining different Digital Elevation Models (DEMs), LULC, Soils, and in situ data. Local DEM (10m × 10m) with in-situ rainfall, soil, and Sentinel-2, Local DEM (10m × 10m) with in-situ rainfall, soil, and LandSat-8; SRTM (30m × 30m) with in-situ rainfall, soil, and Sentinel-2; and SRTM (30m × 30m) with in-situ rainfall, soil, and LandSat-8. This figure also illustrates the performance of these simulations in terms of their matching with observed streamflow data and evaluation using the Nash-Sutcliffe efficiency (NSE) and Relative Volume Error (RVE).
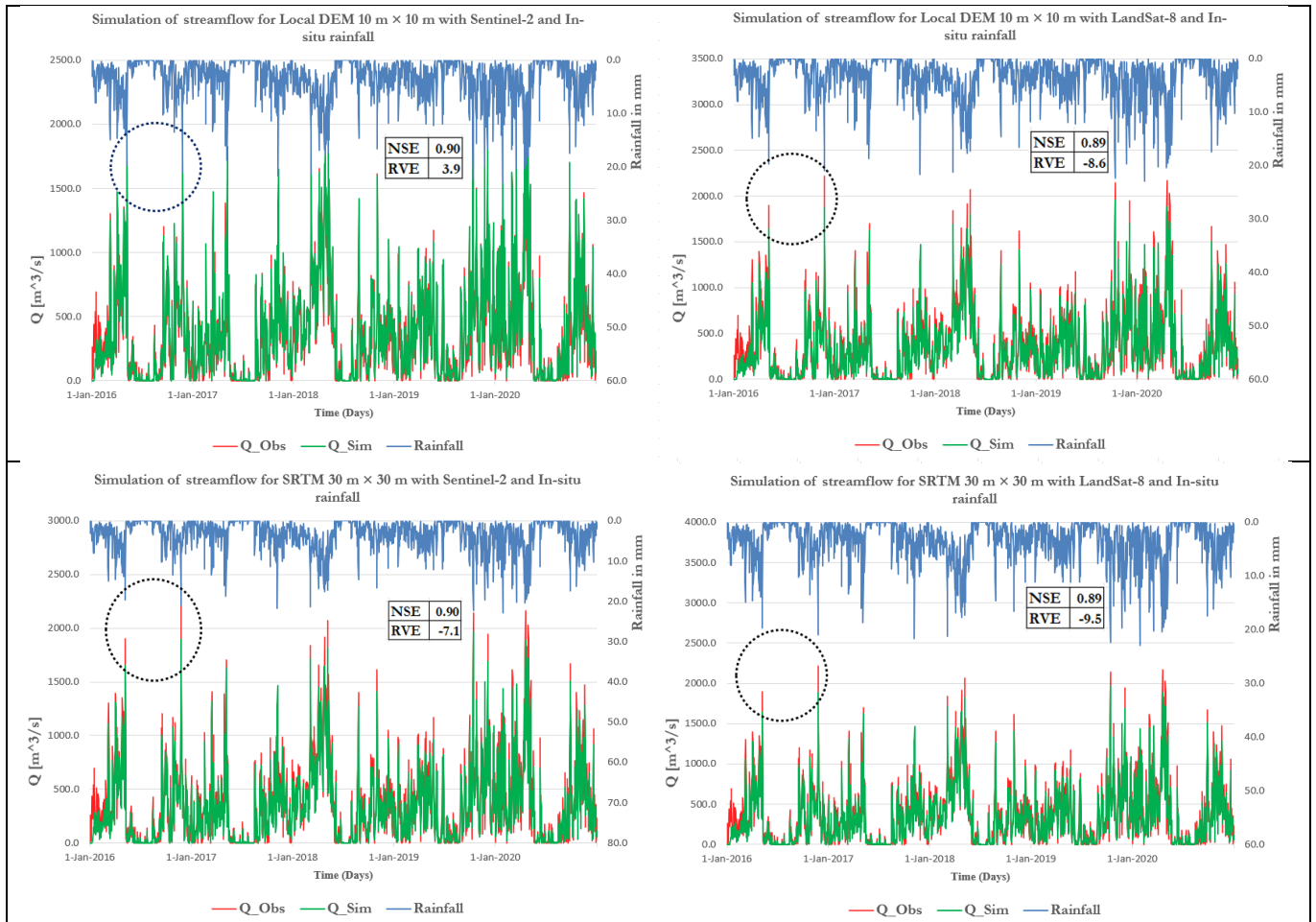
Figure 14: Simulated and observed discharges hydrograph

The first graph in Figure 14 (top left) shows the streamflow simulation results using a high-resolution Local DEM (10m × 10m) in combination with in-situ rainfall data and the Sentinel-2 LULC map. This scenario indicated a high Nash-Sutcliffe efficiency (NSE) of 0.90 and a Relative Volume Error (RVE) of 3.9%. A high NSE value, close to 1, indicates an excellent fit between the observed and simulated streamflow, indicating that the model effectively captures the streamflow dynamics. The low RVE indicates a minimal difference in the total volume of the simulated flow compared to the observed flow, demonstrating the effective results of this combination.

The second graph (top right) illustrates the simulation results using the same Local DEM (10m × 10m) and in situ rainfall, but with LandSat-8 data instead of Sentinel-2. This combination also produced a higher NSE of 0.89, indicating a good match between the simulated and observed streamflow. However, the RVE increased -8.6%, indicating a higher volume difference or discrepancy between the simulated and observed streamflow. While the model fits the observed streamflow, the increased RVE indicates larger errors in the total volume estimation compared with the first scenario.

The third graph (bottom left) presents the results using a coarser-resolution SRTM DEM (30m × 30m) combined with Sentinel-2 data. This scenario achieved an NSE of 0.90 and an RVE of -7.1%. The NSE was

relatively identical to that of the first scenario, indicating a strong model performance even with a coarser DEM resolution. However, there is a significant difference in the RVE for the second scenario, suggesting that coarser resolution affects the accuracy of the catchment representation and flow estimations, leading to comparable volume errors.

The fourth graph (bottom right) shows the simulation results using the SRTM DEM (30m × 30m) with LandSat-8 data. This combination resulted in an NSE of 0.89 and an RVE of -9.5%. The NSE remains high and thus indicates good model performance. The RVE was the largest, indicating the largest volume error. This indicates that the combination of the coarser DEM with LandSat-8 data cannot capture the detailed catchment characteristics.

The analysis of these results shows several key points regarding the impact of DEM resolution and the choice of satellite (LULC) data on rainfall runoff modelling. All four simulations performed well, with NSE values close to or above 0.89, indicating reliable streamflow simulations. However, the fit of the total volume of simulated flow was influenced by both the DEM resolution and satellite LULC map used. Higher resolution Local DEM (10m × 10m) combined with high Sentinel-2 LULC provided better volume fit compared to the courser SRTM DEM (30m × 30m) combined with both Sentinel-2 and LandSta-8 LUL, as evidenced by the lower RVE in the first scenario. This can be aligned with studies conducted and demonstrated that finer-resolution DEMs and finer LULC resolution offer a better representation of catchment characteristics, leading to improved simulation streamflow predictions (Rocha et al., 2020b). Moreover, the choice between Sentinel-2 and LandSat-8 maps affects the model performance. The Sentinel-2 LULC map results in lower RVE values and better NSE values when combined with high-resolution DEM, and it may provide more accurate surface information for streamflow modelling compared to LandSat-8 (Al-Khafaji & Al-Sweiti, 2017).

5.1.1.3. Model calibration

The primary objective of this study was to assess the effect of remote sensing data on the performance of rainfall-runoff modelling in the Nyabarongo catchment area. This was achieved through the calibration of the HEC-HMS semi-distributed model using a reference scenario combining Local DEM (10m × 10m) with in-situ rainfall, soil data, and Sentinel-2 LULC maps, as shown in Figure 15, and the subsequent application of optimized parameters to various other model combinations. This allowed for a comprehensive analysis of how varying data sources (DEMs, LULC maps, and SREs) influence rainfall-runoff simulations.
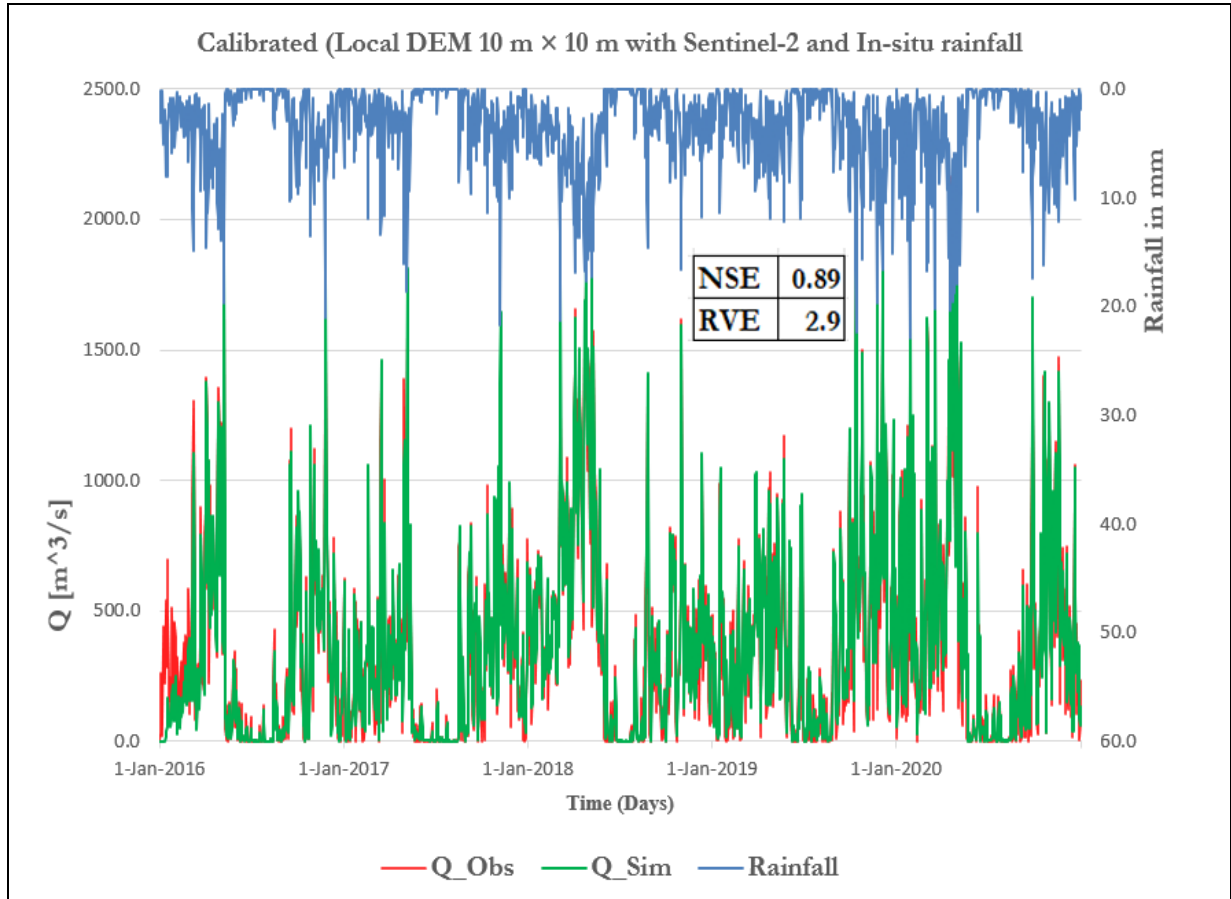
Figure 15: HEC-HMS model calibrated hydrograph

Figure 15 shows the simulated and observed discharge hydrographs as the outcomes of the calibrated HEC-HMS semi-distributed model using the reference case. This model achieved a high Nash-Sutcliffe efficiency (NSE) of 0.89 and a Relative Volume Error (RVE) of 2.9%, from 3.9%. A high NSE value indicates that the model accurately simulates the observed streamflow, showing a good match between the simulated and observed discharges. The low RVE suggests minimum errors in the total volume of the simulated runoff compared to the observed runoff, confirming the effectiveness of the model in volume estimation.

The calibration process involved optimizing parameters within the subbasins, such as Muskingum K and X values on benchmark model. The reference case model was selected for calibration because of its superior initial performance metrics for the first runs compared to other scenarios, as shown in Figure 14, and explained in the section above. The initial Curve Number values reflect the varying infiltration capacities across the sub-basins were not changed or adjusted for all developed models. Additionally, the Lag time initial values, which affect the timing of runoff, indicate that various hydrological responses within the Nyabarongo catchment remained the same for all models. The Muskingum K and X values, critical for routing flows, were optimized between 0.40372 to 0.59127 and 0.19842 to 0.29743, respectively across the sub-basins, reflecting significant control over the storage and translation of runoff or flood waves through the sub-basins. These adjustments in the K and X values influenced the timing and attenuation of peak flows, thereby enhancing the runoff simulations. All the obtained optimized parameter values for each sub-

basin were then applied to other model combinations to evaluate their performance and other data sources under the same calibrated conditions. Therefore, it was possible to assess the impact of different data sources on the model performance.

5.2. Evaluation of data sources on the performance of rainfall-runoff model

5.2.1. Preliminary assessment

5.2.1.1. Land Use Land Cover maps evaluation

Figure 16 was generated from the inter-crossing and comparison of Sentinel-2 and LandSat-8. It presents the area distribution in square kilometers of LULC data sources across various LULC classes, comparing Sentinel-2 and LandSat-8. This distribution highlights the differences between these two datasets in terms of spatial resolution and potential effects on runoff simulations.
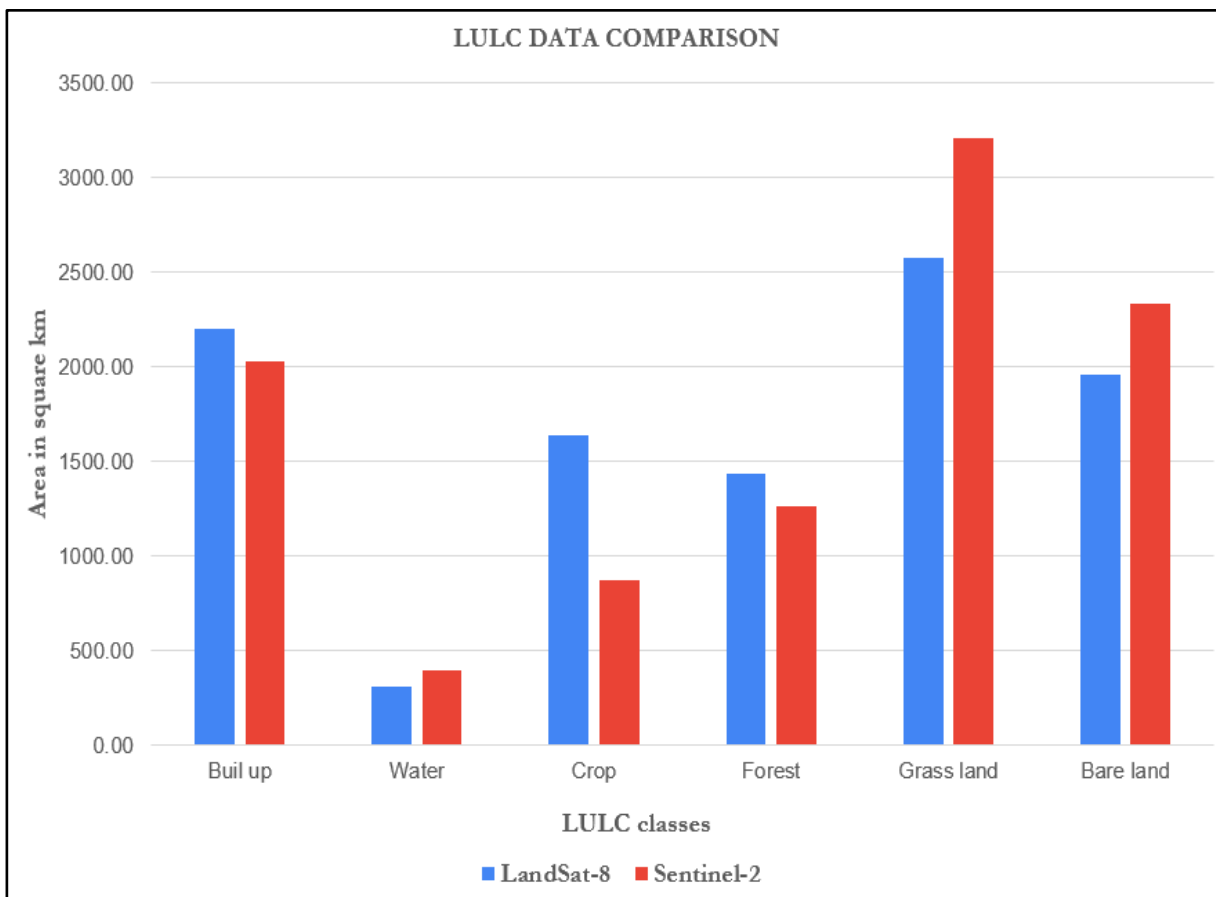
Figure 16: Comparison between LULC maps from Sentinel-2 and LandSat-8

The built-up area showed a minor difference between Sentinel-2 (2032.7 Km², with a rate of 20.1%) and LandSat-8 (2200.3 Km²) (21.8%). This difference could influence the runoff simulation, as urban areas typically generate higher runoff due to impervious surfaces. The higher spatial resolution of Sentinel-2 allowed for a more precise identification of built-up areas compared to LandSat-8 as reported by studies, potentially leading to more accurate runoff simulations (Kuc & Chormański, 2019). The water bodies were

slightly more abundant in Sentinel-2 covering 393.3 Km² (3.9 %) compared to LandSat-8 (310.3 Km², 3.1 %). Therefore, the improved resolution of Sentinel-2 provides the detection of smaller water bodies, which can refine runoff simulations by providing more detailed streams and hydrological networks (Jakovljević et al., 2018).

The cropland area was significantly larger in LandSat-8 (1634.7 Km², 16.2%) than in Sentinel-2 (874.1 Km², 8.7%). This may be due to the seasonal differences in crop visibility. Croplands affect runoff through infiltration and evapotranspiration (ET). The higher resolution of Sentinel-2 may lead to better differentiation between croplands and other land covers, which indicates the accuracy of simulating runoff compared with LandSat-8, which may be lost through infiltration and evapotranspiration processes based on these reclassification results (Etchanchu et al., 2017). Forest areas were also more in LandSat-8 (1435.2 Km², 14.2%) compared to Sentinel-2 (1263.4 Km², 12.5%). These results reflect the reduction in runoff due to the high infiltration capacity and evapotranspiration. The higher spatial resolution of Sentinel-2 could provide a more detailed forest cover map, improving most runoff simulation results for forest-related hydrological processes compared with LandSat-8.

Grassland coverage was higher in Sentinel-2 (3213.9 Km², 31.8%) compared to LandSat-8 (2574.3 Km², 25.5%). Grasslands influence runoff through moderate infiltration and evapotranspiration rates. Sentinel-2, with finer resolution, increases the detection of smaller patches of grassland, potentially leading to more accurate runoff simulations (Etchanchu et al., 2017). Bare land was more in Sentinel-2 (2336.5 Km², 23.1%) compared than in LandSat-8 (1985.2 Km², 19.3%). This implies higher runoff due to minimal infiltration. The higher resolution of Sentinel-2 allows for better detection of bare land patches, which could refine runoff simulations by providing a detailed surface cover map.

The resolution differences between Sentinel-2 (10m × 10m) and LandSat-8 (30m × 30m) significantly affected the accuracy of the LULC classification. For instance, as explained in the data processing section, Sentinel-2 had an overall accuracy of 78.8%, and LandSat-8 achieved 73.1% accuracy. Sentinel-2 higher resolution provided a more detailed and precise land cover map, which can improve the accuracy of rainfall-runoff simulations in the HEC-HMS model in the Nyabarongo catchment, aligned with the research done by Forkuor et al.,2018 showed that finer spatial resolution of LULC maps leads to better delineation of land cover types, which is essential for precise hydrological simulations (Forkuor et al., 2018).

5.2.1.2.   Assessing Digital Elevation data

In this study, SRTM DEM and a local DEM were evaluated. Figures 17 and 18 present the comparative outcomes of stream network delineation and surface volume storage using two different digital elevation models, including the Local DEM with a resolution of 10m × 10m and SRTM of 30m × 30m within the Nyabarongo catchment area.
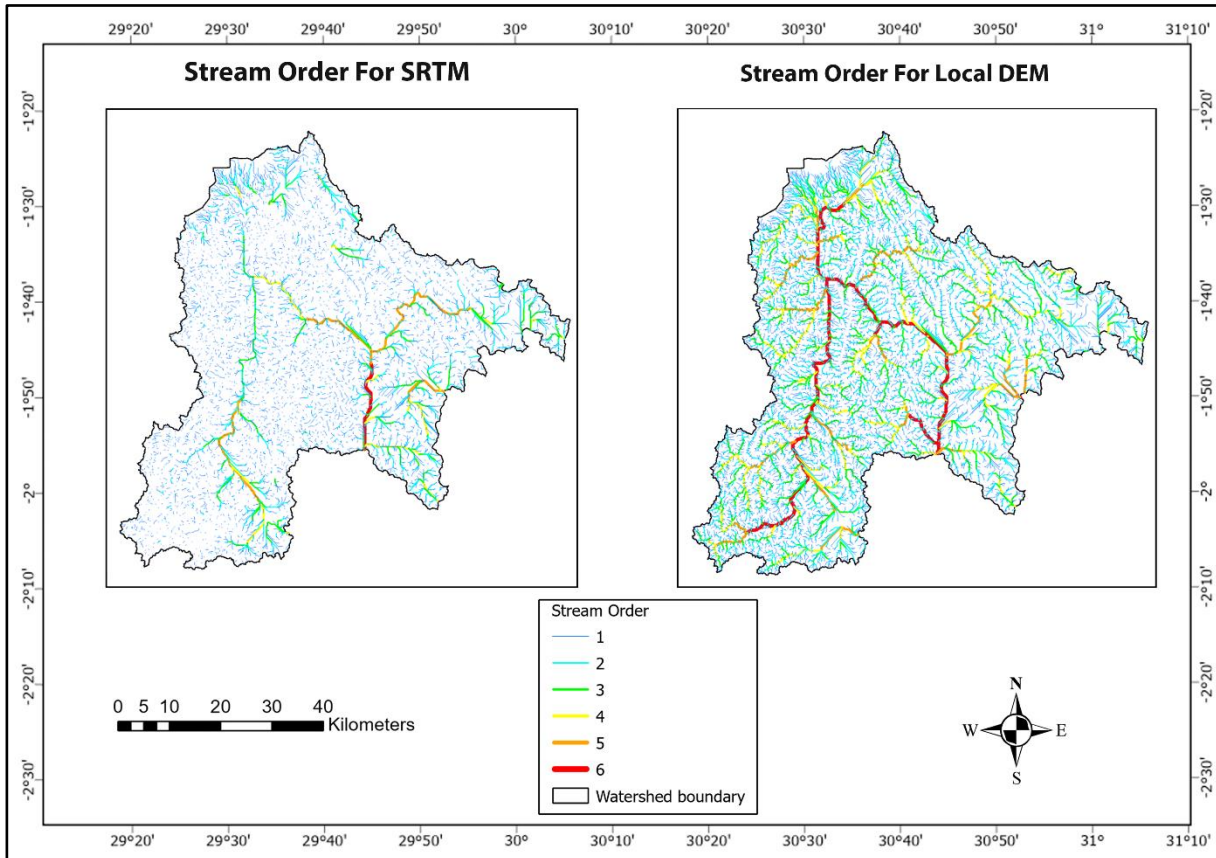
Figure 17: Stream networks delineating using Local DEM 10m×10m and SRTM 30m×30m

Figure 17 shows a comparison of the stream networks delineated using both DEMs. As illustrated in the figure, the stream network delineated using the Local DEM shows more detailed stream networks than SRTM, which are less detailed. Therefore, the higher resolution allows for the capture of finer topographical details, resulting in a more accurate representation of smaller tributaries and minor streams. The detailed stream networks in the Local DEM can potentially lead to more precise rainfall-runoff simulations in the HEC-HMS model compared to the SRTM, which might lead to less accurate runoff simulations due to a less detailed stream network, as indicated in Figure 17.
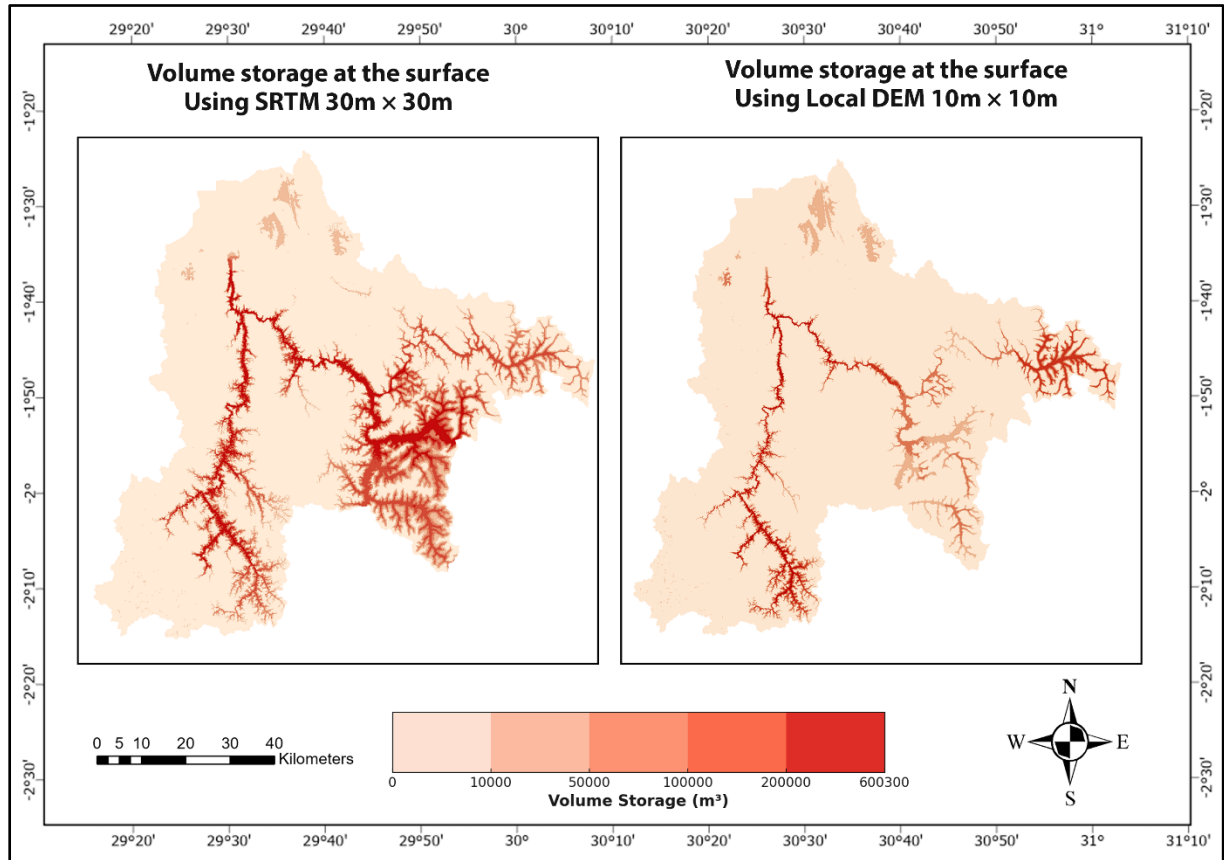
Figure 18: Volume storage at the surface using both Local DEM 10m × 10m and SRTM 30m × 30m

Figure 18 shows the volume storage at the surface using both DEMs, with calculated total volumes of 8,885,700m³ for the Local DEM and 19,562,400m³ for the SRTM DEM, as illustrated in Appendices 1 and 2, respectively. The surface storage volume in the Local DEM (10m × 10m) was significantly lower than that in the SRTM DEM (30m × 30m). High resolution captures more detailed terrain features, such as small depressions and natural storage areas, but these are distributed over a more extensive network, leading to a lower total storage volume (Hou et al., 2021). This higher surface storage volume with the SRTM DEM may occur because the lower resolution tends to generalize the terrain, resulting in larger, smoother depressions and storage areas, which cumulatively account for the higher total volume.

These dissimilarities in surface volume storage may have implications for rainfall-runoff simulations. For instance, a lower volume of surface storage may lead to higher peak flows during rainfall events because there are fewer large storage areas to attenuate the flow. This can result in a more responsive catchment with rapid runoff generation. However, a higher volume of surface storage implies a more significant flow attenuation. Larger storage areas can capture and hold more water during rainfall events, potentially lowering peak flows and delaying runoff response.

The choice of DEM resolution has a notable effect on rainfall-runoff simulations within the Nyabarongo catchment using the HEC-HMS model. The higher-resolution DEM provides a more detailed representation of the terrain, leading to more detailed stream networks and lower storage volumes compared to the lower-resolution DEM (W. Zhang & Montgomery, 1994). The lower-resolution DEM can lead to less accurate runoff simulations, particularly in areas where small topographical features significantly influence hydrological responses. The Local DEM (10m × 10m) provided a more detailed and accurate representation of the Nyabarongo catchment compared to the SRTM DEM (30m × 30m). This resulted in more precise rainfall-runoff simulations in the HEC-HMS model. These findings align with other existing research that focused on the importance of DEM resolution in rainfall runoff modelling. Higher-resolution DEMs are generally preferred for detailed and accurate simulations, especially in locations with complex terrain such as the Nyabarongo catchment area (Moges et al., 2023b).

5.2.1.3.   Rainfall data source analysis

The rainfall distribution maps in Figure 19 show the spatial variability of the daily average rainfall across the study area using both in-situ rainfall and SRE products such as CMORPH, CHIRPS, and GPM-IMERG. From these maps, it is evident that in-situ rainfall and SREs are different within the catchment. The DELTA maps in Figure 20 highlight the differences between in-situ rainfall and various SREs, specifically CMORPH, CHIRPS, and GPM-IMERG. For instance, in the delta map in-situ and CHIRPS, the top-centre map shows the difference between in-situ and CHIRPS. Positive values indicate areas where SREs overestimated precipitation, and negative values indicate underestimated precipitation compared to in-situ data.
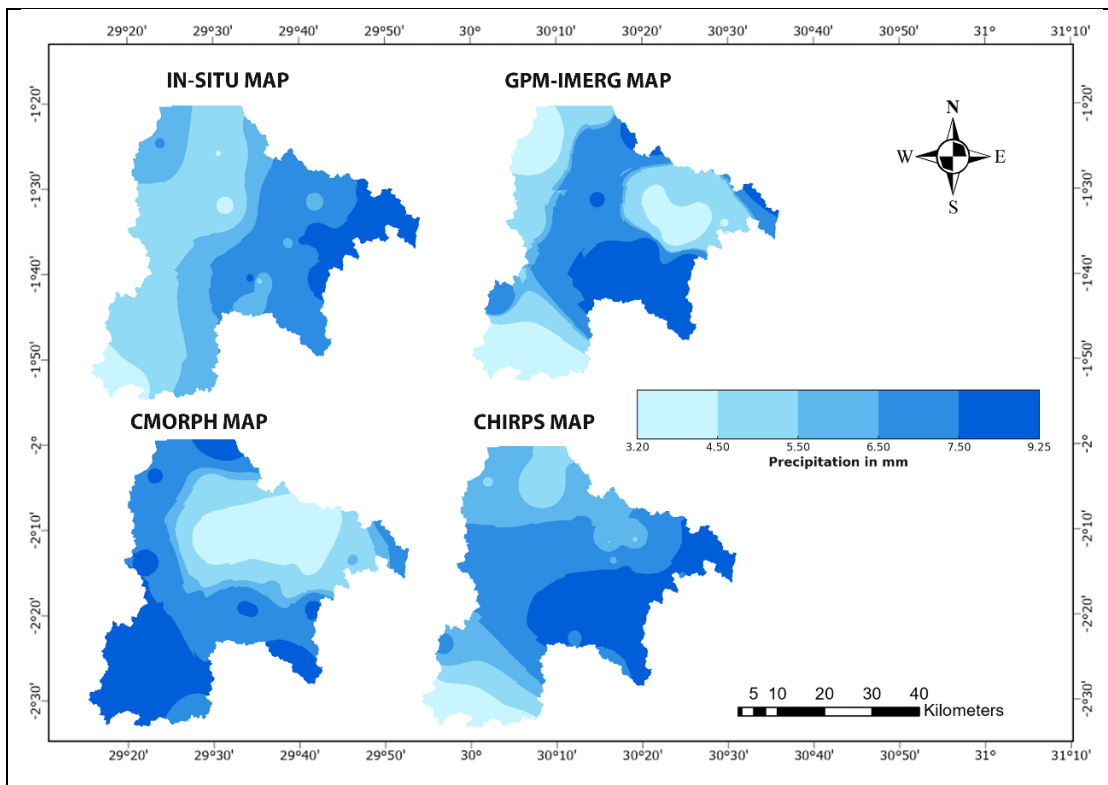
Figure 19: Rainfall maps showing distribution patterns in both in-situ and SREs
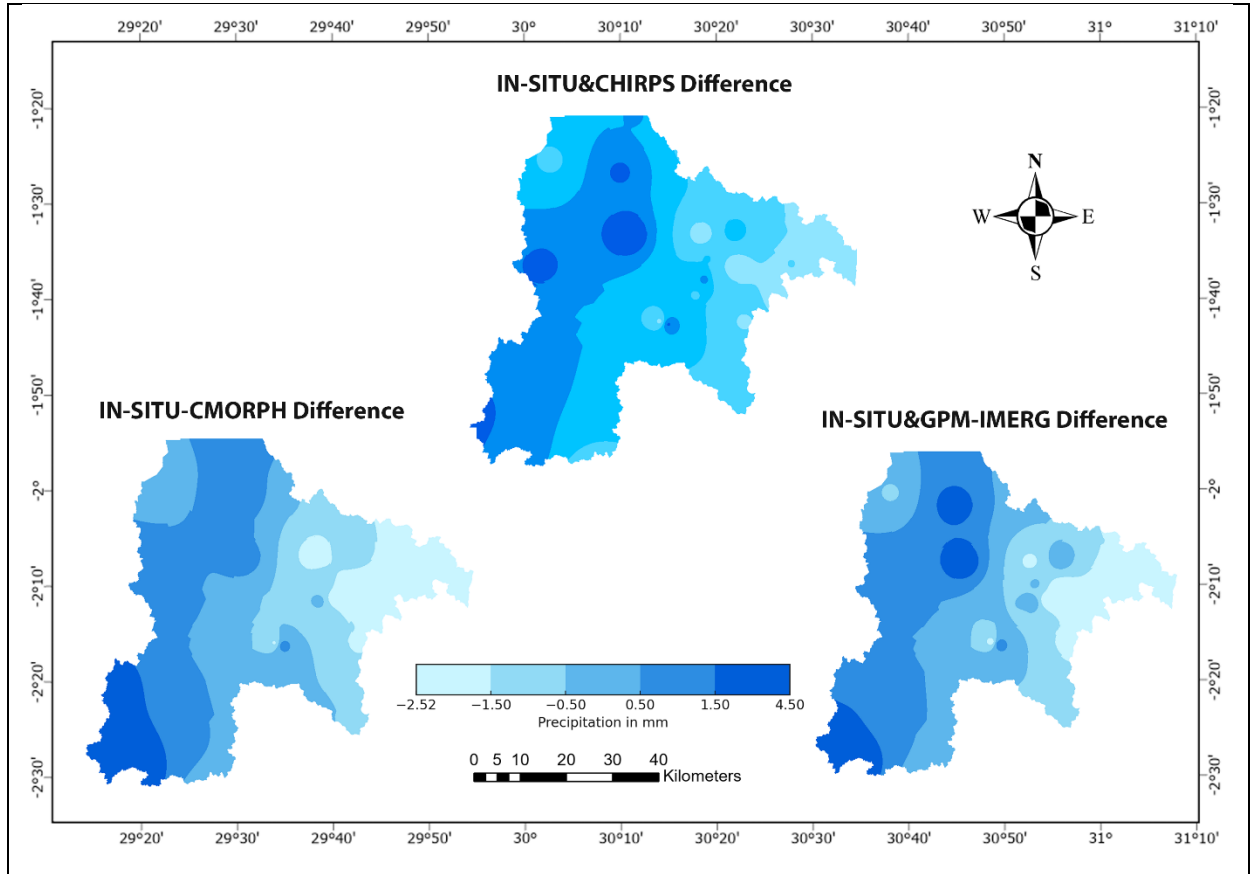
Figure 20: DELTA maps (i.e. difference maps) showing rainfall patterns for SREs

This spatial variability and differences in rainfall data have significant implications for errors in rainfall-runoff simulations using the HEC-HMS semi-distributed model (Troutman, 1983). The spatial variability captured by both SREs, and in-situ rainfall must be the same to achieve good runoff simulation results. Areas with higher precipitation contribute more to runoff than those with lower precipitation, potentially leading to localized flooding if not accurately represented. Therefore, dissimilarities related to overestimations and underestimations for these SREs compared with in-situ rainfall could lead to overprediction and underprediction of runoff simulation within the model. Incorporating bias-corrected rainfall data, such as power transform, time–space variant, and distribution transformation techniques, may improve the accuracy of rainfall-runoff simulations (Sharma et al., 2007).

5.2.2. Effects of data sources on the performance of HEC-HMS rainfall runoff model

Table 6 shows the performance of different data sources for streamflow simulation using the HEC-HMS semi-distributed model. As shown in this table, the effects of data sources are divided into sections that show the Nash-Sutcliffe Efficient (NSE) and Relative Volume Error (RVE) for both initial runs and calibrated models, including the reference case model of Local DEM 10m × 10m with Sentinel-2 and other models of Local DEM 10m × 10m with LandSat-8, SRTM 30m × 30m with Sentinel-2, and SRTM 30m × 30m with LandSat-8. The different rainfall both in situ, uncorrected, and corrected SREs with different bias

correction techniques and the same soil data were received by these developed models, as stipulated in Table 6 and appendix 3.

Table 6: Performance of different data sources on the streamflow simulation

	Local DEM 10m × 10m with Sentinel-2				Local DEM 10m × 10m with LandSat-2			
	Initial runs		Calibrated		Initial runs		Calibrated	
Rainfall	NSE	RVE	NSE	RVE	NSE	RVE	NSE	RVE
In-situ	0.90	3.9	**0.89**	**2.9**	0.89	-8.6	**0.89**	-7.4
CMORPH-Uncorrected	0.24	-9.6	0.38	-7.8	0.23	-13.0	0.30	-10.1
CMORPH-PT	0.71	1.4	**0.77**	**0.4**	0.61	12.0	**0.69**	10.0
CMORPH-TSV	0.38	-8.6	0.49	-7.4	0.40	-11.4	0.50	-9.4
CMORPH-DT	0.33	-1.04	0.43	-0.04	0.30	10.4	0.33	9.4
CHIRPS-Uncorrected	0.17	0.3	0.28	-1.3	0.22	-10.7	0.27	-10.2
CHIPS-PT	0.73	7.2	**0.79**	6.3	0.63	8.1	**0.69**	8.7
CHIPS-TSV	0.30	-2.8	0.43	-1.2	0.37	-10.0	0.41	-7.3
CHIPS-DT	0.20	12.2	0.29	1.3	0.30	10.0	0.31	10.1
IMERG-Uncorrected	0.38	16.8	0.41	14.0	0.34	-17.5	0.40	-11.5
IMERG-PT	0.70	9.0	**0.72**	8.0	0.62	12.7	**0.67**	10.2
IMERG-TSV	0.52	0.9	0.62	2.0	0.60	-10.1	0.60	-10.1
IMERG-DT	0.50	14.3	0.54	12.8	0.44	15.9	0.50	10.6
SRTM 30m × 30m with Sentinel-2					**SRTM 30m × 30m with LandSat-8**			
Rainfall	NSE	RVE	NSE	RVE	NSE	RVE	NSE	RVE
In-situ	0.90	-7.1	**0.89**	-6.1	0.89	-9.5	**0.90**	-8.5
CMORPH-Uncorrected	0.23	-11.9	0.35	-8.9	0.20	-14.2	0.30	-11.2
CMORPH-PT	0.69	4.5	**0.77**	2.5	0.61	13.8	**0.70**	10.8
CMORPH-TSV	0.40	-9.2	0.49	-8.3	0.39	-12.5	0.49	-10.4
CMORPH-DT	0.33	2.4	0.43	1.3	0.29	12.4	0.30	10.4
CHIRPS-Uncorrected	0.20	-14.3	0.26	-13.3	0.16	-15.7	0.20	-13.7
CHIPS-PT	0.68	10.3	**0.70**	8.4	0.60	11.3	**0.60**	10.7
CHIPS-TSV	0.36	-7.0	0.42	-6.0	0.36	-11.3	0.41	-9.4
CHIPS-DT	0.28	14.1	0.31	12.4	2.64	12.5	0.31	12.2
IMERG-Uncorrected	0.37	-11.1	0.40	-10.1	0.36	25.4	0.40	-22.4
IMERG-PT	0.70	10.4	**0.71**	9.1	0.51	24.5	**0.65**	19.0
IMERG-TSV	0.53	-4.9	0.61	-3.8	0.57	-15.8	0.62	-12.2
IMERG-DT	0.48	10.3	0.54	9.5	0.43	20.8	0.49	18.8

The initial runs for the reference case model of Local DEM 10m × 10m with Sentinel-2 using in-situ rainfall data achieved a high NSE of 0.90 and an RVE of 3.9%, indicating a strong match between the observed and simulated streamflow. Uncorrected SREs such as CMORPH, CHIRPS, and GPM-IMERG showed significantly lower performance, with NSE values of 0.24, 0.17, and 0.38, respectively, and significant underestimations of no fit in RVE values of -9.6%, 0.3%, and 16.8% according to the acceptable range of -5% and +5%. The application of the bias correction techniques significantly improved the results. For example, the Power Transform (PT) correction technique for CMORPH increased the NSE to 0.71 and

adjusted the RVE to 1.4%. Similarly, the Time-space Variant (TSV) and Distribution Transformation bias correction techniques also increased the NSE and reduced the RVE, but the Power Transformation performed well. After calibration, the NSE for the reference model with in-situ rainfall remained high at 0.89, with an improved RVE of 2.9%. The calibrated model with uncorrected and corrected SREs further increased performance. For instance, the Power Transform in CMORPH achieved an NSE of 0.77 and RVE of 0.4%. For other corrected SREs such as CHIRPS and GPM-IMERG, the Power Transform also showed significant improvements in both NSE and RVE, indicating effective bias correction.

The initial runs with Local DEM 10m × 10m with LandSat-8 showed an NSE of 0.89 with in-situ rainfall but a notably bad estimation with RVE at -8.6% compared to the reference case. Uncorrected SREs such as CMORPH, CHIRPS, and GPM-IMERG performed poorly, with NSE values of approximately 0.23, 0.22, and 0.34, respectively, and significant underestimations in RVE of approximately -13.0%, -10.7%, and -17.5% compared to the reference case and Local DEM 10m × 10m with LandSat-8 and in-situ rainfall. Bias correction techniques improved these metrics, with the Power Transform, which is the best, in CMORPH, for example, showing an NSE of 0.61 and an RVE of 12.0%, demonstrating a shift to the best results compared to uncorrected. The other techniques and power transforms in all and other SREs, namely CHIRPS and GPM-IMERG, also showed improvements in NSE and RVE. The results of calibration showed that the NSE for the model with in-situ rainfall was 0.89, and the RVE was -7.4%. The corrected SREs showed an NSE of 0.69 and RVE of 10.0% in the Power Transform, indicating improvement. Therefore, Power Transform and other techniques in all SREs improved NSE and RVE values but were still poor compared to the reference case and Local DEM 10m × 10m with LandSat-8 and in-situ rainfall, as shown in Table 6 and Appendix 3.

Using the SRTM 30m × 30m DEM with Sentinel-2 and in situ rainfall, the results showed an NSE of 0.90 and an RVE of -7.1% for the initial runs. Uncorrected SREs showed poor performance, with NSE values of approximately 0.23 and RVE of -11.9% in CMORPH, indicating underestimation and performance for other SREs compared to the reference case and SRTM 30m × 30m DEM with Sentinel-2 and in-situ rainfall. Corrected SREs through the power transform and time–space variant showed improvements. The power Transform in CMORPH achieved an NSE of 0.69 and an RVE of 4.5%, while CHIRPS and GPM-IMEG also enhanced NSE and reduced RVE compared to the uncorrected data. Calibrated runs with SRTM 30m × 30m DEM and Sentinel-2 with in-situ rainfall showed an NSE of 0.89 and an RVE of -6.1%. Corrected SREs by Power Transform, such as CMORPH, achieved an NSE of 0.77 and RVE of 2.5%, indicating a significant improvement over uncorrected data. The power Transform also showed an improved performance, reflecting an effective bias correction.

Initial runs with SRTM 30m × 30m DEM and LandSat-2 had an NSE of 0.89 and -9.5%, respectively, with in-situ rainfall. Uncorrected SREs, such as CMORPH, also performed poorly with an NSE of 0.20 and RVE

of -14.2% compared to the corrected data, and SRTM 30m × 30m DEM and LandSat-2 run with in-situ rainfall and reference cases. Power transformation also outperformed the other techniques for all SRE products. Calibration of the SRTM 30m × 30m DEM and LandSat-2 model with in-situ rainfall resulted in an NSE of 090 and RVE of -8.5 %, which also outperformed the initial runed model.

These overall results on the impacts of various data sources on the performance of the model aligned with other studies that focused on the importance of high-resolution data and effective bias correction. Rocha et al. (2020) found that high-resolution DEMs and land cover significantly increased rainfall-runoff model performance by providing detailed topographic and surface information (Rocha et al., 2020). Gumindoga et al. (2019) and Goshine et al. (2019) demonstrated that bias correction techniques such as Power Transform, Time Space Variant, and Distribution Transformation improve the accuracy of SREs in rainfall-runoff modelling (Goshime et al., 2019). Among these bias correction techniques, the Power Transform (PT) was the most effective, consistently improving NSE and RVE values across different SRE products and model combinations. The comparison of these study findings indicated that models combined with higher-resolution Local DEM (10m × 10m) and LULC maps (Sentinel-2) with in-situ rainfall consistently outperformed those with lower-resolution SRTM (30m × 30m), as evidenced by higher NSE values and lower RVE percentages. This is reliable with the findings of Rocha et al. (2020), who highlighted the influence of detailed terrain data on rainfall-runoff simulations. The resolution of land cover data has also played a crucial role. Models with Sentinel-2 (10m × 10m resolution) generally showed better performance than those with Land Sat-8 (30m × 30m resolution), supporting the conclusions drawn by Hanif et al.,2023) regarding the significant improvement in surface representation with high-resolution land cover data, indicating the best performance in simulating streamflow (Hanif et al., 2023). The reference case model of Local DEM 10m × 10m with Sentinel-2 and in situ rainfall outperformed other models, highlighting the importance of high-resolution DEM and detailed land cover data in achieving good streamflow simulations.

5.3. Evaluation and bias correction of SRE products

5.3.1. Time window defining

The performance metrics were assessed using the Sequential Window (SW) approach over different bias correction time windows (days) at numerous stations. This was performed using both TSV and DT bias correction techniques. The RMSE and other performance metrics, such as ME, RBias, and R^2, were primarily evaluated to determine the optimum time window size for bias correction for SRE. Following Habib et al. (2014), the SW technique was used to identify the optimal time window size for bias correction of the daily SREs. In this research, by examining time windows of 3, 5, 6, 7, 9, and up to 17 days across four rain gauge stations including Gitega, Kabuye SW, Kigali Aero, and Gacurabwenge as samples to test and determine the optimal window size for effectively capturing and correcting SRE biases, the results showed that a 7-day time window provided the greatest performance for all assessed SREs.

For the CHIRPS data, the 7-day time window proved to be the most successful at reducing biases across different parameters. For example, the Gitega station has a significantly lower RMSE value (5.9 for a 7-day window compared to 6.1 for a 3-day window, which appears as the next one after a 7-day time window compared to other remaining time window lengths. The ME for the 7-day window was 3.6, compared to 3.7 for the 3-day window, indicating an improved performance in terms of error reduction. The R^2 value increased from 0.66 for the 3-day window to 0.70 for the 7-day window, indicating improved performance with an optimal window size, as shown in Table 7. At Kabuye station, the 7-day window generated an RMSE of 7.2 compared to 9.1 for the 3-day window. For Gacurabwenge and Kigali Aero stations, the obtained RMSE is significantly lower compared to other time window sizes, with values of 7.1 and 7.0, respectively. However, after considering the RMSE, ME, and R^2 values, a 7-day window was recommended compared to other time window lengths, as displayed in Table 7.

For the CMORPH data, the 7-day time window also performed well. For instance, at the Gacurabwenge station, the RMSE decreased to 9.0 for a 7-day window, while the ME decreased to 4.9, indicating a better fit or optimal time window size with bias correction applied compared to all other time window sizes. The R^2 value was relatively high (close to 0.54), demonstrating consistent performance across a 7-day time window. The RMSE value for the Kigali Aero Station was 8.7 for the 7-day window, which was lower than that for the other time window sizes. The ME decreased to 4.1, indicating an improvement compared to all other time window sizes. The R^2 value increased to 0.55, which is higher and indicates a stronger correlation between the observed (in situ) and corrected (satellite) values after bias correction compared to other time window sizes. Similarly to the Kabuye and Gitega stations, the RMSE has significantly decreased to 8.1 and 6.0 values which are lower compared to other time window sizes.

Table 7: Variation of statistical indicators for the time window length defining

SRE	Metrics	Time window length for Gacurabwenge station								Time window length for Gitega station							
		3 days	5 days	6 days	7 days	10 days	12 days	15 days	17 days	3 days	5 days	6 days	7 days	10 days	12 days	15 days	17 days
CHIRPS	RBias	-0.25	-0.12	-0.05	**-0.01**	-0.21	-0.21	-0.21	-0.21	-0.21	0.00	-0.07	**0.00**	-0.06	-0.01	0.05	-0.03
	RMSE	8.2	9.0	9.7	**7.1**	9.3	9.3	9.3	9.3	6.1	7.2	6.8	**5.9**	7.3	7.5	7.5	7.4
	ME	4.3	4.8	5.2	**4.1**	5.1	5.1	5.1	5.1	3.7	4.6	4.5	**3.6**	4.8	4.9	5.0	4.9
	R²	0.55	0.51	0.42	**0.60**	0.40	0.40	0.40	0.40	0.66	0.54	0.55	**0.70**	0.48	0.48	0.48	0.48
		Time window length for Kabuye station								Time window length for Kigali Aero station							
	RBias	-0.13	-0.02	-0.06	**0.01**	0.13	0.06	0.13	0.18	-0.08	0.02	-0.02	**0.00**	0.01	-0.02	0.03	0.00
	RMSE	9.1	10.1	9.4	**7.2**	11.4	11.2	11.3	11.7	9.2	8.9	9.3	**7.0**	9.9	10.1	10.0	9.9
	ME	4.4	5.2	4.8	**4.0**	6.0	5.8	6.1	6.2	5.3	5.5	5.7	**4.1**	6.1	6.1	6.1	6.1
	R²	0.34	0.24	0.32	**0.55**	0.19	0.22	0.21	0.21	0.39	0.43	0.35	**0.59**	0.24	0.24	0.27	0.22
		Time window length for Gacurabwenge station								Time window length for Gitega station							
CMORPH	RBias	-0.07	-0.12	-0.11	**-0.01**	-0.09	-0.18	-0.17	-0.29	-0.13	-0.08	-0.04	**-0.01**	-0.13	-0.03	-0.16	-0.26
	RMSE	10.6	9.6	9.9	**9.0**	10.3	10.5	10.2	9.6	6.4	6.8	7.3	**6.0**	7.3	9.5	8.3	8.0
	ME	5.6	5.3	5.6	**4.9**	5.8	5.9	5.8	5.4	3.5	3.8	4.1	**3.0**	4.0	5.2	4.4	4.4
	R²	0.44	0.48	0.49	**0.54**	0.42	0.36	0.39	0.40	0.68	0.64	0.60	**0.69**	0.61	0.41	0.43	0.43
		Time window length for Kabuye station								Time window length for Kigali Aero station							
	RBias	-0.20	-0.12	-0.09	**-0.01**	-0.25	-0.13	-0.23	-0.25	-0.14	-0.09	0.00	**0.00**	-0.17	-0.10	-0.13	-0.20
	RMSE	8.6	9.8	9.3	**8.1**	8.8	9.6	9.0	9.3	9.0	9.6	9.5	**8.7**	9.1	9.7	9.5	9.2
	ME	4.1	5.2	5.0	**3.9**	4.8	5.5	5.2	5.3	4.6	5.3	5.3	**4.1**	5.0	5.4	5.2	5.1
	R²	0.57	0.43	0.44	**0.66**	0.50	0.45	0.42	0.40	0.45	0.36	0.45	**0.55**	0.44	0.44	0.40	0.40
		Time window length for Gacurabwenge station								Time window length for Gitega station							
GPM-IMERG	RBias	-0.02	-0.06	-0.05	**-0.01**	-0.03	0.03	0.02	-0.07	0.00	0.00	0.00	**0.00**	-0.03	0.03	0.02	0.06
	RMSE	6.8	6.4	7.0	**6.1**	7.2	9.6	9.6	8.9	5.7	5.4	5.7	**5.1**	5.8	6.2	6.0	6.6
	ME	3.5	3.7	3.7	**3.3**	4.0	5.4	5.0	4.8	3.1	3.1	3.3	**2.9**	3.5	3.9	3.6	4.0
	R²	0.74	0.77	0.73	**0.80**	0.74	0.51	0.53	0.54	0.74	0.75	0.72	**0.79**	0.72	0.65	0.72	0.65
		Time window length for Kabuye station								Time window length for Kigali Aero station							
	RBias	-0.04	0.01	-0.04	**0.00**	-0.01	-0.05	-0.04	-0.03	0.00	0.00	-0.01	**0.00**	0.00	-0.01	0.01	0.01
	RMSE	4.3	5.9	6.1	**4.1**	5.9	6.3	6.6	6.3	4.8	5.6	6.2	**4.3**	6.6	6.8	6.8	6.5
	ME	2.5	3.5	3.5	**2.2**	3.7	3.8	4.0	3.9	2.5	3.2	3.6	**2.3**	3.8	4.0	4.1	3.8
	R²	0.89	0.79	0.76	**0.91**	0.79	0.73	0.71	0.74	0.83	0.76	0.72	**0.86**	0.67	0.65	0.65	0.69

For GPM-IMERG, the 7-day time window provided the best results across all the tested stations. At Gacurabwenge station, the RMSE for the 7-day window was 6.1, which was lower compared to other time window sizes, demonstrating a decrease in error predicting. The ME decreased significantly to 3.3, which was also the lowest compared with the other time window sizes. At the other stations including Kabuye, Kigali Aero and Gitega stations, the 7-day window's RMSE was also notably lower and showed improvement over all obtained for all remaining time window sizes with values of 4.1, 4.3, and 5.1, respectively. The other indicators like ME, and R^2 showed notable improvement, showing better data fit and consistency with an optimal time window size of 7 days.

The 7-day time window consistently provided the best bias correction for SREs across all tested meteorological stations and satellite products in the Nyabarongo catchment area. Research conducted by Bhatti et al. (2016) and Habib et al. (2014) demonstrated that a 7-day time window was most effective for bias correction in similar hydrological situations. The 7-day time window was confirmed to be applicable over all 28 rain gauge stations within and outside the catchment area of this study. The improved RMSE, ME, and R^2 values for the CHIRPS, CMORPH, and GPM-IMERG products confirmed that the 7-day time window approach was reliable and suitable for reducing errors from SREs for efficient rainfall-runoff modeling in the research area, as shown in Table 7.

5.3.2. Testing of Bias Correction Techniques

Uncorrected SREs in CHIRPS data showed considerable errors for all rain gauge stations, with RMSE values ranging from 7.4 mm/day at Gitega station to 11.03 mm/day at Kabuye SW stations. The TSV technique reduced the RMSE to 5.9 mm/day at Gitega station and to 7.2 mm/day at Kabuye SW station, indicating improvement in all stations by reducing errors but with significant inaccuracies, particularly at stations with high original RMSE (uncorrected) values. The DT approach did not improve accuracy in all rain gauge stations, it increased the RMSE at four stations including Gitega, Kabuye SW, Kigali Aero, and Gacurabwenge. The PT technique achieved a significant reduction in errors, with the lowest RMSE values among all rain gauge stations compared to the other bias correction techniques, as shown in Table 8. Furthermore, PT showed a significant difference in improving all other performance metrics, including the R^2, ME, and RBias values, as displayed in Figure 21 and Table 8. The method consistently yielded the highest R^2 values and lowest ME and RBias values, indicating better error correction performance with perfect values compared to the other methods.

The uncorrected CMORPH data showed high RMSE values, particularly at Kigali Aero and Kabuye SW, with values of 10.0 mm/day. The TSV technique reduced the RMSE to 8.7 mm/day at the Kigali Aero station and 8.1 mm/day in Kabuye SW. The TSV showed a moderate decrease in the RMSE for all stations. The DT technique significantly reduced RMSE values for three stations of Gitega, Kabuye SW, and Kigali Arero and increased RMSE in the Gacurabwenge station. The PT technique was the most successful, with

RMSE values as low as 0.005 mm/day at Gacurabwenge and other stations, compared to all tested bias correction techniques. The PT once again outperformed the others with ME, R^2, and RBias, with significant values across all stations in the CMORPH product.

 The GPM-IMERG data showed that the uncorrected RMSE values ranged from 7.0 mm/d at Kabuye SW to 9.7 mm/d at Gacurabwenge. The TSV bias correction technique reduced the RMSE to 4.1 mm/d at Kabuye SW and 6.1 mm/d at Gacurabwenge. The DT technique was further improved, with RMSE values ranging from 6.0 mm/day at Kabuye SW to 8.4 mm/day at Gacurabwenge. The PT approach produced the best results, with RMSE values as low as 0.027 mm/day at Kabuye SW and Gacurabwenge. Generally, all bias correction techniques decreased the RMSE in the GPM-IMERG data, but PT was the most followed by TSV and the last one was DT.

Table 8: Testing of bias correction techniques

Gauge Station	Method	CHIRPS				CMORPH				GPM-IMERG			
		Rbias	RMSE	ME	R²	Rbias	RMSE	ME	R²	Rbias	RMSE	ME	R²
Gitega	Uncorrected	-0.03	7.4	4.9	0.48	-0.01	9.9	5.3	0.38	0.11	7.1	4.4	0.64
	TSV	**0.00**	5.9	3.6	0.70	-0.01	6.0	3.04	0.69	**0.00**	5.1	2.9	0.79
	DT	0.25	7.6	5.4	0.48	0.08	7.7	4.6	0.51	0.17	6.5	4.3	0.64
	PT	**0.00**	**0.1**	**0.03**	**1.00**	**0.002**	**0.1**	**0.03**	**1.00**	-0.001	**0.01**	**0.004**	**1.00**
Kabuye SW	Uncorrected	-0.07	11.0	5.9	0.21	-0.17	10.0	5.6	0.39	0.10	7.0	4.1	0.71
	TSV	0.01	7.2	4.0	0.55	-0.01	8.1	3.9	0.66	0.00	4.1	2.2	0.91
	DT	0.36	11.4	6.2	0.37	-0.07	8.7	5.1	0.51	0.15	6.0	3.9	0.79
	PT	**0.001**	**0.02**	**0.01**	**1.00**	**0.001**	**0.02**	**0.01**	**1.00**	-0.002	**0.03**	**0.01**	**1.00**
Kigali Aero	Uncorrected	-0.15	9.7	5.8	0.21	-0.08	10.0	5.4	0.40	0.09	7.9	4.4	0.60
	TSV	**0.00**	7.0	4.1	0.59	**0.00**	8.7	4.1	0.55	**0.00**	4.3	2.3	0.86
	DT	0.03	9.96	6.1	0.24	0.13	8.8	5.4	0.46	0.19	6.5	4.2	0.68
	PT	0.002	**0.1**	**0.0**	**1.00**	0.003	**0.05**	**0.03**	**1.00**	-0.001	**0.02**	**0.01**	**1.00**
Gacurabwenge	Uncorrected	-0.21	9.3	5.1	0.40	-0.29	9.6	5.4	0.40	-0.09	9.7	5.2	0.50
	TSV	-0.01	7.1	4.1	0.60	-0.01	9.0	4.9	0.54	-0.01	6.1	3.3	0.80
	DT	0.08	9.3	5.6	0.40	0.41	10.4	6.3	0.49	0.17	8.4	5.01	0.62
	PT	**-0.001**	**0.1**	**0.04**	**1.00**	**0.00**	**0.005**	**0.002**	**1.00**	**0.001**	**0.03**	**0.02**	**1.00**

Gitega station	Kabuye SW station	Kigali Aero station	Gacurabwenge station
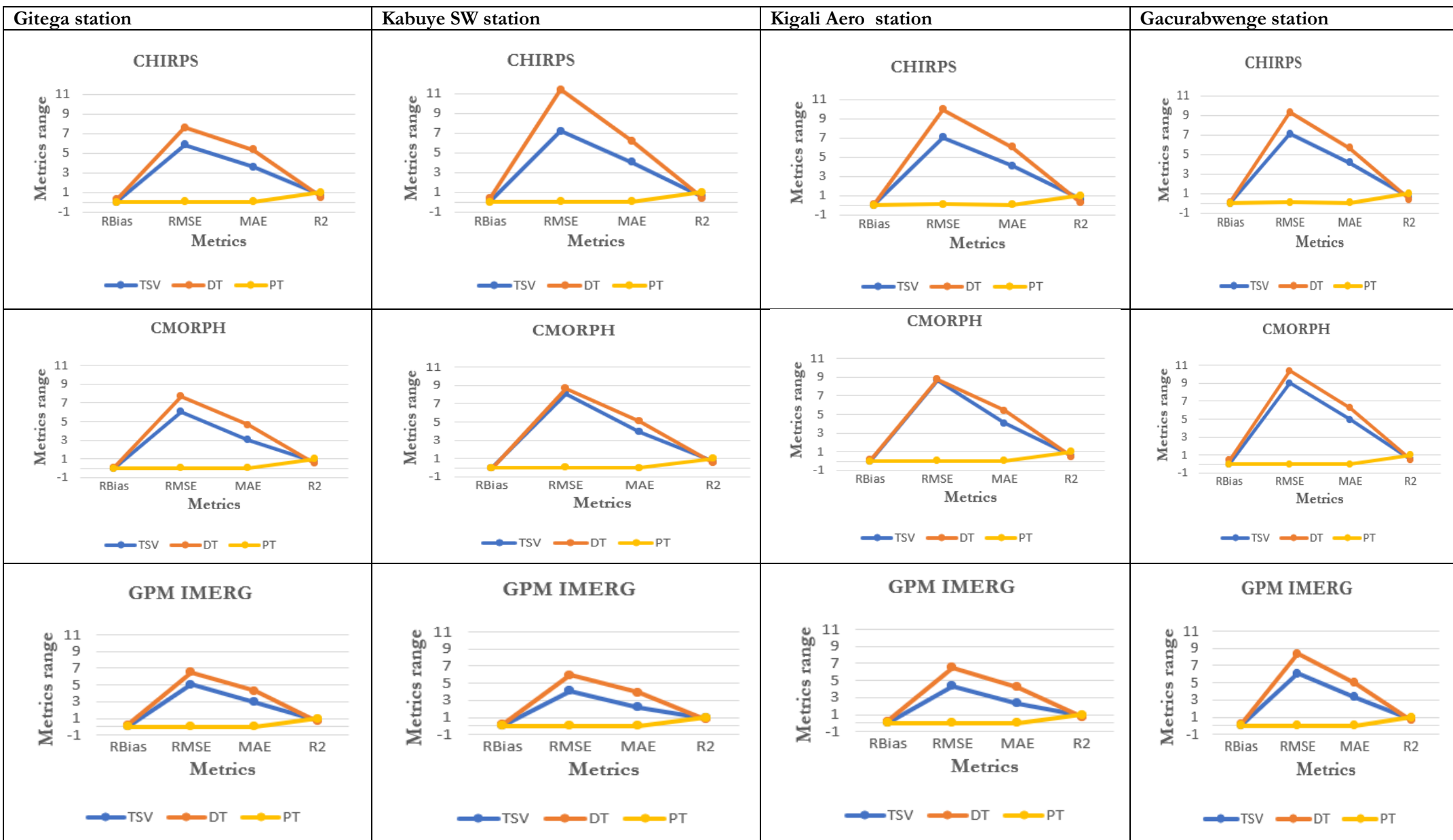
Figure 21: Results on testing of bias correction methods for four stations on the SRE products

The results show that the Power Transformation (PT) technique consistently outperformed the Time-Space Variable (TSV) and Distribution Transform (DT) methods across all SREs. This finding correlates with those of previous studies. For instance, the study carried out by Habib et al. (2014) and Xiao et al. (2022) demonstrated the effectiveness of the PT method in reducing bias and improving the accuracy of satellite-derived rainfall data. The PT correction effectively improved rainfall estimates in the Nyabarongo catchment area, as evidenced by a significant reduction in RMSE and MAE and an increase in R^2 values. The PT approach was proven for bias correction in SREs because it reduces errors and improves the correlation with ground-based observations in the Nyabarongo catchment area.

5.3.3.   Assessment of SREs bias correction effect

The analysis presented in Figure 22 indicates a comprehensive evaluation of various SREs both before and after applying different bias correction techniques within the Nyabarongo catchment area. The Taylor diagram visually compares these SREs based on the correlation coefficient, standard deviation, and centered Root Mean Square Error against ground observations, serving as a key reference for assessing the effectiveness of each SREs and bias correction technique.
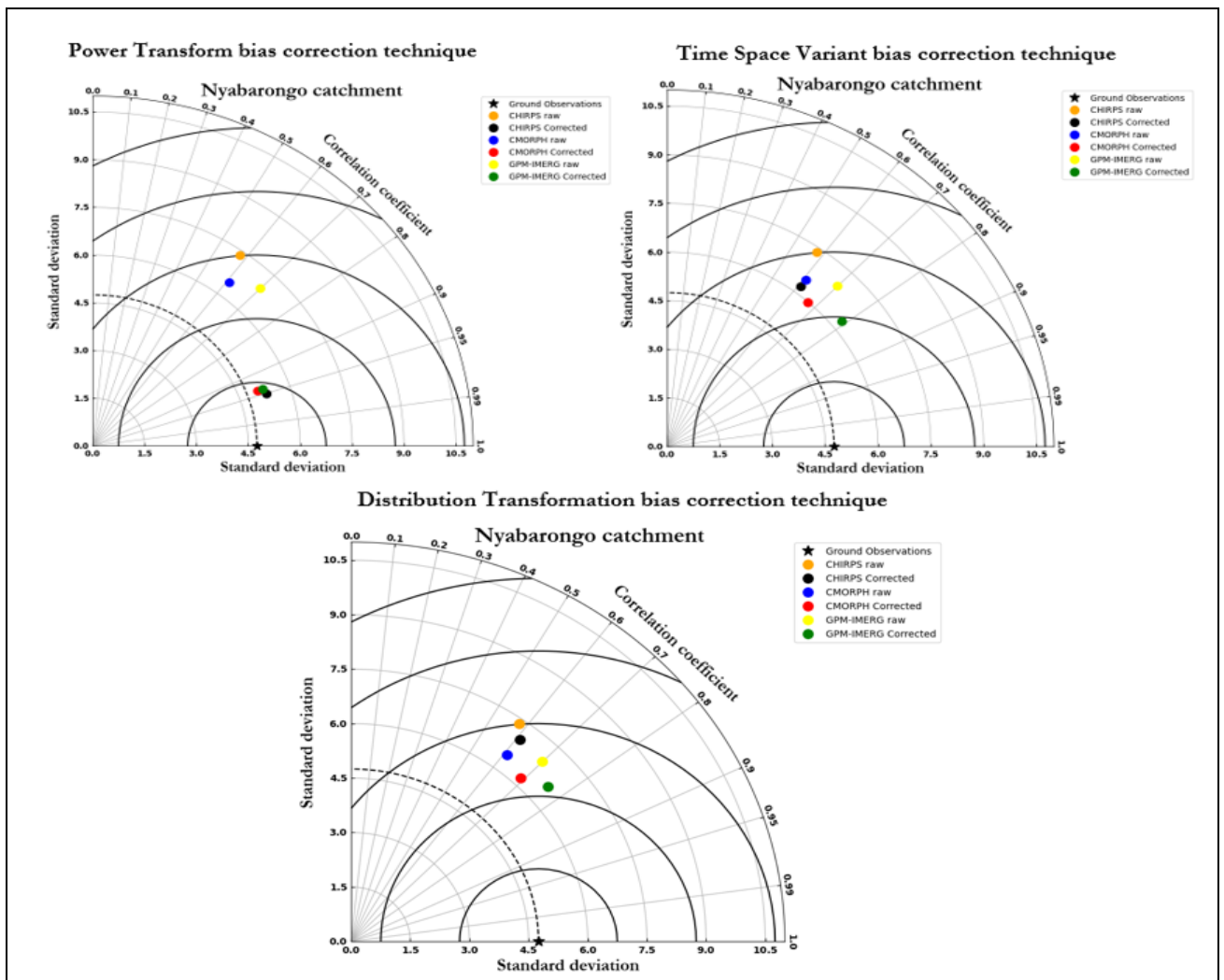
Figure 22: Taylor diagram showing the statistical performance of both corrected and uncorrected SREs

As illustrated in Figure 22, uncorrected CMORPH slightly outperformed the other uncorrected SRE products. The Power Transform bias correction technique significantly improves the performance accuracy of CMORPH, CHIRPS, and GPM-IMERG, reducing the standard deviation closer to that of in-situ measurements (4.75) from the values of 6.48 to 5.07, 7.35 to 5.29, and 6.93 to 5.22, respectively, and significantly enhancing the correlation from 0.61 to 0.94, 0.58 to 0.95 and 0.7 to 0.94, respectively, indicating a strong match in the pattern and distribution of rainfall estimates compared to reference in-situ measurements and other bias correction techniques. CMORPH, CHIRPS, and GPM-IMERG showed difference from the in situ standard deviation, with CMORPH having a slightly higher standard deviation compared to other SREs. The time-space variant bias correction technique showed a moderate improvement, especially in aligning the standard deviation of SREs with the in-situ data. The Distribution Transformation demonstrated a lower performance compared with other bias correction techniques, as detailed by the Taylor diagram in Figure 22.

5.3.4. Effects of error propagation in streamflow simulations

To evaluate how remote sensing data can affect the performance of rainfall runoff modelling in the Nyabarongo catchment area, this study specifically aimed to assess the effects of error propagation, mostly from both uncorrected and corrected SREs data, on streamflow simulations employing the HEC-HMS semi-distributed model in the Nyabarongo catchment. Figure 23 and appendix 4 present the statistical indicator ratios of error propagation for SREs applied to various combinations of developed models from different data sources.
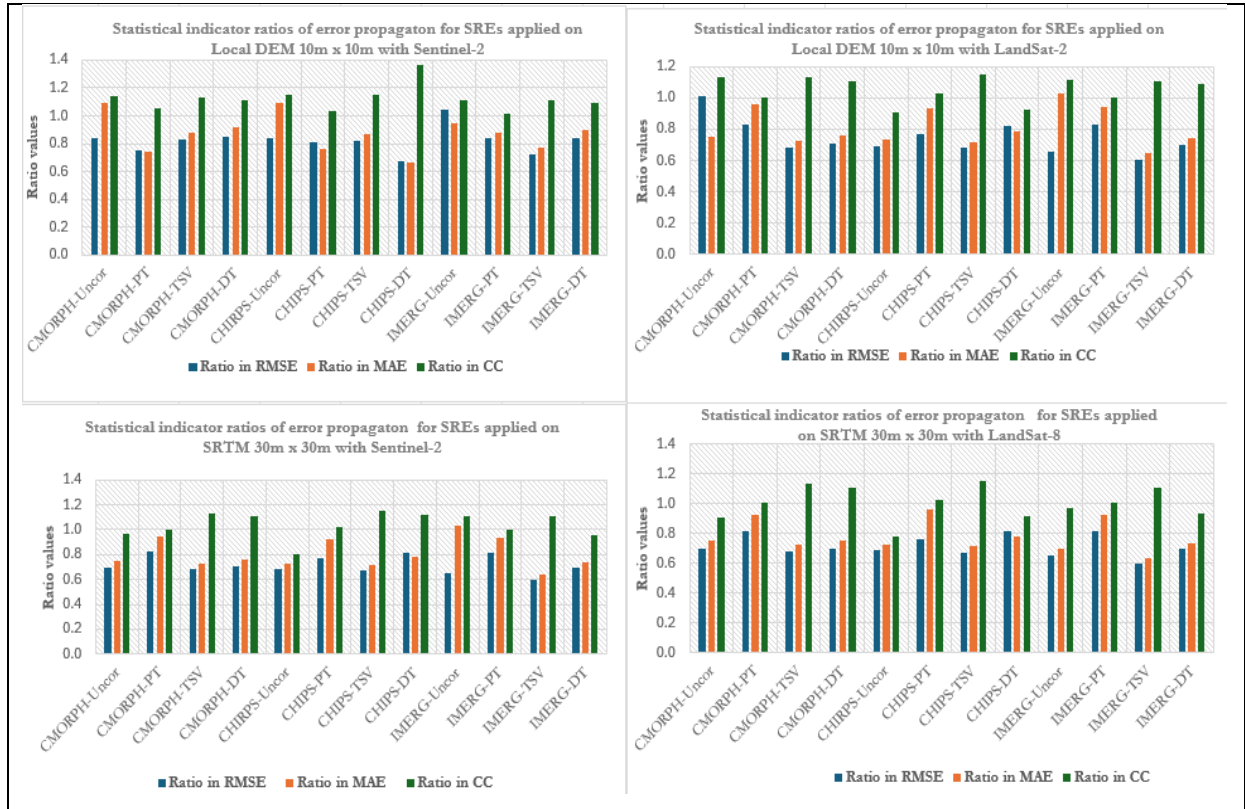
Figure 23: Error propagation effects on streamflow simulations

As illustrated in Figure 23, for the Local DEM 10m × 10m with Sentinel-2, the uncorrected CMORPH dataset showed significant error propagation in streamflow simulations with a MAE (MAE_{QS}/MAE_R) ratio of 1.1, which is larger than 1. The other ratios in this uncorrected product show error attenuation as fit with an acceptable range where $RMSE_{QS}/RMSE_R$ was 0.8, which is below 1, and CC_{QS}/CC_R was 1.14, which is greater than 1, suggesting attenuation of errors. The uncorrected CHIRPS dataset showed an increase in MAE ratio of 1.1, indicating the need for bias correction to achieve good streamflow simulations. In addition, uncorrected GPM-IMERG indicated an error propagation (increase) with an $RMSE_{QS}/RMSE_R$ of 1.04, which is above 1. Bias correction techniques generally reduced these errors, indicating notable attenuation of errors in the CMORPH, CHIRPS, and GPM-IMERG products, as depicted in Appendix 4. These results align with other studies conducted by Gumindoga et al., 2021 that focus the effectiveness of bias correction methods in reducing the propagation of errors from SREs to streamflow simulations where their findings cofirmed that the uncorrected CMORPH showed increases of error propagation compared to corrected dataset (Gumindoga et al., 2021).

Using Local DEM 10m × 10m with LandSat-8, the uncorrected CMORPH data again showed increase in errors with an RMSE ratio of 1.01, which was above 1. Uncorrected CHIRPS and GPM-IMERG also indicated an increase in errors with a CC_{QS}/CC_R of 0.91 which is lower than 1, and MAE_{QS}/MAE_R of 1.03, which is greater than 1 in GPM-IMERG. After applying bias correction techniques, the techniques showed improvements indicating effective error attenuation, except distribution transformation (DT) for CHIRPS,

which showed an increase in error with a CC_{QS}/CC_R of 0.92, which is lower than 1, as shown in Figure 23 and Appendix 4.

For the SRTM 10m × 10m with Sentinel-2, uncorrected CMORPH, CHIRPS and GPM IMERG datasets indicated an error increase with CC_{QS}/CC_R of 0.97 and 0.803, respectively, which are lower than 1 for CMORPH and CHIRPS and MAE_{QS}/MAE_R of 1.03, which is greater than 1 for GPM-IMERG. The bias correction techniques showed a reduction in errors for all SREs except for the distribution transformation for GPM-IMERG with a CC_{QS}/CC_R of 0.96, which is lower than 1, indicating an increase in errors. Lastly, the SRTM 10m × 10m with LandSat-2 combination, the uncorrected CMORPH, CHIRPS, and GPM-IMERG datasets showed a notable increase in errors with CC_{QS}/CC_R of 0.91, 0.78, and 0.97, respectively, which are lower than 1, suggesting error augmentation in streamflow simulations, as indicated in Appendix 4. The bias correction techniques reflected improved performance with error attenuation except distribution transformation (DT) for the CHIRPS and GPM-IMERG datasets with CC_{QS}/CC_R of 0.91 and 0.93, respectively, which are lower than 1, indicating an error increase in streamflow simulations.

Across all the developed models, it is evident that the Local DEM 10m × 10m with the Sentinel-2 model generally had lower error propagation ratios than the other models. This indicates that higher-resolution DEMs and LULC maps coupled with bias-corrected SREs provide more accurate streamflow simulations. Uncorrected SREs generally showed higher error propagation than corrected data.

5.3.5. Runoff coefficient assessment in streamflow

Figure 24 presents the runoff coefficient at the outlet in the Nyabarongo catchment area, comparing and indicating the outcomes of four models developed with various combinations of Digital Elevation Models (DEMs) and LULC data sources. These models were forced with various rainfall data sources, including in-situ rainfall data (reference) and both uncorrected and corrected SRE data.

The model using the Local DEM 10m × 10m with Sentinel-2 showed varying runoff coefficient values across different rainfall data sources. The in-situ rainfall served as a reference, with a runoff coefficient of approximately 0.61. Uncorrected CMORPH, CHIRPS and GPM-IMERG data significantly underestimated the runoff coefficient compared with in-situ rainfall at 0.40, 0.39 and 0.40 respectively, indicating the need for bias correction. The corrected SREs increased the runoff coefficient, with the Power Transform (PT) bias correction technique showing most closely runoff coefficient to the reference at about 0.59, 0.57 and 0.58 for CMORPH, CHIRPS and GPM-IMERG, respectively, indicating its higher performance in this model compared to other bias correction techniques. Furthermore, the time space variant and distribution transformation improved the runoff coefficient compared to the uncorrected SREs, as illustrated in Figure 24.
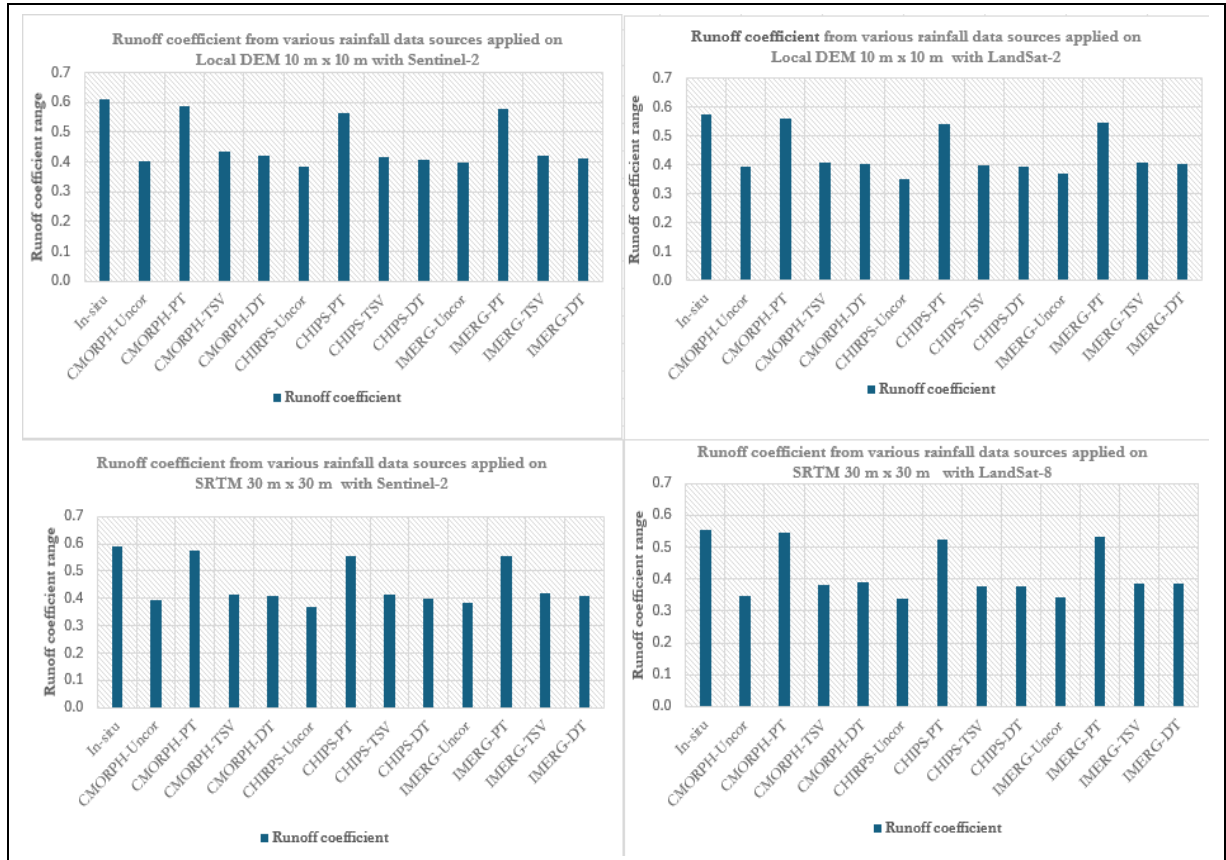
Figure 24: Runoff coefficient at the outlet in the Nyabarongo catchment area

For the Local DEM 10m × 10m with LandSat-2, the in-situ rainfall data generated a different runoff coefficient value of approximately 0.57 compared to the previously discussed model, highlighting the impact of LULC data. LandSat-8 LULC data, while still having a coarser resolution than Sentinel-2, can affect the precision of land cover classifications and subsequently influence runoff coefficient. Uncorrected SRE data also underestimated with in-situ runoff coefficient with 0.39, 0.35, and 0.37 for CMORPH, CHIRPS and GPM-IMEG, respectively. All bias correction techniques showed improvements, but notably, the Power Transform provided higher runoff coefficient compared to other techniques.

In SRTM DEM 30m × 30m with Sentinel-2, the in-situ rainfall data indicated a runoff coefficient of 0.59. Uncorrected CMORPH, CHIRPS and GPM-IMERG products still underestimated runoff coefficient compared to reference data with values of 0.40, 0.37 mm and 0.38, respectively. The bias correction techniques improved the runoff coefficient with the Power Transform, which showed a more runoff coefficient than the other techniques in this model.

Lastly, in the model using SRTM DEM 30m × 30m with LandSat-8, the in-situ rainfall showed a runoff coefficient of 0.56. Uncorrected CMORPH, CHIRPS and GPM-IMERG data showed lower values of runoff coefficient to 0.35, 0.34, and 0.34, respectively compared to in-situ. The bias-correction techniques increased the runoff coefficient, and the Power Transform outperformed the other bias-correction

techniques in this model. The combination of coarser DEM and LULC data can increase the errors in runoff estimations due to less precise representation of topographic features and land cover classifications, which may lead to different influences compared with finer resolution datasets.

The comparison indicated that the combination of Local DEM 10m × 10m with Sentinel-2 and in-situ rainfall produced the highest runoff coefficients across all models. Moreover, the study demonstrated that the Power Transform bias correction technique was the most effective in correcting errors in all SRE products, resulting in runoff coefficient estimates closest to those obtained from in-situ data. The DEM resolution and type of LULC data significantly affect the runoff coefficient. Specifically, this model using the Local DEM (10m × 10m) and Sentinel-2 consistently produced higher runoff coefficients compared to those using the SRTM DEM (30m × 30m) and LandSat-8 due to more detailed topographic representation and good captures land cover details, which can influence water flow and storage estimations and impact evapotranspiration rates and surface runoff estimations.

6. CONCLUSION AND RECOMMENDATION

6.1. Conclusion

This study aimed to evaluate how remote sensing data sources affect the performance of the HEC-HMS semi-distributed rainfall-runoff model in the Nyabarongo catchment area. One of the main problems encountered during this research was the quality of in-situ data, especially discharge data, which are necessary for model calibration and validation. The findings of this study show that the performance of rainfall-runoff model simulations is highly dependent on the quality and resolution of the input data such as Digital Elevation Models (DEMs), Land Use Land Cover (LULC) maps, and both in-situ and SREs.

To achieve the defined objectives of this study, four models were developed such as Local DEM (10m × 10m) with Sentinel-2, Local DEM (10m × 10m) with LandSat-8, SRTM (30m × 30m) with Sentinel-2, and SRTM (30m × 30m) with LandSat-8. Initially, the study assessed the quality and effects of DEMs, LULC data, and both in-situ rainfall data and SRE products on rainfall-runoff modelling. The comparison between the Local DEM 10m × 10m and SRTM DEM 30m × 30m showed that the Local DEM 10m × 10m with higher spatial resolution provided more details on catchment delineation and stream network analysis and low-volume water storage, which directly affected the precision of the runoff simulation compared with the coarser SRTM DEM 30m ×30m. The LULC data, Sentinel-2 and LandSat-8, which are essential for producing the Curve Numbers (CN), were used in the HEC-HMS semi-distributed model. The sentinel-2 data provided more detailed land cover types, which led to higher model performance in surface runoff simulation compared with the LandSat-8 data, resulting in less runoff simulations due to its lower resolution. The assessment of in-situ and SREs such as CMORPH, CHIRPS, and GPM-IMERG, showed variations in rainfall representation within the Nyabarongo catchment area. The analysis indicated that CHIRPS and GPM-IMERG overestimated the in-situ data, and CMORPH generally underestimated rainfall.

Relating to model performance, the study found that the model using the reference scenario, which combined Local DEM 10m × 10m, in-situ rainfall, and Sentinel-2 LULC map, showed the best performance compared to other developed models. This combination resulted in a high Nash-Sutcliffe Efficiency (NSE) of 0.89 and Relative Volume Error (RVE) of 2.9%, indicating a good match between the observed and simulated streamflow. Models that used lower resolution data, such as the SRTM DEM or LandSat-8 LULC map, showed reduced performance, with lower NSE and higher RVE values, demonstrating the critical role of high-resolution data in rainfall-runoff modelling. The study also assessed and compared in-situ rainfall data with uncorrected and corrected SREs. The analysis showed that uncorrected SREs generally performed less, leading to lower NSE and higher RVE values compared with acceptable ranges and reference scenario.

To perform error correction for SREs, the study focused on defining the optimal time window for bias correction techniques. After assessing different window sizes using the Sequential Window approach, the findings showed that a time window of 7 days was the most effective. Among the bias correction techniques tested, the Power Transform (PT) technique was the most effective compared with other techniques, such as Time Space Variant (TSV), and Distribution Transformation (DT), consistently improving the correlation between SREs and in-situ rainfall data. This technique significantly reduces errors, as indicated by improvements in RMSE and ME.

Furthermore, this study assessed how errors in different data sources propagate through the model, affecting the precision of streamflow simulations. It was found that uncorrected SREs showed error propagation in the model, leading to differences in streamflow simulations. However, after applying the bias correction technique, the errors were reduced, and the Power Transform performed well. Finally, the study assessed the effect of different data sources on the runoff coefficient in the Nyabarongo catchment area. The results indicated that the runoff coefficients varied significantly depending on the data source used. Models that received high-resolution local DEMs 10m× 10m, detailed LULC maps from Sentinel-2, in-situ and corrected SREs produced high runoff coefficients compared to other combinations.

In the absence or poor in-situ rainfall data, this study showed that SREs, after appropriate bias correction, can be effectively applied in the Nyabarongo catchment area. The results indicated that, following Power Transform (PT) bias correction, the findings from SREs are relatively close to the outcomes from in-situ rainfall data, making them an effective origin of data for rainfall-runoff modelling in regions with limited in-situ data such as Nyabarongo catchment area.

6.2.   Recommendation

Different limitations were encountered during conducting this study, particularly related to data quality and the use of WetSpa modelling tools. Based on the findings of this study, the following recommendations are proposed to improve future studies.

- The study faced problems related to in-situ data due to the unequal distribution of rain gauges and poor quality of discharge data, which affect the performance of the model during calibration. To address this issue, it is recommended that the Government of Rwanda invest in advanced data collection systems. This should include increasing the number of rain gauges and improving the methods used to record discharge data. Improved data quality and availability will support good planning and forecasting of floods occurring in Rwanda using hydrologic and hydrodynamic models in Rwanda.

- Due to time constraints, the study was unable to fully optimize the α and β coefficients for the Power Transform bias correction technique across all years of time series. For future studies, it is recommended that sufficient time be allocated to optimize these coefficients. This ensures that the bias correction process is more accurate, leading to a better performance of the rainfall-runoff model.

- During this study, I planned to use fully distributed WetSpa model. Therefore, the model failed because it was designed and compatible with the older ArcView 3.2 software version and expired XP window, which are no longer used. It is recommended that developers update the WetSpa model to work and compatible with advanced GIS software such as the latest versions of ArcGIS. Additionally, future studies could use other advanced distributed rainfall runoff models that provide detailed representations of spatial variations within the catchment compared to a semi-distributed model, which will improve the performance of runoff simulations using the model.

6.3. Ethical statement and considerations

This study was conducted in compliance with the ethical guidelines and policies of the University of Twente. It used both confidential and publicly available data on open online datasets, with careful consideration given to the ethical handling of these datasets.

Confidential data, such as in-situ rainfall and streamflow related data, were obtained from Rwanda. As citizen of Rwanda, I requested these datasets through formal requests from the Rwanda Water Board and Rwanda Meteorological Agency. Additionally, the Local DEM 10m × 10m was acquired from the Rwanda National Land Authority. These datasets were used in compliance with the legal frameworks governing data use in Rwanda. The study also used publicly available datasets, such as SRE products (CHIRPS, CMORPH, and GPM-IMERG), soil data from FAO, and LULC maps from Sentinel-2, LandSat-8 and SRTM 30m × 30m. These datasets were downloaded from open-source platforms.

Given the recognized limitations and quality issues associated with in-situ data in Rwanda, particularly streamflow data, a lot effort has been used to process these datasets to improve them before use in model calibration. All data, especially confidential data, were handled carefully with respect of legal compliance of the Rwandan government to ensure privacy in line with the ethical standards required.

LIST OF REFERENCES

Abraham, S., Huynh, C., & Vu, H. (2019). Classification of Soils into Hydrologic Groups Using Machine Learning. International Conference on Data Technologies and Applications, 5(1). https://doi.org/10.3390/DATA5010002

Afonso de Oliveira Serrão, E., Silva, M. T., Ferreira, T. R., Paiva de Ataide, L. C., Assis dos Santos, C., Meiguins de Lima, A. M., de Paulo Rodrigues da Silva, V., de Assis Salviano de Sousa, F., & Cardoso Gomes, D. J. (2022). Impacts of land use and land cover changes on hydrological processes and sediment yield determined using the SWAT model. International Journal of Sediment Research, 37(1), 54–69. https://doi.org/10.1016/j.ijsrc.2021.04.002

Aghakouchak, A., Mehran, A., Norouzi, H., & Behrangi, A. (2012). Systematic and random error components in satellite precipitation data sets. Geophysical Research Letters, 39(9), 3–6. https://doi.org/10.1029/2012GL051592

Ahn, G., Gordon, S., & Merry, C. (2014). Impacts of Remotely Sensed Land Use Data on Watershed Hydrologic Change Assessment.

Al-Khafaji, M., & Al-Sweiti, F. H. (2017). Integrated Impact of Digital Elevation Model and Land Cover Resolutions on Simulated Runoff by SWAT Model. Hydrology and Earth System Sciences Discussions. https://doi.org/10.5194/HESS-2017-653

Amekudzi, L. K., Osei, M. A., Atiah, W. A., Aryee, J. N. A., Ahiataku, M. A., Quansah, E., Preko, K., Danuor, S. K., & Fink, A. H. (2016a). Validation of TRMM and FEWS Satellite Rainfall Estimates with Rain Gauge Measurement over Ashanti Region, Ghana. Applied Categorical Structures, 06(04), 500–518. https://doi.org/10.4236/ACS.2016.64040

Amekudzi, L. K., Osei, M. A., Atiah, W. A., Aryee, J. N. A., Ahiataku, M. A., Quansah, E., Preko, K., Danuor, S. K., & Fink, A. H. (2016b). Validation of TRMM and FEWS Satellite Rainfall Estimates with Rain Gauge Measurement over Ashanti Region, Ghana. Atmospheric and Climate Sciences, 06(04), 500–518. https://doi.org/10.4236/acs.2016.64040

Amorati, R., Alberoni, P. P., Levizzani, V., & Nanni, S. (2000). IR-based satellite and radar rainfall estimates of convective storms over northern Italy. Meteorological Applications, 7(1), 1–18. https://doi.org/10.1017/S1350482700001328

Aonashi, K., & Ferraro, R. R. (2020). Microwave Sensors, Imagers and Sounders. Advances in Global Change Research, 67, 63–81. https://doi.org/10.1007/978-3-030-24568-9_4

Ara, Z., & Zakwan, M. (2018). Rainfall runoff modelling for Eastern Canal Basin. Water and Energy International, 61RNI(6), 63–67.

Arlen D. Feldman. (2000). Hydrologic Modeling System Technical Reference Manual. Hydrologic Modeling System HEC-HMS Technical Reference Manual, March, 148.

Asadi, A., & Boustani, F. (2013). Performance Evaluation of the HEC-HMS Hydrologic Model for Lumped and Semi-distributed Stormflow Simulation (Study Area:Delibajak Basin).

Babaremu, K. O. (2024). A Review of Current Understanding and Implications for Watershed and Water. March. https://doi.org/10.5281/zenodo.10049652

Ball, J. E., & Luk, K. C. (1998). Modeling Spatial Variability of Rainfall over a Catchment. Journal of Hydrologic Engineering, 3(2), 122–130. https://doi.org/10.1061/(asce)1084-0699(1998)3:2(122)

Belayneh, A., Sintayehu, G., Gedam, K., & Muluken, T. (2020). Evaluation of satellite precipitation products using HEC-HMS model. Modeling Earth Systems and Environment, 6(4), 2015–2032. https://doi.org/10.1007/s40808-020-00792-z

Beven, K. (2012). Rainfall-Runoff Modelling. In Rainfall-Runoff Modelling. https://doi.org/10.1002/9781119951001

Bitew, M. M., & Gebremichael, M. (2011a). Evaluation of satellite rainfall products through hydrologic simulation in a fully distributed hydrologic model. Water Resources Research, 47(6). https://doi.org/10.1029/2010WR009917

Bitew, M. M., & Gebremichael, M. (2011b). Evaluation of satellite rainfall products through hydrologic simulation in a fully distributed hydrologic model. Water Resources Research, 47(6). https://doi.org/10.1029/2010WR009917

Brocca, L., Filippucci, P., Hahn, S., Ciabatta, L., Massari, C., Camici, S., Schüller, L., Bojkov, B., & Wagner, W. (2019). SM2RAIN-ASCAT (2007-2018): Global daily satellite rainfall data from ASCAT soil moisture observations. Earth System Science Data, 11(4), 1583–1601. https://doi.org/10.5194/essd-11-1583-2019

Chalkias, C., Stathopoulos, N., Kalogeropoulos, K., & Karymbalis, E. (2016). Applied Hydrological Modeling with the Use of Geoinformatics: Theory and Practice. Empirical Modeling and Its Applications. https://doi.org/10.5772/62824

Chow, V. Te, Maidment, D. R., Mays, L. W., & Ven Te Chow, David R. Maidment, L. W. M. (1988). Applied Hydrology Chow 1988.pdf (pp. 1–294).

Devia, G. K., Ganasri, B. P., & Dwarakish, G. S. (2015). A Review on Hydrological Models. Aquatic Procedia, 4(December), 1001–1007. https://doi.org/10.1016/j.aqpro.2015.02.126

Dold, B. (2016). Infrared Radiation in Modern Technology Infrared Radiation in Modern Technology. Brigham Young University, April, 8. https://doi.org/10.13140/RG.2.1.3430.4409

D'souza, G., Barrett, E. C., & Power, C. H. (1990). Satellite rainfall estimation techniques using visible and infrared imagery. Remote Sensing Reviews, 4(2), 379–414. https://doi.org/10.1080/02757259009532111

Elaji, A., & Ji, W. (2020). Urban Runoff Simulation: How Do Land Use/Cover Change Patterning and Geospatial Data Quality Impact Model Outcome? Water, 12(10). https://doi.org/10.3390/W12102715

Etchanchu, J., Rivalland, V., Gascoin, S., Cros, J., Brut, A., & Boulet, G. (2017). Effects of multi-temporal high-resolution remote sensing products onsimulated hydrometeorological variables in a cultivated area(southwestern France). Hydrology and Earth System Sciences Discussions. https://doi.org/10.5194/HESS-2016-661

Feudale, L., & Manzato, A. (2014). Cloud-to-ground lightning distribution and its relationship with orography and anthropogenic emissions in the Po Valley. Journal of Applied Meteorology and Climatology, 53(12), 2651–2670. https://doi.org/10.1175/JAMC-D-14-0037.1

Forkuor, G., Dimobe, K., Serme, I., & Tondoh, J. E. (2018a). Landsat-8 vs. Sentinel-2: examining the added value of sentinel-2's red-edge bands to land-use and land-cover mapping in Burkina Faso. GIScience & Remote Sensing, 55(3), 331–354. https://doi.org/10.1080/15481603.2017.1370169

Forkuor, G., Dimobe, K., Serme, I., & Tondoh, J. E. (2018b). Landsat-8 vs. Sentinel-2: examining the added value of sentinel-2's red-edge bands to land-use and land-cover mapping in Burkina Faso. GIScience & Remote Sensing, 55(3), 331–354. https://doi.org/10.1080/15481603.2017.1370169

Funk, C., Peterson, P., Landsfeld, M., Pedreros, D., Verdin, J., Shukla, S., Husak, G., Rowland, J., Harrison, L., Hoell, A., & Michaelsen, J. (2015). The climate hazards infrared precipitation with stations - A new environmental record for monitoring extremes. Scientific Data, 2, 1–21. https://doi.org/10.1038/sdata.2015.66

Fylstra, D., Lasdon, L., Watson, J., & Waren, A. (1998). Design and use of the Microsoft Excel Solver. Interfaces, 28(5), 29–55. https://doi.org/10.1287/inte.28.5.29

Gebre, S. L. (2015). Application of the HEC-HMS Model for Runoff Simulation of Upper Blue Nile River Basin. Journal of Waste Water Treatment & Analysis, 06(02). https://doi.org/10.4172/2157-7587.1000199

Getnet Adugna. (2021). Flood Modeling of Jemo River Catchement in Addis Ababa City, Ethiopia. International Journal of Engineering Research And, V10(01), 86–93. https://doi.org/10.17577/ijertv10is010035

Godara. (2019). Choosing an Appropriate Hydrologic Model. 1–18.

Goez, H. H. (2011). Runoff modelling of the Upper Cabra river basin Panama.

Goshime, D. W., Absi, R., & Ledésert, B. (2019). Evaluation and Bias Correction of CHIRP Rainfall Estimate for Rainfall-Runoff Simulation over Lake Ziway Watershed, Ethiopia. Hydrology, 6(3). https://doi.org/10.3390/HYDROLOGY6030068

Govender, T., Dube, T., & Shoko, C. (2022). Remote sensing of land use-land cover change and climate variability on hydrological processes in Sub-Saharan Africa: key scientific strides and challenges. Geocarto International, 37(25), 10925–10949. https://doi.org/10.1080/10106049.2022.2043451

Guermazi, E., Milano, M., & Reynard, E. (2019). Performance evaluation of satellite-based rainfall products on hydrological modeling for a transboundary catchment in northwest Africa. Theoretical and Applied Climatology, 138(3–4), 1695–1713. https://doi.org/10.1007/s00704-019-02928-3

Guide, U., & Manual, T. R. (2008). Technical Reference Manual. Texas Instruments, December, 155.

Gumindoga, W., Rientjes, T. H. M., Haile, A. T., Makurira, H., & Reggiani, P. (2016). Bias correction schemes for CMORPH satellite rainfall estimates in the Zambezi River Basin. Hydrology and Earth System Sciences Discussions, 0(February), 1–36. https://doi.org/10.5194/hess-2016-33

Gumindoga, W., Rientjes, T. H. M., Haile, A. T., Reggiani, P., & Makurira, H. (2021). Journal of Hydrology : Regional Studies Propagation of CMORPH rainfall errors to REW streamflow simulation mismatch in the upper Zambezi Basin. Journal of Hydrology: Regional Studies, 38(July 2020), 100966. https://doi.org/10.1016/j.ejrh.2021.100966

Gumindoga, W., Rientjes, T. H. M., Tamiru Haile, A., Makurira, H., & Reggiani, P. (2019). Performance of bias-correction schemes for CMORPH rainfall estimates in the Zambezi River basin. Hydrology and Earth System Sciences, 23(7), 2915–2938. https://doi.org/10.5194/hess-23-2915-2019

Hanif, F., Kanae, S., Farooq, R., Iqbal, M. R., & Petroselli, A. (2023). Impact of Satellite-Derived Land Cover Resolution Using Machine Learning and Hydrological Simulations. Remote Sensing, 15(22). https://doi.org/10.3390/RS15225338

Hong, Y., & Adler, R. F. (2008). Estimation of global SCS curve numbers using satellite remote sensing and geospatial data. International Journal of Remote Sensing, 29(2), 471–477. https://doi.org/10.1080/01431160701264292

Hou, J., Li, X., Pan, Z., Wang, J., & Wang, R. (2021). Effect of digital elevation model spatial resolution on depression storage. Hydrological Processes, 35(10). https://doi.org/10.1002/HYP.14381

Huffman, G. J., Stocker, E. F., Bolvin, D. T., Nelkin, E. J., & Jackson, T. (2019). GPM IMERG Early Precipitation L3 Half Hourly 0.1 degree x 0.1 degree V06. Goddard Earth Sciences Data and Information Services Center (GES DISC), March.

Hussein, A. A., & Baylar, A. (2023). Hydrological Model Evaluation of Ground, GPM IMERG, and CHIRPS precipitation data for Shabelle Basin in Ethiopia. Journal of Electronics,Computer Networking and Applied Mathematics, 31, 41–60. https://doi.org/10.55529/JECNAM.31.41.60

Islam, Z. (2011). A Review on Physically Based Hydrologic Modeling on Submitted by Zahidul Islam Department of Civil and Environmental Engineering University of Alberta May , 2011. February, 46. https://doi.org/10.13140/2.1.4544.5924

J. Herben Huddleston. (1996). How soil properties affect groundwater vulnerability to pesticide contamination. Oregon State University Extension Service, October.

Jakovljević, G., Govedarica, M., & Álvarez-Taboada, F. (2018). Waterbody mapping: a comparison of remotely sensed and GIS open data sources. International Journal of Remote Sensing, 40(8), 2936–2964. https://doi.org/10.1080/01431161.2018.1538584

Joyce, R. J., Janowiak, J. E., Arkin, P. A., & Xie, P. (2004). CMORPH: A method that produces global precipitation estimates from passive microwave and infrared data at high spatial and temporal resolution. Journal of Hydrometeorology, 5(3), 487–503. https://doi.org/10.1175/1525-7541(2004)005<0487:CAMTPG>2.0.CO;2

Khan, S. I., Hong, Y., Wang, J., Yilmaz, K. K., Gourley, J. J., Adler, R. F., Brakenridge, G. R., Policelli, F., Habib, S., & Irwin, D. (2011). Satellite Remote Sensing and Hydrologic Modeling for Flood Inundation Mapping in Lake Victoria Basin: Implications for Hydrologic Prediction in Ungauged Basins. IEEE Transactions on Geoscience and Remote Sensing, 49(1 PART 1), 85–95. https://doi.org/10.1109/TGRS.2010.2057513

Kidd, C., Kniveton, D. R., Todd, M. C., & Bellerby, T. J. (2003). Satellite rainfall estimation using combined passive microwave and infrared algorithms. Journal of Hydrometeorology, 4(6), 1088–1104. https://doi.org/10.1175/1525-7541(2003)004<1088:SREUCP>2.0.CO;2

Knudsen, J., Thomsen, A., & Refsgaard, J. C. (1986). WATBAL: A Semi-Distributed, Physically Based Hydrological Modelling System. Hydrology Research, 17(4–5), 347–362. https://doi.org/10.2166/NH.1986.0026

Koneti, S., Sunkara, S. L., & Roy, P. S. (2018). Hydrological Modeling with Respect to Impact of Land-Use and Land-Cover Change on the Runoff Dynamics in Godavari River Basin Using the HEC-HMS Model. ISPRS Int. J. Geo Inf., 7(6). https://doi.org/10.3390/IJGI7060206

Kuc, G., & Chormański, J. (2019). SENTINEL-2 IMAGERY FOR MAPPING AND MONITORING IMPERVIOUSNESS IN URBAN AREAS. The International Archives of the Photogrammetry, Remote Sensing and Spatial Information Sciences, 42(1/W2), 43–47. https://doi.org/10.5194/ISPRS-ARCHIVES-XLII-1-W2-43-2019

Lanza, L. G., & Vuerich, E. (2009). The WMO Field Intercomparison of Rain Intensity Gauges. Atmospheric Research, 94(4), 534–543. https://doi.org/10.1016/j.atmosres.2009.06.012

Lee, G., Tachikawa, Y., & Takara, K. (2009). Interaction between Topographic and Process Parameters due to the Spatial Resolution of DEMs in Distributed Rainfall-Runoff Modeling. Journal of Hydrologic Engineering, 14(10), 1059–1069. https://doi.org/10.1061/(ASCE)HE.1943-5584.0000098

Legates, D. R., & McCabe, G. J. (1999). Water Resources Research - 1999 - Legates - Evaluating the use of goodness-of-fit Measures in hydrologic and.pdf. In Water Resour. Res (Vol. 35, pp. 233–241).

Levizzani, V., Porcú, F., Marzano, F. S., Mugnai, A., Smith, E. A., & Prodi, F. (2007). Investigating a SSM/I microwave algorithm to calibrate Meteosat infrared instantaneous rainrate estimates. Meteorological Applications, 3(1), 5–17. https://doi.org/10.1002/MET.5060030102

Ma, Q., Zavattero, E., Du, M., Vo, N. D., & Gourbesville, P. (2016). Assessment of High Resolution Topography Impacts on Deterministic Distributed Hydrological Model in Extreme Rainfall-runoff Simulation. Procedia Engineering, 154(December), 601–608. https://doi.org/10.1016/j.proeng.2016.07.558

Manyifika, M. (2015). Diagnostic assessment on urban floods using satellite data and hydrologic models in Kigali, Rwanda. Thesis, 88.

Marzano, F. S., Palmacci, M., Cimini, D., Giuliani, G., & Turk, F. J. (2004). Multivariate statistical integration of Satellite infrared and microwave radiometric measurements for rainfall retrieval at the geostationary scale. IEEE Transactions on Geoscience and Remote Sensing, 42(5), 1018–1032. https://doi.org/10.1109/TGRS.2003.820312

McCauley, A., Jones, C., & Jacobsen, J. (2005). Basic Soil Properties. Soil and Water, 1–12.

Meng, C., Mo, X., Liu, S., & Hu, S. (2021). Extensive evaluation of IMERG precipitation for both liquid and solid in Yellow River source region. Atmospheric Research, 256(March), 105570. https://doi.org/10.1016/j.atmosres.2021.105570

Moges, D. M., Virro, H., Kmoch, A., Cibin, R., Rohith, A. N., Martínez-Salvador, A., Conesa-García, C., & Uuemaa, E. (2023a). How does the choice of DEMs affect catchment hydrological modeling? Science of the Total Environment, 892. https://doi.org/10.1016/J.SCITOTENV.2023.164627

Moges, D. M., Virro, H., Kmoch, A., Cibin, R., Rohith, A. N., Martínez-Salvador, A., Conesa-García, C., & Uuemaa, E. (2023b). How does the choice of DEMs affect catchment hydrological modeling? Science of the Total Environment, 892. https://doi.org/10.1016/J.SCITOTENV.2023.164627

Moradkhani, H., & Sorooshian, S. (2009). General Review of Rainfall-Runoff Modeling: Model Calibration, Data Assimilation, and Uncertainty Analysis. Hydrological Modelling and the Water Cycle, 1–24. https://doi.org/10.1007/978-3-540-77843-1_1

Morrison, R. E., Bryant, C. M., Terejanu, G., Prudhomme, S., & Miki, K. (2013). Data partition methodology for validation of predictive models. Computers and Mathematics with Applications, 66(10), 2114–2125. https://doi.org/10.1016/j.camwa.2013.09.006

Mushore, T., Dube, T., Shoko, C., Mazvimavi, D., & Masocha, M. (2019). Progress in rainfall-runoff modelling – contribution of remote sensing. Transactions of the Royal Society of South Africa, 74(2), 173–179. https://doi.org/10.1080/0035919X.2019.1589600

Najmaddin, P. M., Whelan, M. J., & Balzter, H. (2017). Estimating daily reference evapotranspiration in a semi-arid region using remote sensing data. Remote Sensing, 9(8). https://doi.org/10.3390/rs9080779

Nasiri, V., Deljouei, A., Moradi, F., Sadeghi, S., & Borz, S. (2022). Land Use and Land Cover Mapping Using Sentinel-2 , Landsat-8 Two Composition Methods. Remote Sensing, 14(9), 1977.

Ntawukuriryayo. (2022). Application of Satellite-based rainfall estimates and Inundation extent for Flood in the Sebeya Catchment, Rwanda. August, 87.

Omondi, C. K. (2017). Assessment of bias corrected satellite rainfall products for streamflow simulation : A TOPMODEL application in the Kabompo River Basin , Zambia Assessment of bias corrected satellite rainfall products for streamflow simulation : A TOPMODEL application in .

Rawls, W. J., Shalaby, A., & McCuen, R. H. (1981). Evaluation of Methods for Determining Urban Runoff Curve Numbers. Transactions of the ASABE, 24(6), 1562–1566. https://doi.org/10.13031/2013.34490

REMA. (2019). Republic of Rwanda Rwanda Environment Management Authority Assessment of Climate Change Vulnerability in.

Richer-de-Forges, A. C., Chen, Q., Baghdadi, N., Chen, S., Gomez, C., Jacquemoud, S., Martelet, G., Mulder, V. L., Urbina-Salazar, D., Vaudour, E., Weiss, M., Wigneron, J. P., & Arrouays, D. (2023). Remote Sensing Data for Digital Soil Mapping in French Research—A Review. Remote Sensing, 15(12), 1–38. https://doi.org/10.3390/rs15123070

Rientjes, T. H. M. (2016). Hydrologic modelling for Integrated Water Resource Assessments. Lecture Book for Modules 9-10 Surface Water Stream, March, 255.

Rietz, D. A., & Hawkins, R. H. (2004). Effects of land use on runoff Curve Number. Watershed Management and Operations Management 2000, 105. https://doi.org/10.1061/40499(2000)110

Rocha, J., Duarte, A., Silva, M., Fabres, S., Vasques, J., Revilla-Romero, B., & Quintela, A. (2020a). The Importance of High Resolution Digital Elevation Models for Improved Hydrological Simulations of a Mediterranean Forested Catchment. Remote Sensing, 12(20), 1–17. https://doi.org/10.3390/RS12203287

Rocha, J., Duarte, A., Silva, M., Fabres, S., Vasques, J., Revilla-Romero, B., & Quintela, A. (2020b). The Importance of High Resolution Digital Elevation Models for Improved Hydrological Simulations of a Mediterranean Forested Catchment. Remote Sensing, 12(20), 1–17. https://doi.org/10.3390/RS12203287

Rocha, J., Duarte, A., Silva, M., Fabres, S., Vasques, J., Revilla-Romero, B., & Quintela, A. (2020c). The Importance of High Resolution Digital Elevation Models for Improved Hydrological Simulations of a Mediterranean Forested Catchment. Remote Sensing, 12(20), 1–17. https://doi.org/10.3390/RS12203287

Roostaee, M., & Deng, Z. (2020). Effects of Digital Elevation Model Resolution on Watershed-Based Hydrologic Simulation. Water Resources Management, 34(8), 2433–2447. https://doi.org/10.1007/S11269-020-02561-0

RoR, R. of R. (2018). Upper Nyabarongo Catchment Management Plan (2018-2014). Republic of Rwanda/ Ministry of Environments, 1–317.

Sanchez, P. A., Ahamed, S., Carré, F., Hartemink, A. E., Hempel, J., Huising, J., Lagacherie, P., McBratney, A. B., McKenzie, N. J., De Lourdes Mendonça-Santos, M., Minasny, B., Montanarella, L., Okoth, P., Palm, C. A., Sachs, J. D., Shepherd, K. D., Vågen, T. G., Vanlauwe, B., Walsh, M. G., … Zhang, G. L. (2009). Digital soil map of the world. Science, 325(5941), 680–681. https://doi.org/10.1126/science.1175084

Santos, F., Tevar, F., Sablan, K. A., & Lagmay, E. (2022). Evaluation of the Effect of Varying Digital Elevation Model (DEM) Resolutions on Hydrologic Model Performance of a Tropical Watershed. Proceedings - 2022 2nd International Conference in Information and Computing Research, ICORE 2022, 170–176. https://doi.org/10.1109/ICORE58172.2022.00050

Sartika, F. A., Sutjiningsih, D., & Anggraheni, E. (2020a). Analysis of classification hydrologic soil group distribution based on infiltration rate of horton method in the upper Ciliwung watershed. IOP Conference Series: Earth and Environmental Science, 426(1). https://doi.org/10.1088/1755-1315/426/1/012030

Sartika, F. A., Sutjiningsih, D., & Anggraheni, E. (2020b). Analysis of classification hydrologic soil group distribution based on infiltration rate of horton method in the upper Ciliwung watershed. IOP Conference Series: Earth and Environmental Science, 426(1). https://doi.org/10.1088/1755-1315/426/1/012030

Sharma, D., Gupta, A. Das, & Babel, M. S. (2007). Spatial disaggregation of bias-corrected GCM precipitation for improved hydrologic simulation: Ping River Basin, Thailand. Hydrology and Earth System Sciences, 11(4), 1373–1390. https://doi.org/10.5194/HESS-11-1373-2007

Singh, V. P., & Woolhiser, D. A. (2003). Mathematical Modeling of Watershed Hydrology. Perspectives in Civil Engineering: Commemorating the 150th Anniversary of the American Society of Civil Engineers, 345–367. https://doi.org/10.1061/(asce)1084-0699(2002)7:4(270)

Smith, B., & Sandwell, D. (2003). Accuracy and resolution of shuttle radar topography mission data. Geophysical Research Letters, 30(9), 3–6. https://doi.org/10.1029/2002GL016643

Solakian, J., Maggioni, V., & Godrej, A. (2020). Investigating the error propagation from satellite-based input precipitation to output water quality indicators simulated by a hydrologic model. Remote Sensing, 12(22), 1–23. https://doi.org/10.3390/rs12223728

Stisen, S., & Sandholt, I. (2010). Evaluation of remote-sensing-based rainfall products through predictive capability in hydrological runoff modelling. Hydrological Processes, 24(7), 879–891. https://doi.org/10.1002/hyp.7529

Trinh, T., Kavvas, M. L., Ishida, K., Ercan, A., Chen, Z. Q., Anderson, M. L., Ho, C., & Nguyen, T. (2018). Integrating global land-cover and soil datasets to update saturated hydraulic conductivity parameterization in hydrologic modeling. Science of the Total Environment, 631–632, 279–288. https://doi.org/10.1016/J.SCITOTENV.2018.02.267

Troutman, B. M. (1983). Runoff prediction errors and bias in parameter estimation induced by spatial variability of precipitation. Water Resources Research, 19(3), 791–810. https://doi.org/10.1029/WR019I003P00791

USACE. (2022). HEC-HMS User's Manual. US Army Corps of Engineers Hydrologic Engineering Center.

Vaze, J., & Teng, J. (2007). Impact of DEM Resolution on Topographic Indices and Hydrological Modelling Results.

Vernimmen, R. R. E., Hooijer, A., Mamenun, Aldrian, E., & Van Dijk, A. I. J. M. (2012). Evaluation and bias correction of satellite rainfall data for drought monitoring in Indonesia. Hydrology and Earth System Sciences, 16(1), 133–146. https://doi.org/10.5194/hess-16-133-2012

Vrugt, J. A., Diks, C. G. H., Gupta, H. V., Bouten, W., & Verstraten, J. M. (2005). Improved treatment of uncertainty in hydrologic modeling: Combining the strengths of global optimization and data assimilation. Water Resources Research, 41(1), 1–17. https://doi.org/10.1029/2004WR003059

Zambrano-Bigiarini, M., Nauditt, A., Birkel, C., Verbist, K., & Ribbe, L. (2016). Temporal and spatial evaluation of satellite-based rainfall estimates across the complex topographical and climatic gradients of Chile. Hydrology and Earth System Sciences, 21(2), 1295–1320. https://doi.org/10.5194/HESS-21-1295-2017

Zelelew, D. G., & Melesse, A. M. (2018). Applicability of a spatially semi-distributed hydrological model for watershed scale runoff estimation in Northwest Ethiopia. Water (Switzerland), 10(7). https://doi.org/10.3390/w10070923

Zhang, C., Chen, X., Shao, H., Chen, S., Liu, T., Chen, C., Ding, Q., & Du, H. (2018). Evaluation and intercomparison of high-resolution satellite precipitation estimates-GPM, TRMM, and CMORPH in the Tianshan Mountain Area. Remote Sensing, 10(10). https://doi.org/10.3390/rs10101543

Zhang, W., & Montgomery, D. R. (1994). Digital elevation model grid size, landscape representation, and hydrologic simulations. Water Resources Research, 30(4), 1019–1028. https://doi.org/10.1029/93WR03553

Zhou, Y. (2020). Watershed Hydrology and Land-Use and Land-Cover Change (LULCC). Fresh Water and Watersheds, 221–224. https://doi.org/10.1201/9780429441042-32

APPENDIX

Appendix 1: Volume storage at the surface calculated for Local DEM 10m x 10m

Elevation for pixel in m	Count	Area (m²)	Volume(m³)	Elevation for pixel in m	Count	Area (m²)	Volume(m³)	Elevation for pixel in m	Count	Area (m²)	Volume(m³)
0	9580470	900	0	43	12046	900	38700	86	2960	900	77400
1	66307	900	900	44	12209	900	39600	87	3088	900	78300
2	49645	900	1800	45	11656	900	40500	88	2938	900	79200
3	42693	900	2700	46	11776	900	41400	89	3156	900	80100
4	38536	900	3600	47	11660	900	42300	90	2858	900	81000
5	36284	900	4500	48	10221	900	43200	91	2758	900	81900
6	33782	900	5400	49	9773	900	44100	92	2686	900	82800
7	34407	900	6300	50	9512	900	45000	93	2475	900	83700
8	35549	900	7200	51	9017	900	45900	94	2555	900	84600
9	36012	900	8100	52	9112	900	46800	95	2815	900	85500
10	38062	900	9000	53	8629	900	47700	96	2572	900	86400
11	35700	900	9900	54	8209	900	48600	97	2491	900	87300
12	36166	900	10800	55	8079	900	49500	98	2604	900	88200
13	35033	900	11700	56	8336	900	50400	99	2787	900	89100
14	32710	900	12600	57	8037	900	51300	100	2820	900	90000
15	32836	900	13500	58	8001	900	52200	101	2755	900	90900
16	33453	900	14400	59	7838	900	53100	102	2512	900	91800
17	32090	900	15300	60	7399	900	54000	103	2273	900	92700
18	31032	900	16200	61	7779	900	54900	104	2007	900	93600
19	30985	900	17100	62	7598	900	55800	105	1508	900	94500
20	29886	900	18000	63	7040	900	56700	106	1190	900	95400
21	28533	900	18900	64	7059	900	57600	107	1267	900	96300
22	27052	900	19800	65	7472	900	58500	108	1266	900	97200
23	25042	900	20700	66	6933	900	59400	109	928	900	98100
24	24065	900	21600	67	6396	900	60300	110	864	900	99000
25	23999	900	22500	68	6442	900	61200	111	642	900	99900
26	22608	900	23400	69	6132	900	62100	112	514	900	100800
27	21057	900	24300	70	7059	900	63000	113	573	900	101700
28	20870	900	25200	71	6720	900	63900	114	481	900	102600
29	19469	900	26100	72	7304	900	64800	115	572	900	103500
30	18855	900	27000	73	6462	900	65700	116	649	900	104400
31	17877	900	27900	74	6621	900	66600	117	496	900	105300
32	16953	900	28800	75	6934	900	67500	118	325	900	106200
33	17000	900	29700	76	7346	900	68400	119	221	900	107100
34	16464	900	30600	77	7653	900	69300	120	256	900	108000
35	14163	900	31500	78	6586	900	70200	121	192	900	108900
36	12478	900	32400	79	5600	900	71100	122	100	900	109800
37	12154	900	33300	80	4684	900	72000	123	33	900	110700
38	12162	900	34200	81	3805	900	72900	124	9	900	111600
39	11999	900	35100	82	3276	900	73800	125	1	900	112500
40	11943	900	36000	83	3107	900	74700	665	35	900	598500
41	11356	900	36900	84	3066	900	75600	666	36	900	599400
42	12136	900	37800	85	2903	900	76500	667	15	900	600300
									SUM		**8,885,700**

Appendix 2: Volume storage at the surface calculated for SRTM DEM 30m x 30m

Elevation (m)	Count	Area (m²)	Volume (m³)	Elevation (m)	Count	Area (m2)	Volume (m3)	Elevation (m)	Count	Area (m²)	Volume (m³)
0	7919803	900	0	70	20743	900	63000	140	4025	900	126000
1	77126	900	900	71	20146	900	63900	141	3616	900	126900
2	58197	900	1800	72	19997	900	64800	142	3459	900	127800
3	50007	900	2700	73	20271	900	65700	143	3457	900	128700
4	45471	900	3600	74	20006	900	66600	144	3454	900	129600
5	43365	900	4500	75	19871	900	67500	145	3111	900	130500
6	41690	900	5400	76	19633	900	68400	146	2935	900	131400
7	39841	900	6300	77	19464	900	69300	147	3018	900	132300
8	39660	900	7200	78	18814	900	70200	148	2934	900	133200
9	39208	900	8100	79	19194	900	71100	149	3079	900	134100
10	38406	900	9000	80	21235	900	72000	150	2866	900	135000
11	39616	900	9900	81	22235	900	72900	151	2670	900	135900
12	40119	900	10800	82	20458	900	73800	152	2631	900	136800
13	41324	900	11700	83	19112	900	74700	153	2586	900	137700
14	40338	900	12600	84	18695	900	75600	154	2361	900	138600
15	39539	900	13500	85	17474	900	76500	155	2275	900	139500
16	39699	900	14400	86	17800	900	77400	156	2325	900	140400
17	39429	900	15300	87	17540	900	78300	157	2163	900	141300
18	37892	900	16200	88	17929	900	79200	158	2250	900	142200
19	37222	900	17100	89	17727	900	80100	159	2239	900	143100
20	35491	900	18000	90	17126	900	81000	160	2215	900	144000
21	33520	900	18900	91	16341	900	81900	161	2203	900	144900
22	32605	900	19800	92	16508	900	82800	162	2314	900	145800
23	32049	900	20700	93	16687	900	83700	163	2339	900	146700
24	31665	900	21600	94	16856	900	84600	164	2520	900	147600
25	31873	900	22500	95	17063	900	85500	165	2449	900	148500
26	31428	900	23400	96	16052	900	86400	166	2369	900	149400
27	30534	900	24300	97	14392	900	87300	167	2249	900	150300
28	29556	900	25200	98	13860	900	88200	168	2121	900	151200
29	29529	900	26100	99	13792	900	89100	169	1919	900	152100
30	28566	900	27000	100	13215	900	90000	170	1778	900	153000
31	28639	900	27900	101	13180	900	90900	171	1541	900	153900
32	28299	900	28800	102	13112	900	91800	172	1304	900	154800
33	28288	900	29700	103	13077	900	92700	173	995	900	155700
34	27972	900	30600	104	12998	900	93600	174	955	900	156600
35	28383	900	31500	105	12886	900	94500	175	952	900	157500
36	28355	900	32400	106	12625	900	95400	176	1012	900	158400
37	28691	900	33300	107	12397	900	96300	177	1038	900	159300
38	27922	900	34200	108	12273	900	97200	178	1063	900	160200
39	27556	900	35100	109	11884	900	98100	179	1147	900	161100
40	26982	900	36000	110	12076	900	99000	180	1032	900	162000
41	26094	900	36900	111	12796	900	99900	181	953	900	162900
42	25355	900	37800	112	12835	900	100800	182	758	900	163800
43	24997	900	38700	113	11982	900	101700	183	614	900	164700
44	24980	900	39600	114	11845	900	102600	184	566	900	165600
45	25039	900	40500	115	10619	900	103500	185	492	900	166500
46	24841	900	41400	116	10070	900	104400	186	483	900	167400
47	24709	900	42300	117	9988	900	105300	187	484	900	168300
48	24442	900	43200	118	9488	900	106200	188	475	900	169200
49	24134	900	44100	119	9347	900	107100	189	460	900	170100
50	23910	900	45000	120	9741	900	108000	190	451	900	171000
51	23854	900	45900	121	9699	900	108900	191	453	900	171900
52	23785	900	46800	122	10321	900	109800	192	482	900	172800
53	23290	900	47700	123	10369	900	110700	193	515	900	173700
54	23550	900	48600	124	10221	900	111600	194	563	900	174600
55	23255	900	49500	125	10262	900	112500	195	515	900	175500
56	22974	900	50400	126	10233	900	113400	196	508	900	176400
57	22883	900	51300	127	10635	900	114300	197	365	900	177300
58	22916	900	52200	128	10976	900	115200	198	227	900	178200
59	22701	900	53100	129	11067	900	116100	199	150	900	179100
60	22588	900	54000	130	11601	900	117000	200	73	900	180000
61	22516	900	54900	131	12407	900	117900	201	46	900	180900
62	22346	900	55800	132	13099	900	118800	202	22	900	181800
63	22057	900	56700	133	12643	900	119700	203	7	900	182700
64	21994	900	57600	134	11828	900	120600	204	4	900	183600
65	21669	900	58500	135	10609	900	121500	205	3	900	184500
66	21232	900	59400	136	9182	900	122400	206	2	900	185400
67	21111	900	60300	137	7602	900	123300	207	1	900	186300
68	21162	900	61200	138	5963	900	124200	208	1	900	187200
69	20868	900	62100	139	4749	900	125100				
								SUM			19562400

Appendix 3: Performance of various developed models with different data sources inputs

Run	Rain	Soils	Local DEM 10m × 10m	SRTM 30m × 30m	Sentinel-2	LandSat-8	Initial runs		Calibrated	
							NS	RVE	NS	RVE
1	In-Situ (ref case1)	+	+		+		0.90	3.9	0.89	2.9
2	In-Situ (ref case 2)	+	+			+	0.89	-8.6	0.89	-7.4
3	In-Situ (ref case1)	+		+	+		0.90	-7.1	0.89	-6.1
4	In-Situ (ref case 2)	+		+		+	0.89	-9.5	0.90	-8.5
5	CMORPH-Uncorrected	+	+		+		0.24	-9.6	0.38	-7.8
6	CMORPH- Uncorrected	+	+			+	0.23	-13.0	0.30	-10.1
7	CMORPH- Uncorrected	+		+	+		0.23	-11.9	0.35	-8.9
8	CMORPH- Uncorrected	+		+		+	0.20	-14.2	0.30	-11.2
9	CMORPH- PT	+	+		+		0.71	1.4	0.77	0.4
10	CMORPH- PT	+	+			+	0.61	12.0	0.69	10.0
11	CMORPH- PT	+		+	+		0.69	4.5	0.77	2.5
12	CMORPH- PT	+		+		+	0.61	13.8	0.70	10.8
13	CMORPH- DT	+	+		+		0.33	-1.0	0.43	0.0
14	CMORPH- DT	+	+			+	0.30	10.4	0.33	9.4
15	CMORPH- DT	+		+	+		0.33	2.4	0.43	1.3
16	CMORPH- DT	+		+		+	0.29	12.4	0.30	10.4
17	CMORPH- TVS	+	+		+		0.38	-8.6	0.49	-7.4
18	CMORPH- TVS	+	+			+	0.40	-11.4	0.50	-9.4
19	CMORPH- TVS	+		+	+		0.40	-9.2	0.49	-8.3
20	CMORPH- TVS	+		+		+	0.39	-12.5	0.49	-10.4
21	CHIRPS - Uncorrected	+	+		+		0.17	0.3	0.28	-1.3
22	CHIRPS - Uncorrected	+	+			+	0.22	-10.7	0.27	-10.2
23	CHIRPS - Uncorrected	+		+	+		0.20	-14.3	0.26	-13.3
24	CHIRPS - Uncorrected	+		+		+	0.16	-15.7	0.20	-13.7
25	CHIRPS -PT	+	+		+		0.73	7.2	0.79	6.3
26	CHIRPS -PT	+	+			+	0.63	8.1	0.69	8.7
27	CHIRPS -PT	+		+	+		0.68	10.3	0.70	8.4
28	CHIRPS -PT	+		+		+	0.60	11.3	0.60	10.7
29	CHIRPS – DT	+	+		+		0.20	12.2	0.29	1.3
30	CHIRPS – DT	+	+			+	0.30	10.0	0.31	10.1
31	CHIRPS – DT	+		+	+		0.28	14.1	0.31	12.4
32	CHIRPS – DT	+		+		+	0.23	18.3	0.31	12.2
33	CHIRPS-TVS	+	+		+		0.30	-2.8	0.43	-1.2
34	CHIRPS-TVS	+	+			+	0.37	-10.0	0.41	-7.3
35	CHIRPS-TVS	+		+	+		0.36	-7.0	0.42	-6.0
36	CHIRPS-TVS	+		+		+	0.36	-11.3	0.41	-9.4
37	GMP-IMERG- Uncorrected	+	+		+		0.38	16.8	0.41	14.0
38	GMP-IMERG- Uncorrected	+	+			+	0.34	-17.5	0.40	-11.5
39	GMP-IMERG- Uncorrected	+		+	+		0.37	-11.1	0.40	-10.1
40	GMP-IMERG- Uncorrected	+		+		+	0.36	-25.4	0.40	-22.4
41	GMP-IMERG-PT	+	+		+		0.70	9.0	0.72	8.0
42	GMP-IMERG-PT	+	+			+	0.62	12.7	0.67	10.2
43	GMP-IMERG-PT	+		+	+		0.70	10.4	0.71	9.1
44	GMP-IMERG-PT	+		+		+	0.51	24.5	0.65	19.0
45	GMP-IMERG-DT	+	+		+		0.50	14.3	0.54	12.8
46	GMP-IMERG-DT	+	+			+	0.44	15.9	0.50	10.6
47	GMP-IMERG-DT	+		+	+		0.48	10.3	0.54	9.5
48	GMP-IMERG-DT	+		+		+	0.43	20.8	0.49	18.8
49	GMP-IMERG-TVS	+	+		+		0.52	0.9	0.62	2.0
50	GMP-IMERG-TVS	+	+			+	0.60	-10.1	0.60	-10.1
51	GMP-IMERG-TVS	+		+	+		0.53	-4.9	0.61	-3.8
52	GMP-IMERG-TVS	+		+		+	0.57	-15.8	0.62	-12.2

Appendix 4: Error propagation effects on streamflow simulations

SREs	RMSE$_R$	MAE$_R$	CC$_R$	RMSE$_{QS}$	MAE$_{QS}$	CC$_{QS}$	RMSE$_{QS}$/ RMSE$_R$	MAE$_{QS}$/ MAE$_R$	CC$_{QS}$/ CC$_R$
Local DEM 10m x 10m with Sentinel-2									
CMORPH-Uncorrected	3.8	2.3	0.61	3.2	2.5	0.70	0.8	**1.1**	1.14
CMORPH-PT	1.6	0.5	0.94	1.2	0.4	0.99	0.8	0.7	1.06
CMORPH-TSV	3.4	2.1	0.68	2.8	1.8	0.77	0.8	0.9	1.13
CMORPH-DT	3.4	2.1	0.70	2.9	1.9	0.78	0.9	0.9	1.11
CHIRPS- Uncorrected	4.0	2.4	0.58	3.3	2.6	0.67	0.8	**1.1**	1.15
CHIPS-PT	1.6	0.5	0.94	1.3	0.4	0.97	0.8	0.8	1.04
CHIPS-TSV	3.7	2.3	0.61	3.0	2.0	0.71	0.8	0.9	1.15
CHIPS-DT	3.8	2.6	0.61	2.6	1.8	0.83	0.7	0.7	1.36
IMERG- Uncorrected	3.4	1.9	0.71	3.5	1.8	0.79	**1.04**	0.9	1.11
IMERG-PT	1.9	0.7	0.94	1.6	0.6	0.96	0.8	0.9	1.02
IMERG-TSV	2.7	1.7	0.8	1.98	1.3	0.88	0.7	0.8	1.11
IMERG-DT	3.0	1.95	0.76	2.6	1.8	0.83	0.8	0.9	1.1
Local DEM 10m x 10m with LandSat-2									
CMORPH- Uncorrected	3.8	2.3	0.61	3.9	1.7	0.69	**1.01**	0.8	1.13
CMORPH-PT	1.6	0.5	0.94	1.3	0.5	0.94	0.8	1.0	1.003
CMORPH-TSV	3.4	2.1	0.68	2.3	1.5	0.77	0.7	0.7	1.13
CMORPH-DT	3.4	2.1	0.70	2.4	1.6	0.77	0.7	0.8	1.11
CHIRPS- Uncorrected	4.0	2.4	0.58	2.8	1.8	0.53	0.7	0.7	**0.91**
CHIPS-PT	1.6	0.5	0.94	1.3	0.5	0.96	0.8	0.9	1.02
CHIPS-TSV	3.7	2.3	0.61	2.5	1.6	0.70	0.7	0.7	1.15
CHIPS-DT	3.8	2.6	0.61	3.2	2.1	0.56	0.8	0.8	**0.92**
IMERG- Uncorrected	3.4	1.9	0.71	2.2	2.0	0.79	0.7	**1.03**	1.11
IMERG-PT	1.9	0.7	0.94	1.6	0.7	0.95	0.8	0.9	1.01
IMERG-TSV	2.7	1.7	0.79	1.6	1.1	0.88	0.6	0.6	1.11
IMERG-DT	3.0	2.0	0.76	2.1	1.5	0.83	0.7	0.7	1.09
SRTM 30m x 30m with Sentinel-2									
CMORPH- Uncorrected	3.8	2.3	0.61	2.7	1.7	0.59	0.7	0.8	**0.97**
CMORPH-PT	1.6	0.5	0.94	1.3	0.5	0.94	0.8	0.9	1.003
CMORPH-TSV	3.4	2.1	0.68	2.3	1.5	0.76	0.7	0.7	1.13
CMORPH-DT	3.4	2.1	0.70	2.4	1.6	0.77	0.7	0.8	1.11
CHIRPS- Uncorrected	4.0	2.4	0.58	2.7	1.8	0.47	0.7	0.7	**0.803**
CHIPS-PT	1.6	0.5	0.94	1.2	0.5	0.96	0.8	0.9	1.02
CHIPS-TSV	3.7	2.3	0.61	2.5	1.6	0.70	0.7	0.7	1.15
CHIPS-DT	3.8	2.6	0.61	3.1	2.1	0.68	0.8	0.8	1.12
IMERG- Uncorrected	3.4	1.9	0.71	2.2	2.0	0.79	0.7	**1.03**	1.11
IMERG-PT	1.9	0.7	0.94	1.6	0.7	0.95	0.8	0.9	1.01
IMERG-TSV	2.7	1.7	0.79	1.6	1.1	0.88	0.6	0.6	1.11
IMERG-DT	3.0	2.0	0.76	2.1	1.4	0.73	0.7	0.7	**0.96**
SRTM 30m x 30m with LandSat-8									
CMORPH- Uncorrected	3.8	2.3	0.61	2.6	1.7	0.56	0.7	0.7	**0.91**
CMORPH-PT	1.6	0.5	0.94	1.3	0.5	0.94	0.8	0.9	1.003
CMORPH-TSV	3.4	2.1	0.68	2.3	1.5	0.77	0.7	0.7	1.13
CMORPH-DT	3.4	2.1	0.70	2.4	1.5	0.77	0.7	0.8	1.11
CHIRPS- Uncorrected	4.0	2.4	0.58	2.7	1.7	0.46	0.7	0.7	**0.78**
CHIPS-PT	1.6	0.5	0.94	1.2	0.5	0.96	0.8	1.0	1.03
CHIPS-TSV	3.7	2.3	0.61	2.5	1.6	0.70	0.7	0.7	1.15
CHIPS-DT	3.8	2.6	0.61	3.1	2.0	0.56	0.8	0.8	**0.91**
IMERG- Uncorrected	3.4	1.9	0.71	2.2	1.4	0.69	0.7	0.7	**0.97**
IMERG-PT	1.9	0.7	0.94	1.6	0.7	0.95	0.8	0.9	1.01
IMERG-TSV	2.7	1.7	0.79	1.6	1.1	0.88	0.6	0.6	1.11
IMERG-DT	3.0	2.0	0.76	2.1	1.4	0.71	0.7	0.7	**0.93**

Appendix 5: Runoff coefficient at the outlet in the Nyabarongo catchment area

Rainfall	Rainfall	Discharge	Runoff coefficient	NSE	RVE
Local DEM 10 × 10m with Sentinel-2					
In-situ	6058.9	3695.9	0.61	0.89	2.9
CMORPH-Uncorrected	4205.7	1687.1	0.40	0.38	-7.8
CMORPH-PT	6635.8	3902.1	0.59	0.77	0.4
CMORPH-TSV	4384.5	1901.2	0.43	0.49	-7.4
CMORPH-DT	6610.5	2795.5	0.42	0.43	0.0
CHIRPS- Uncorrected	5942.8	2288.0	0.39	0.28	-1.3
CHIPS-PT	6717.7	3800.2	0.57	0.79	6.3
CHIPS-TSV	5996.6	2496.5	0.42	0.43	-1.2
CHIPS-DT	6985.7	2852.2	0.41	0.29	1.3
IMERG- Uncorrected	6037.4	2408.3	0.40	0.41	14.0
IMERG-PT	6658.7	3850.3	0.58	0.72	8.0
IMERG-TSV	6033.5	2548.2	0.42	0.62	2.0
IMERG-DT	6579.0	2703.5	0.41	0.54	12.8
Local DEM 10m ×10m with LandSat-2					
In-situ	6058.9	3478.7	0.57	0.89	-7.4
CMORPH- Uncorrected	4205.7	1659.9	0.39	0.30	-10.1
CMORPH-PT	6635.8	3702.9	0.56	0.69	10.0
CMORPH-TSV	4384.5	1784.0	0.41	0.50	-9.4
CMORPH-DT	6610.5	2648.3	0.40	0.33	9.4
CHIRPS- Uncorrected	5942.8	2070.8	0.35	0.27	-10.2
CHIPS-PT	6717.7	3621.0	0.54	0.69	8.7
CHIPS-TSV	5996.6	2379.3	0.40	0.41	-7.3
CHIPS-DT	6985.7	2735.0	0.39	0.31	10.1
IMERG- Uncorrected	6037.4	2241.1	0.37	0.40	-11.5
IMERG-PT	6658.7	3643.1	0.55	0.67	10.2
IMERG-TSV	6033.5	2471.0	0.41	0.60	-10.1
IMERG-DT	6579.0	2656.3	0.40	0.50	10.6
SRTM 30m × 30m with Sentinel-2					
In-situ	6058.9	3585.6	0.59	0.89	-6.1
CMORPH- Uncorrected	4205.7	1666.7	0.40	0.35	-8.9
CMORPH-PT	6635.8	3809.8	0.57	0.77	2.5
CMORPH-TSV	4384.5	1820.9	0.42	0.49	-8.3
CMORPH-DT	6610.5	2705.2	0.41	0.43	1.3
CHIRPS- Uncorrected	5942.8	2177.7	0.37	0.26	-13.3
CHIPS-PT	6717.7	3727.9	0.55	0.70	8.4
CHIPS-TSV	5996.6	2486.2	0.41	0.42	-6.0
CHIPS-DT	6985.7	2801.9	0.40	0.31	12.4
IMERG- Uncorrected	6037.4	2308.0	0.38	0.40	-10.1
IMERG-PT	6658.7	3710.0	0.56	0.71	9.1
IMERG-TSV	6033.5	2537.9	0.42	0.61	-3.8
IMERG-DT	6579.0	2703.2	0.41	0.54	9.5
SRTM 30m × 30m with LandSat-8					
In-situ	6058.9	3372.2	0.56	0.90	-8.5
CMORPH- Uncorrected	4205.7	1453.3	0.35	0.30	-11.2
CMORPH-PT	6635.8	3636.3	0.55	0.70	10.8
CMORPH-TSV	4384.5	1677.5	0.38	0.49	-10.4
CMORPH-DT	6610.5	2591.8	0.39	0.30	10.4
CHIRPS- Uncorrected	5942.8	2004.3	0.34	0.20	-13.7
CHIPS-PT	6717.7	3514.5	0.52	0.60	10.7
CHIPS-TSV	5996.6	2272.7	0.38	0.41	-9.4
CHIPS-DT	6985.7	2628.5	0.38	0.31	12.2
IMERG- Uncorrected	6037.4	2074.6	0.34	0.40	-22.4
IMERG-PT	6658.7	3556.6	0.53	0.58	19.0
IMERG-TSV	6033.5	2324.5	0.39	0.62	-12.2
IMERG-DT	6579.0	2549.8	0.39	0.49	18.8